SENSING THE LIGHT: DESIGN OF PHOTOACTIVATABLE PROTEIN-PROTEIN INTERACTIONS USING THE LOV2 DOMAIN

Oana Izabela Lungu

A dissertation submitted to the faculty of the University of North Carolina at Chapel Hill in partial fulfillment of the requirements for the degree of Doctor of Philosophy in the Department of Biochemistry and Biophysics.

Chapel Hill
2012

Approved by:

Brian Kuhlman, Ph.D.

Klaus Hahn, Ph.D.

Charles Carter, Ph.D.

Sharon Campbell, Ph.D.

Rihei Liu, Ph.D.

ABSTRACT

OANA IZABELA LUNGU: Sensing the Light: Design of Photoactivatable Protein-Protein Interactions Using the LOV2 Domain
(Under the direction of Brian Kuhlman, Ph.D. and Klaus Hahn, Ph.D.)

Photocontrol of protein-protein interactions is a powerful tool for precise spatial and temporal control of cell signaling networks. This dissertation has sought to expand the use of naturally occurring, light-sensitive proteins to photocontrol protein-protein interactions. This method allows for genetically encoded, reversible photoacitvation, or caging, of critical protein-protein interactions in a signaling network cascade. The small, globular GTPase protein Rac1 was caged through the use of the light-sensitive LOV2 domain as steric block to Rac1 effector binding in the dark. The resulting photoswitch which was created, PA-Rac, was able to induce membrane ruffling, protrusions, and directed cell movement upon blue light irradiation at the leading edge of mammalian cells. Its use has resulted in deeper understanding of the role of Rac1 in mammalian cell motility. Modeling and characterization of PA-Rac enabled caging of the related GTPase Cdc42 in a similar manner. The LOV2 domain was also used to create a photoactivatable peptide, LOV-ipaA. The photoswitch, which binds the adhesion protein vinculin, was designed by embedding a peptide sequence by into the Jα helix of the LOV2 domain. As a model case, LOV-ipaA demonstrated the ability to alter the sequence of the LOV2 domain Jα helix while maintaining its photoswitching capacity in order to introduce new functionality into the helix. LOV-ipaA light activated heterodimerization to vinculin was used as tool for light-induced protein expression in *S. cerevisiae*. This tool allowed for photoactivatable overexpression of the proteins Ste4 and Gpa1, which are critical components in regulation of the yeast pheromone mating response pathway. Through this work, significant progress was achieved toward being able to photactivate two classes of proteins, and using those proteins as tools to manipulate biological systems.

To my grandmother, Dr. Elena Antone Decu

ACKNOWLEDGEMENTS

First and foremost, I would like to thank my two advisors, Brian Kuhlman and Klaus Hahn for their unyielding support throughout my time in graduate school. Their mentorship has helped grow personally and professionally. I have become a better scientist because of it.

My many wonderful labmates have all been a a great asset without which I could have never accomplished so much. Some have particularly gone out of their way to lend me a had. I would like to thank Yi Wu, who first started the research into creating photoactivatable proteins using the LOV2 domain, engineering PA-Rac. He helped me set the stage for all of my dissertation work. I would like to thank Ryan Hallett and Jeannette Aiken; not only were they wonderful rotation students, they also helped me put together a manuscript. I would like to thank Carrie Purbeck, Ben Stranges, Steven Lewis, Eun Jung Choi, Gurkan Guntas, and Bryan Der in the Kuhlman lab for their help in troubleshooting experiments, technical matters, and having great conversations. In the Hahn lab, I would like to thank Christopher Welch, John Zawistowski, Evan Trudeau, Akash Gulani, Pei-Hsuan Chu, and Marie Rougie for help with the microscopes and mammalian cell experiments.

My collaborators in the Campbell and Dohlman labs have been of great importance to the creation of this work. Moriah Beck and Ashley Clarke helped me set up vinculin assays. Steve Cappell, Sarah Clement, and Joshua Kelley took time out of their lives to teach me how to work with yeast.

I would like to thank my committee and various professors at UNC who have shaped this project; Dr. Sharon Campbell, Dr. Rihe Liu, Dr. Charles Carter, Dr. Brian Strahl, Dr. John Sondek, Dr. Henrik Dohlman, and Dr. Ashutosh Tirpathy.

On a personal note, I would like to thank my family, Anca and Claudiu Lungu for their

always helpful advice and never ending support. I would also like to thank my partner, Rudresh Ghosh for the many times he escorted me to lab in the middle of the night so I could get my experiments done.

TABLE OF CONTENTS

LIST OF TABLES

LIST OF FIGURES

LIST OF ABBREVIATIONS

AD	Activation Domain
BD	Binding Domain
CBM	Chromophore Binding Module
CD	Circular Dichroism
ChR2	Channelrhodopsin2
CPRG	Chlorophenol red-β-D-galactopyranoside
CRY2	Cryptochrome2
DHFR	Dihydrofolate Reductase
FAD	Flavin-Adenine Dinucleotide
FMN	Flavin Mononucleotide
GDP	Guanosine-5'-Diphosphate
GEF	Guanine Nucleotide Exchange Factor
GTP	Guanosine-5'-Triphosphate
LOV	Light Oxygen Voltage
ITC	Isothermal Titration Calorimetry
NADPH	Nicotinamide Adenine Dinucleotide Phosphate
NMR	Nuclear Magnetic Resonance
NpHR	Halorhodopsin
PA-Rac	Photoactivatable Rac1
PCB	Phycocyanobilin

PΦB	Phytochromobilin
PYP	Photoactive Yellow Protein
RMSD	Root Mean Square Deviation
SD	Synthetic Dextrose
SPR	Surface Plasmon Resonance
TAMRA	5-(and-6)-Carboxytetramethylrhodamine
VBS	Vinculin Binding Site
WASP	Wiskott-Aldrich Syndrome Protein
X-α-gal	5-bromo-4-chloro-3-indolyl-α-D-gactopyranoside

CHAPTER 1

INTRODUCTION

1.1 Photoactivation as a tool for cell biology

Perturbing protein-protein interactions in a biological process and observing the outcome is a valuable method for understanding how signaling networks are modulated. This method has been used to understand basic biological processes such as cell division, signaling, and motility (1). Yet, questions remain as to how proteins interact with each other, and thus regulate biological responses, in a dynamic manner. How are protein-protein interactions regulated spatially and temporally? How do these regulatory events translate into cellular events, such as motility, that occur at the sub-micron and second scales?

Traditional methods of perturbing a signaling pathway have relied on biochemical, genetic, and chemical approaches. Constitutively active, inactive, and dominant negative mutations are used instead of wild type versions of key signaling proteins (2; 3; 4). RNA interference knock-downs eliminate a protein from a signaling network (5; 6). Small molecules can act as chemical activators and inhibitors for signaling proteins (7). While these methods have been successfully used in cellular studies, they suffer from certain limitations. Biochemical and genetic perturbations are slow processes that allow time for a cell to compensate for aberrant signaling through other means. Chemical activators and inhibitors generally do not have a high specificity for protein targets. In addition, none of these methods are able to finely disrupt signaling events in a spatially and temporally controllable manner.

Photoactivation is a useful tool to solve these problems. Photoactivation, or caging, involves trapping a protein in a inactive conformation. The protein is then activated using light,

enabling it to interact with downstream effectors to activate or inhibit pertinent signalling networks. In this way, one can express a caged protein in a cell, irradiate subsection of that cell using a laser beam, thus photoactivating, or uncaging the protein, and observe the downstream signaling events that occur in a precise spatially and temporally controlled manner. In tissues or whole organisms, groups of cells may be photoactivated in order to understand intercellular signalling.

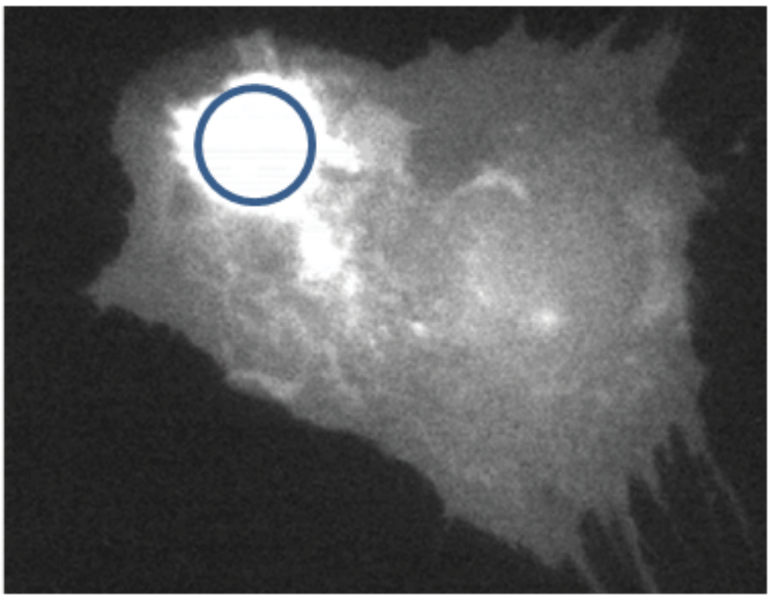

Figure 1.1: Photoactivation of Rac1 using light. A mouse embryo fibroblast expressing Photoactivatable Rac (PA-Rac) is selectively irradiated by a laser. The Rac1 protein is only uncaged in the area of irradiation (blue circle).

In order to perturb protein signaing networks through caging, interactions that propagate downstream functional or physiological changes in a cell or tissue must be inhibited under dark conditions, but allowed under particular wavelengths of light. Many of the most important such interactions in signaling networks are protein-protein interactions.

Two principle methods have been developed for photoactivation of peptides and proteins. The first method relies on photocleavable chemical agents to inhibit protein-protein interactions in the dark, while allowing for protein-protein signaling interactions in the light, when the chemical agent is removed. The second method relies on naturally occurring light sensing proteins. Such proteins undergo conformational changes upon irradidiation with wavelengths

of light absorbed by their chromophores. These conformational changes have been taken advantage of to create general mechanism of caging. In one tissue-level caging mechanism, photoactivtable ion channnels are used to propagate signaling networks controlled by ion gradients and action potentials rather than protein-protein interactions. Other systems use interactions between light sensitive proteins and their effectors to enable light-activated heterodimerization of proteins linked to the light sensor and effector. Yet other systems directly use a naturally occurring protein as a caging agent, enabling a dark state steric block of the targeted protein interactions. Light irradiation alters the conformation of the photosensitive protein, relieving the block and allowing for desired protein interactions.

In this work, naturally occurring photoactivatable proteins are used to cage proteins as well as peptides. Both proteins and peptides are caged by sterically blocking protein-protein interactions in the dark using a genetically encoded, naturally occurring protein as a caging agent, and releasing that steric block in the the light. As an application, the peptide photoswitch is used to induce transcription through light-activated heterodimerization in yeast.

1.2 Chemical caging of proteins

The use of chemical compounds to cage peptides and proteins is technically challenging. Caging of signaling proteins overcomes many of the limitations of using traditional perturbation techniques and is spatially and temporally controllable. In order to achieve perturbation of signaling events through the use of light, key macromolecules controlling a biological process are modified using photo-cleavable chemical compounds. These chemicals block activity of the macromolecule, and irradiation with light of a specific wavelength in the UV range removes the modification, regenerating activity. Chemicals typically used in light activated caging include derivatives of the 2-nitrobenzyl group and the coumarin moiety (8). Activating these caged molecules is not reversible and often requires high intensity UV light, which can be damaging to cellular processes.

Disruption of protein-protein complexes that modulate signaling events can often be achieved with chemically caged peptides that allow for control over when and where cellular signaling

events are disrupted (9). The first *in vivo* use of peptide chemical caging technology probed the role of calcium- calmodulin and myosin light chain kinase in amboid locomotion of eosinophil cells (10). Subsequently, caged analogs of inhibitory phosphopeptides examined the function of 14-3-3 proteins in control of the cell cycle (11). More recently, Caged protein localization peptides were used to direct proteins to subcellular locations (12). However, one chemical caging strategy cannot be easily transferable from one peptide inhibitor to another due to the fact that only certain residues are chemically reactive to covalent modification, and so changing the sequence of a peptide changes the positions available for its caging.

While various small caged peptides have been used in many studies, caging of full length proteins with chemical compounds poses a number of challenges. In order for caging to be successful, chemical modifications must occur only on particular residues of the protein. This is hard to control for, as generally all solvent exposed residues able to interact with the photo-cleavable compound get modified.

Some methods for overcoming the labeling challenge have been developed and recently used *in vivo*. Semi-synthesis of proteins has been employed to label only one selected peptide sequence of a protein, after which it is expressed ligated onto the whole polypeptide (13). In this way, the protein Smad2 was caged and studied for its ability to trimerize only when located in a cell nucleus. The addition of unnatural amino acids has also shown promise as an alternative way to chemically label proteins. Nonnatural, photo-cleavable amino acids are incorporated into a protein using chemically synthesized misacylated tRNAs (14; 8). The technology has been used to control activity of potassium ion channels and nicotinic acetylcholine receptors in *Xenopus* oocytes (15; 16). While the method ensures site-specific incorporation of caging groups into proteins, the difficulty of synthesizing misacylated tRNAs limits its efficiency.

In order to overcome the synthesis limitation, orthogonal tRNA- tRNA synthetase pairs that only allow the addition of caged tyrosine (17; 18), caged cysteine (19), and caged serine (20) residues into polypeptide chains have been engineered for use in yeast and bacterial cells. The caged serine was used to observe the spatial regulation and kinetics of the transcription factor Pho4 in yeast cells. One of the limitations of this technology is the limited possibilities of placing a caging group only on tyrosine, serine, and cystine residues. Also, if such a protein

were to be used in mammalian cell studies, it would have to be microinjected.

One of the most significant finding to come out of protein caging involves the protein cofilin. Cofilin was caged on a residue that is usually phosphorylated, leading to inactivation of the protein. Upon photo-illumination, the caging group fell off, restoring the protein's activity (21). The caged protein was used in live cell studies to determine whether it is a polymerizing or depolymerizing factor of actin. It was determined that cofilin polymerized actin and that it contributed to the directionality of cell motility (22).

More recent advances in chemical caging have lead to the development of multiple photoactivatable enzymes. DNA polymerases (23), RNA polymerases (24), as well as zinc finger nucleases (25) have been designed to regulate gene expression (26). The development of photocleavable rapamycin enabled caging of kinases, including focal adhesion kinase and MEK1 (27; 28).

Although great progress has been made, caging of macromolecules using photo-cleavable chemicals for in vivo studies is technically challenging. It is difficult to covalently modify only a desired key residue to be used for caging. Additionally, most large chemically labeled caged peptides and all proteins must be microinjected into mammalian cells, an often tedious process that limits the number of cells in an experiment. Lastly, because of the specific sterics involved in each caged interaction, there is no method of caging that is easily transferable from target to target.

1.3 Strategies for genetically encoded photoactivation of proteins

As an alternative to chemical caging of proteins, various naturally occurring photosensing proteins have been used as genetically encoded caging agents. All of these proteins are found fungal, plant, or algal organisms. Using such proteins alleviates certain problems associated with chemical caging agents. Proteins may be engineered and constructed with a wide latitude of conformations, regardless of which labile amino acids are available at the desired site of caging. Light activation in these proteins in reversible. Microinjecting genetically encoded proteins into cells is unnecessary. Lastly, organismal-derived photosensory proteins can gener-

ally sense a wide range of colors, including red (29), yellow (30), and blue (31; 32; 33; 34; 35), abolishing the need for use of damaging ultraviolet light.

Channelrhodopsins have been used for optogenetic control of neuronal as well as cardiac cells. They are part of the family of Rhodopsin proteins that are integral membrane proteins found in plants, animals, and microorganisms. Rhodopsins have long been identified as photoreceptors in animal retinas (36). Channelrhodopsins2 (ChR2), used in optogentetics studies, was discovered in the *Chlamydomonas reinhardtii* organism and acts as light-gated cation channel (37). The channel is composed of seven transmembrane helices connected by short loops, and a retinol cofactor in the middle (Figure 1.2). The channel undergoes very rapid (within 30 μs) light-induced conformational changes (38; 39) in response to light of around 500 nm wavelength (31). It closes quickly in darkness.

Channelrhodopsins have been used to quickly depolarize neurons and trigger trains of neuronal spikes. This has allowed researchers to study patterns of spike activity in a precise spatial and temporal manner, and understand various functions of neural circuits. In one such study, in zebrafish, ChR2 was used to activate individual mechanosensory neurons (40). In another study, Alilain *et al.* restored function to damaged neuronal circuits by activating ChR2 in rat spinal chords (41; 42).

Another variant of the rhodopsin family, halorhodopsin (NpHR), is a yellow-light driven chloride ion pump from halobacteria (30; 43). Genetically expressing this pump in organisms allows for hyperpolarization of cells and suppression of action potentials in response to light activation. ChR2 and NpHR have been used together in zebrafish brains and hearts to map out small groups of neurons in the brain that control directional swimming and rapid eye movement (44), as well as to study cardiac pacemaker function during organ development (45).

Although they have been have been critical to advancing the field of neurobiology, channelrhodopsins are not optimal for all applications. They are best used in cells that signal through large electrophysiological changes in ion gradients and through action potentials. Channelrhodopsins also must be used in groups of cells, rather than to study spatially and temporally mediated phenotypic change in a single cell.

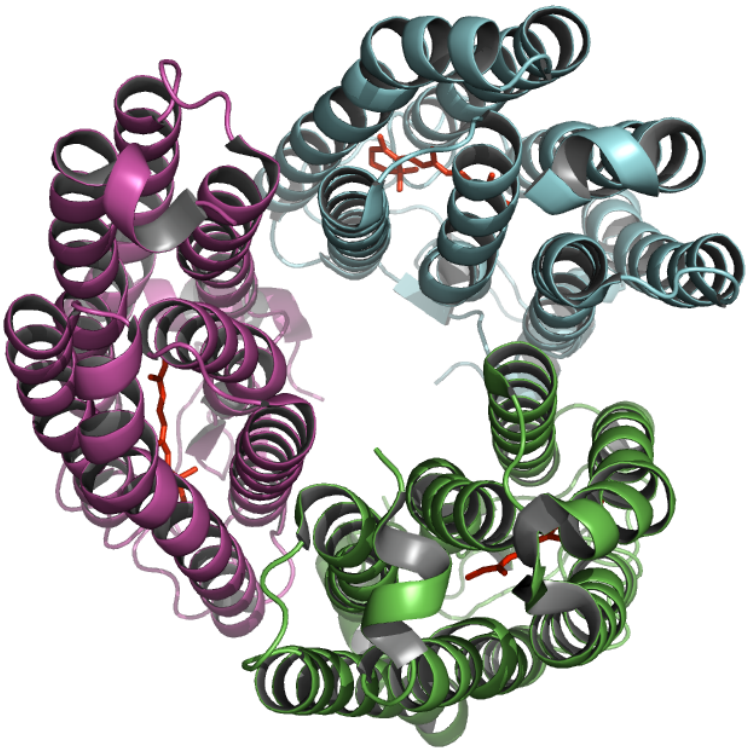

Figure 1.2: Structure of the halorhodopsin protein. Protein is from the *Natronomonas pharaonis* organism. Individual domains of the biological unit from are shown in cyan, green, and purple. The retionol chromophore is shown in red (PDB code 3ABW).

Other systems have taken advantage of naturally occurring phytochrome proteins to photoactivate signaling pathways *in vitro* and *in vivo*. Found in plants as well as microbes, phytochromes (46) and baceriophytochromes (47; 48) respectively, act as red light to far-red light photoreceptors. In plants, these receptors regulate aspects of photomorphogenesis. Phytochromes use a bilin cofactor for red and far-red light absorption, with bacteriophytochromes binding biliverdin, and plant phytochromes binding phycocyanobilin (PCB) or phytochromobilin (PΦB) (49; 50). The four pyrrole ring bilin chromophore of a phytochrome protein in its Pr state absorbs a photon of red light around 660 nm in wavelength (29). This leads to isomerization of a double bond in the chromophore, and the flipping of its D ring (Figure 1.3) (51; 52; 53). The protein then adopts the Pfr conformation, wherein the pyrrole ring shifts slightly, and side chains around the chromophore alter their positions and interacting partners (53). The phytochrome Pfr state reverses back to the Pr state through the absorption of a

photon of far-red light of around 750 nm in wavelength (29).

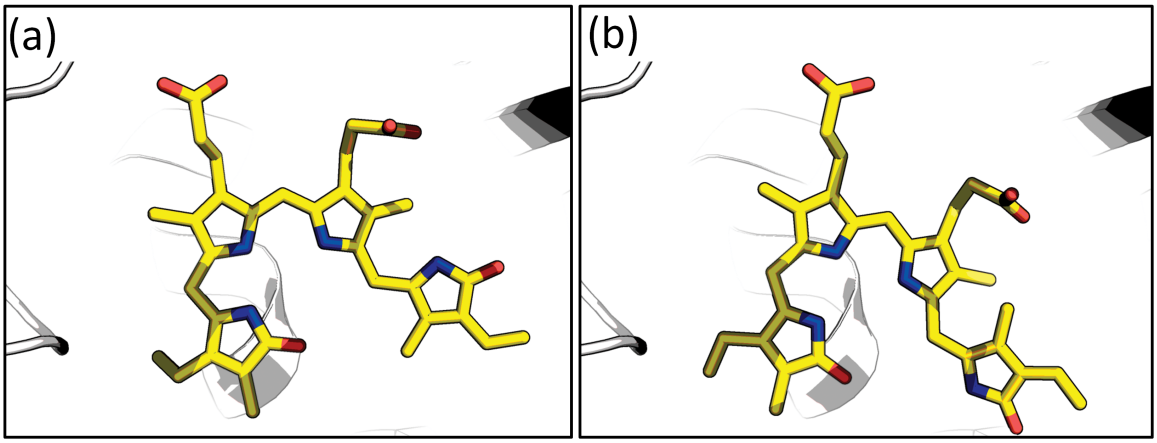

Figure 1.3: The Pr and Pfr states of the bacteriophytochrome biliverdin chromophore. Protein is from the *Pseudomonas aeruginosa* organism. The (a) Pr and (b) Pfr states of the chromophore are shown in yellow. The protein main chain is shown in white (PDB code 3IBR).

Phytochromes contain two domains, the PAS and GAF domains that together comprise the chromophore binding module (CBM) (50). By itself the CBM has reduced photoactivity. C-terminal to the CBM is a phytochrome-specific PHY domain in most such proteins, which together with the CBM is responsible for the full activity of the protein.

The *A. thaliana* CBM of PhyB binds the PIF3 protein upon irradiation with red light in the presence of chromophore PΦB (54). Irradiation with far red light releases this heterodimerization. This system was used by Shimizu *et al.* (29) to activate transcription through the GAL1 promoter in budding yeast. The GAL4 activation domain was linked to PIF3, while the GAL4 binding domain was linked to PhyB. Irradiation with red light in the presence of the PΦB chromophore led to binding of PhyB to PIF3, bringing the GAL4 domains into proximity, and activating transcription of the LacZ reporter gene downstream of the GAL1 promoter. Red light irradiation produced a thousand-fold increase in LacZ activation, and irradiation with far-red light quickly decreased activity (29).

Tyszkiewicz *et al.* extended this work to generate a light-controlled conditional protein splicing system (CPS) in budding yeast (55). In this system, the actions of an intein are red-light regulated. Inteins are protein domains that autocatalytically splice themselves out

of a larger protein, concurrently ligating together the extein polypeptides on either side of the splice (56). The vacuolar ATPase intein was artificially split into two fragments, with one fragment fused to PhyB, while the other was joined to PIF3. Irradiation with blue light led to joining of the two intein fragments and splicing of the polypeptide, leading to the formation of an MBP-FLAG reporter fusion protein.

Phytochromes were utilized to photoactivate signaling networks modulating cell motility (57; 58). PIF3 was linked to the Wiskott-Aldrich Syndrome protein (WASP), while an inactive, GDP-bound Cdc42 protein was linked to PhyB. Normally Cdc42, when GTP bound, activates WASP (59; 60), thus allowing for actin nucleation through activation of the Arp2/3 complex (61; 62). Through irradiation with red light, PhyB-Cdc42 activated PIF3-WASP while in the GDP bound state, allowing for actin filament formation *in vitro* through Arp2/3 activation. Activation of WASP was reversible through irradiation with far-red light. Levskaya *et al.* performed cell motility studies in mammalian cells using PhyB and the PIF6 protein (58). In these studies, the PhyB protein was linked to a membrane localization tag, while PIF6 was linked to the DH-PH catalytic domain cassette of the Tiam or intersectin Rac1 or Cdc42 specific GEFs, respectivley (63; 64). Irradiation with patterns of red and far-red light led to the recruitment of the GEFs to the cell membrane in specific subcellular locations, allowing for activation of Rac1 and Cdc42, and localized patterns of membrane protrusion and filopodial formation.

In one instance, bacteriophytochromes were used for creating a photosensitive bacterial film. Levskaya *et al.* fused a cyannobacterial phytochrome containing a membrane-bound, extracellular light receptor (65) and an *E. coli* the EnvZ-OmpR histidine kinase domain (66). This particular domain was able to activate the OmpR dependent ompC promoter, allowing for transcription of the downstream lacZ reporter (67), which generated a black dye. Light irradiation repressed lacZ transcription, allowing for light-driven gradient projections of designs into a biological film. The mechnism of light sensing in the cyannobacterial phytochrome is unknown.

While phytochromes have been used extensively for light driven signalling, and particulary heterodimerization, the system poses certain challenges. The bilin chromophores used by

phytochromes must be either supplied exogenously, or introduced into host organisms through gene manipulations. The phytochromes are also very large, making them cumbersome to work with. Full-length phytochrome protein structures are unavailable, and the overall mechanism of light-induced switching in the proteins is still a mystery. These two factors combine to make design of phytochromes in order to generalize the switches for caging many types of protein-protein interactions challenging.

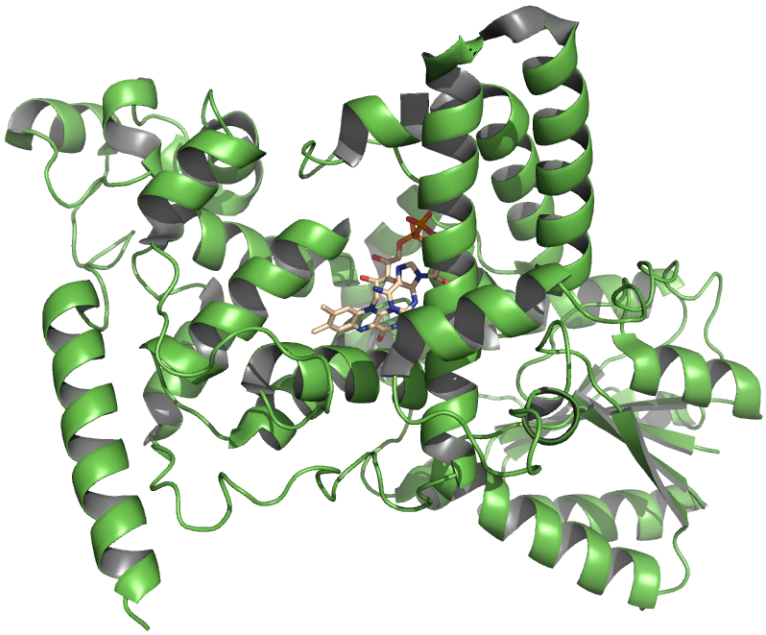

Figure 1.4: Structure of the PHR domain of Cryptochrome1. The domain from *A. thaliana* is shown in green, and the FAD chromophore is shown in tan (PDB code 1U3C).

Cryptochromes, like phytochromes, have also been used for light-mediated dimerization of proteins. Cryptochrome proteins are found in plants as well as animals (68; 69; 70; 71; 72; 73) and entrain circadian rhythms in these organisms (74; 75) by absorbing blue light from 390-480 nm in wavelength (32). Structurally, these proteins contain a U-shaped photolyase homology region (PHR) or domain linked to a C-terminal extension (Figure 1.4) (76). The center of PHR domain holds a non-covalently bound flavin-adenine dinucleotide (FAD), the primary chromophore of the system. Little is know of how light absorption in the system results in signal transduction.

Kennedy *et al.* determined that the PHR domain is the minimal region of Cryptochrome2

(CRY2) from *Arabidopsis thaliana* required for signal phototransduction (77). The protein CIB1, a basic loop-helix-loop domain, naturally interacts with the CRY2 PHR domain in a light-dependent manner (78). In order to induce photodimerization of the two proteins in mammalian cells, CRY2 was fused to a red fluorescent mCherry protein, while CIB1 was fused to a prenylated, membrane-interacting GFP protein. Dimerization, and subsequent localization of CIB1 to the plasma membrane, was observed a lightning-fast 10 s after blue light irradiation. The light induced heterodimerization system was then used to generate light induced DNA recombination in mammalian cells (77). The CRY2 protein was fused to the N terminal portion of a Cre recombinase, while CIB1 was fused to the Cre C-terminal portion and introduced into HEK293 cells. Upon irradiation with continuously pulsed blue light, the system allowed for transcription of an EGFP sequence when downstream of a stop codon but flanked by loxp sites (77).

While the cryptochrome system has proved very useful, CRY2 and CIB1 proteins are quite large, limiting their application. The proteins are challenging to express and not very stable (77). Due to this limitation, little is known about how the CRY2- CIB1 heterodimerization occurs. In fact, little is known about the structure or the mechanism of light induced signal transduction in the CRY2 protein, rendering this a poor system for extending genetically encoded protein light activation to other applications, and particularly poor for designable applications (79).

Photoactive yellow protein (PYP) has been used to photocontrol DNA binding proteins (80; 81; 82). PYP is a small photoreceptor that is part of the PAS domain family. PYP structures have been well-characterized through NMR and crystallographic techniques (83; 84; 85; 86; 87). PYP undergoes a reversible photocycle when its chromophore, a 4-hydroxycinnamic acid, absorbs blue light (33; 34). The chromophore is buried within the PAS fold and covalently linked by a thioester bond to a cysteine residue (88). Cis to trans isomerization of the double bond of the chromophore upon light absorption leads to strain in the PAS core, causing large structural changes within the protein, including exposure of the chromophore to solvent and unfolding of two helices at the N-terminus of the protein (Figure 1.5) (33; 34; 89). No PYP interacting partner or biological role has been identified.

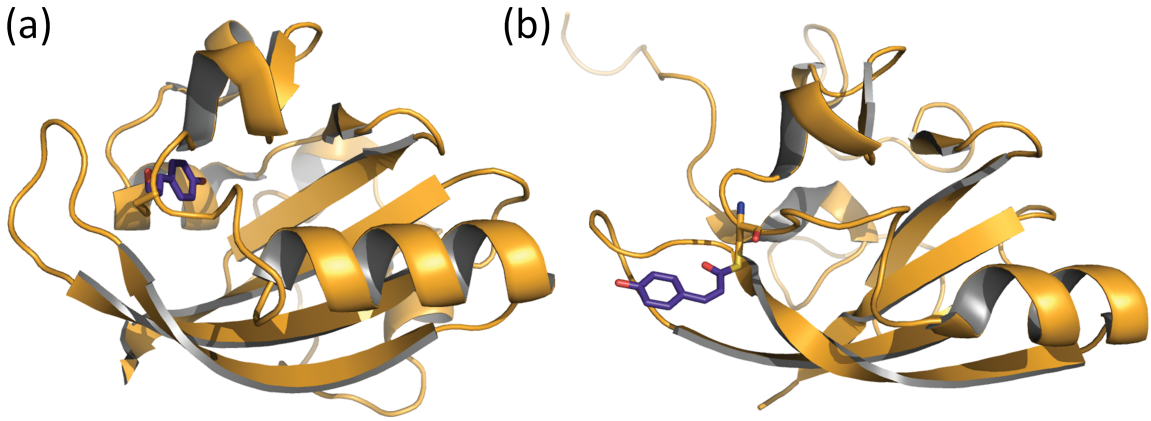

Figure 1.5: Structures of the dark state and blue light activated state of PYP. (a) Dark state crystal structure of PYP from *Halorhodospira halophila* (PDB code 2PHY) (b) Light activated NMR structure of the protein. Main chain is shown in yellow, and the 4-hydroxycinnamic acid chromophore is shown in blue (PDB code 2KX6).

Morgan *et al.* (80) fused the N-terminus of PYP from *Halorhodospira halophila* (86) to the C-terminus of GCN4-bZIP, a lecuine-zipper DNA binding protein (90; 91; 92). The GCH4-bZIP is kept in a sterically blocked conforation when PYP is in the dark state and the N-terminus helices remain folded. Upon irradiation with blue light, the N-terminal helices unfold, and the GCN4-bZIB proteins are able to dimerize. This leads to a small, 2-fold change in binding affinity of the designed protein to DNA in light versus the dark state conditions (80). The switch was then engineered to act in reverse, with 3- fold enhanced affinity in the dark versus under light conditions (81). The switch was slightly improved through design of a chimeric sequence between PYP and GCN4-bZIP, to have a 3.5-fold difference between lit and dark state binding of DNA (82).

The PYP domain hold promise as genetically encoded caging agent due to its small size and well investigated structure. Current work, though, suggests it might be difficult to achieve a photoswitch with a substantial dynamic range using the domain. Additionally, the 4-hydroxycinnamic acid chromophore must be synthesized added to protein cultures, potentially limiting in-cell uses for PYP. LOV domains, whose structures are similar to that of PYP do not share this problem, and also have a number of well-characterized structures.

LOV domains (Light Oxygen and Voltage) are found in many plant, fungal, and bacterial

proteins (79). They have been used extensively as genetically-encoded caging domains for proteins. Three families of LOV domain have been identified; those from phototropin proteins that control aspects of phototropism (93; 94); those from ZEITLUPE circadian photoreceptors (95; 96); and those from aureochrome proteins which are found in certain diatoms (97). LOV domains, like PYP, adopt a putative PAS fold (98). They may contain either a N-terminal or C-terminal helical extension. A flavin-adenine dinucleotide (FAD) or flavin mononucleotide (FMN) is located at the center of the PAS fold, and is the primary chormophore of the domain.

The ZEITLUPE LOV domain from the *A. thaliana* organism has also been used as a tool for light-induced heterodimerization. In a concept similar to that of the phytochrome and cryptochrome designed photoswitches, Yazawa *et al.* utilized two proteins that naturally interact only upon blue light activation: the LOV domain FKF1 and GIGANTEA (GI) (35; 99). This system was used to target FKF1-linked Rac1 protein the the plasma membrane through light-induced heterodimerization to CAAX-box containing, membrane-associated GI. Through recruitment to the plasma membrane, Rac1 was able to activate signal transduction and induce membrane protrusions in areas of light activation (35). The system was further tested to induce gene transcription through the Gal4 transcription factor, VP16 transactivation domain, and UAS gene promoter, a commonly used transcription activation method in fly and rodent organisms. The VP16 and Gal4 domains need to bind in order to induce UAS promoter transcrption activation (100; 101). Gal4 was fused to GI, while FKF1 was fused to VP16. Blue light irradiation induced measurable transcription of a luciferase reporter gene downstream of the UAS promoter (35).

Generalizing the FKF1-GI system for use in other applications poses certain problems. As is the case for the Cry2-CIB1 system, the proteins are large and difficult to characterize (35). Affinity of FKF1 to GI is fairly strong even in the absence of light. Mutations in FKF1 weaken the affinity of the two proteins for each other, but no quantification of the system exists (35). With no structures or other biophysical knowledge of how light activation in the system induces heterodimerization, design in this system is challenging. Lastly, the FKF1-GI heterodimerization interaction occurs very slowly, and the two proteins associated for hours, limiting spatial and temporal control of activated signaling networks (77).

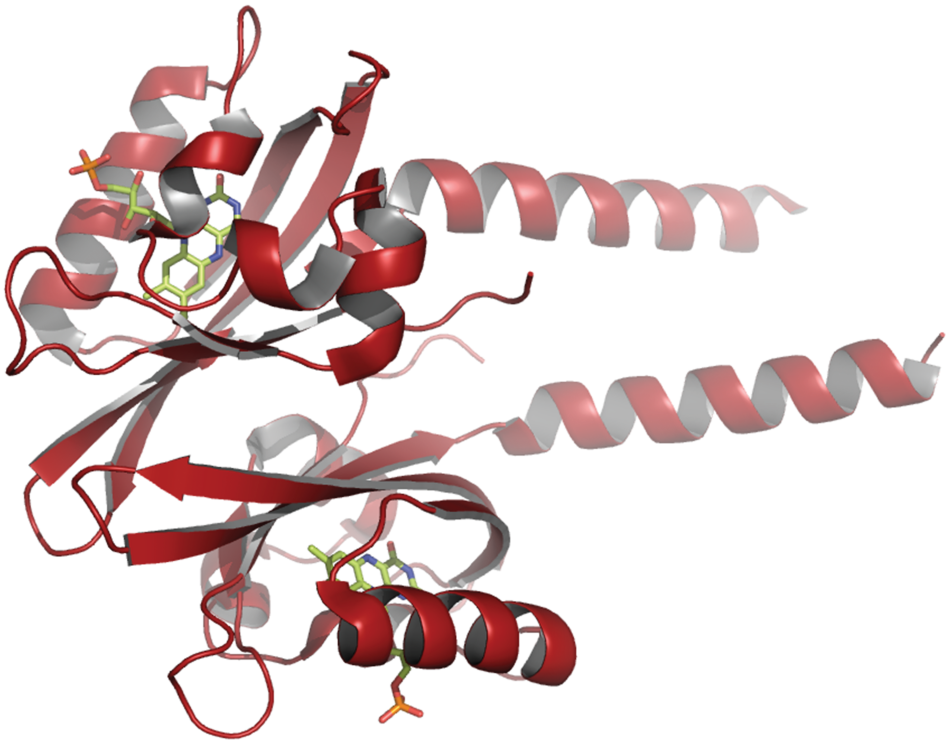

Figure 1.6: Structure of the LOV domain of YtVa. The domain from *Bacillus subtilis* is shown in red, and the FMN chromophore is shown in green (PDB code 2PR5).

Also in the family of LOV domains, the YtVa protein was used to create a light-switchable kinase (Figure 1.6) (102). The heme-binding PAS domain of the FixL protein that normally responds to oxygen was replaced with the structurally similar YtVa LOV domain of *Bacillus subtilis*. The FixL protein of *Bradyrhizobium japonicum* is involved in the organism's nitrogen fixation. FixL is initially autophosphorylated, and then transfers the phosphate moiety to a response regulator protein, FixJ, enabling activation of nitrogen metabolism genes (103; 104; 105). Möglich *et al.* were able to regulate the kinase activity of FixL through light activation in the designed fusion protein, leading to a thousand-fold decrease in kinase activation of the protein under dark conditions *in vitro*. The photoswitch also showed significant transcription *in vivo* of a reporter gene downstream of the $FixK_2$ promoter, which responds to phospho-FixJ.

As structures are available, the YtVa domain might prove useful for other applications. Not much, however is known about the domain's light activation mechanism.

The LOV2 domain is the best characterized of the LOV domains, in terms of structure,

function, and photoswitching mechanism. The LOV2 domain shows great promise as a genetically encoded caging agent due to its large dark state to lit state conformational change. The domain has been used successfully in many instances for genetically encoded photoactivation of protein-protein interactions.

1.4 Structural and photochemical properties of the LOV2 domain

The LOV2 domain plays a critical role in the ability of plants to sense light. Found in higher plants, it is part of the phototropin1 (phot1) kinase protein that allows plants to grow directionally toward sunlight (106). The LOV2 domain acts as an inhibitory domain for the kinase domain of phot1. Upon irradiation with blue light, the LOV2 domain undergoes a conformational change, releasing inhibition of the kinase domain (107).

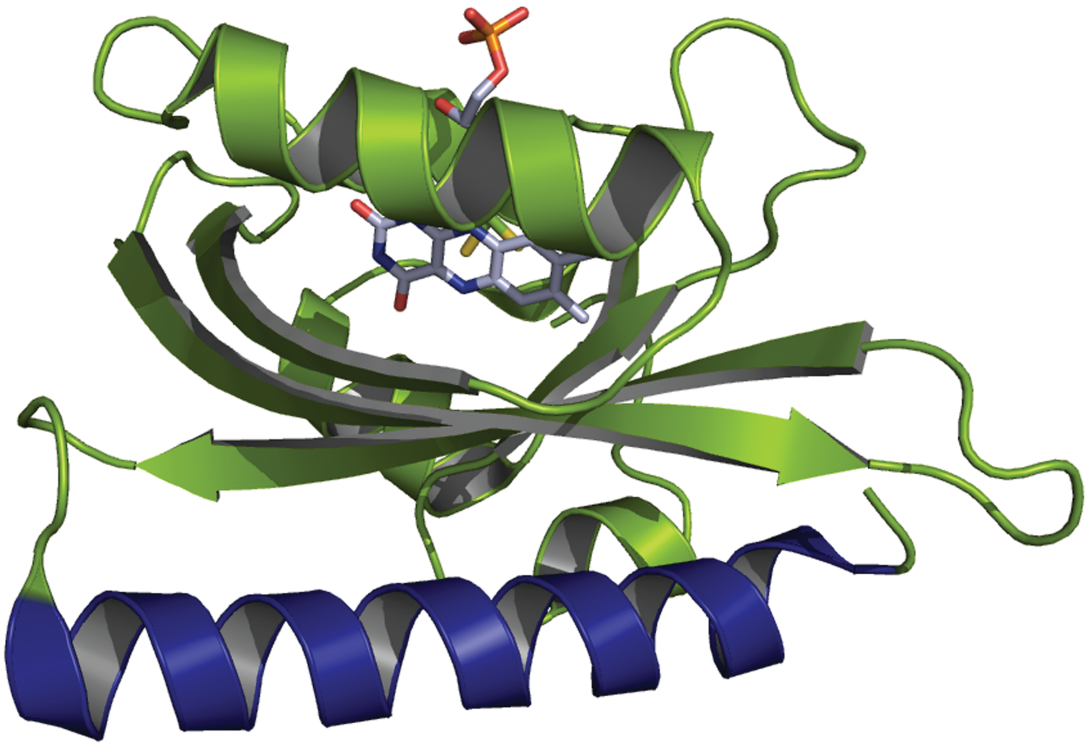

Figure 1.7: Structure of the LOV2 domain. The LOV2 domain from phototropin1 of *Avena sativa* is in the dark state, inactive conformation (PDB code 2V0U). The PAS fold is in green, Jα helix is in navy and the flavin mononucleotide (FMN) is in light blue.

LOV2 has a typical PAS fold, characterized by a central 5-stranded anti-parallel sheet

flanked by four α-helices (Figure 1.7). (98; 108; 109). The center of the protein binds a flavin mononucleotide (FMN) that is responsible for absorption of light. The FMN cofactor is kept in place through contacts with residues in virtually all domain helices and strands (110). This creates a very rigid core that is sensitive to small changes in conformation caused by light absorption. Outside of the core, a large helix, termed the Jα helix, links the LOV2 domain to the kinase domain in phot1.

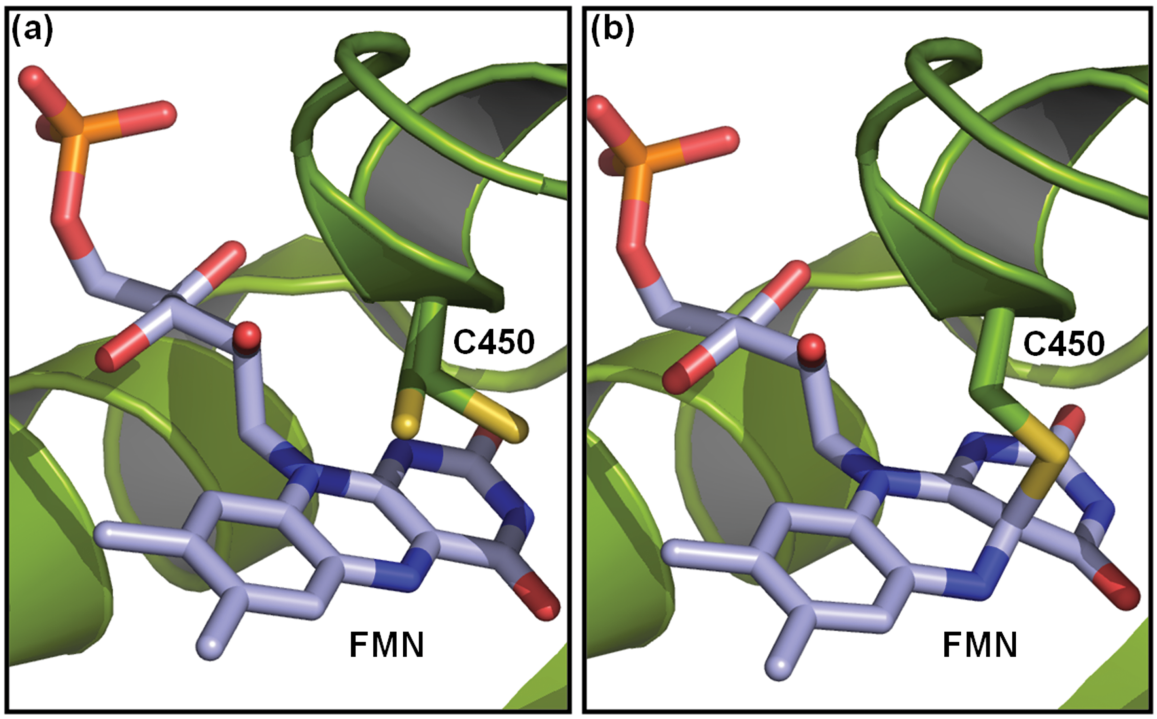

Figure 1.8: The LOV2 domain thiol adduct. A thiol bond forms between LOV2 domain residue C450 (green) and FMN (blue) upon light-induced activation. (a) The dark state structure (PDB code 2V0U) is shown on the left. (b) The lit state structure is shown on the right (PDB code 2V0W).

The FMN cofactor catalyzes a conformational change in the LOV2 domain through the absorption of light. A covalent adduct is formed between a cysteine side chain and a carbon atom of an FMN ring upon irradiation with a photon of blue light (109). In *A. sativa*, this residue is Cys450 (Figure 1.8). FMN is able to absorb light of 400 to 500 nm wavelength, having a principle peak absorption at 447 nm and a secondary peak at 478 nm (111; 112). Once formed, the thiol adduct shifts the LOV2 absorption spectrum, to a principle peak in

the ultra violet range, centered at 378 nm. Upon thiol bond formation, the LOV2 domain undergoes a significant structural change. The thiol bond within the FMN ring causes a ring pucker, leading to a 6 degree tilt of the tricyclic isoalloxazine FMN ring and slight movements of the side chains surrounding it (79). In particular, a glutamine residue (Q513) in the 5-stranded β sheet alters its hydrogen bonding partners due to this shift. Mutation of this residue to a leucine leaves the LOV2 domain in a pseudo dark state (113). Mutation of the glutamine to an asparagine, on the other hand, leaves the LOV2 domain in a pseudo lit state (113).

The LOV2 domain further experiences large conformational changes in its Jα helix region upon thiol bond formation. NMR and spectroscopic studies indicate the Jα helix unfolds with exposure to blue light (114; 115; 116), in a process that has not been fully elucidated. The helix seems to unfold in a cooperative manner (117). The change in free energy resulting from this conformational change has been calculated at 3.8 kcal mol^{-1}, whereas 15 times more energy enters the LOV2 domain when a single photon of blue light is absorbed (117). This indicates a large amount of energy is dissipated in the system, and there is enough energy introduced into the LOV2 domain for the dark state to lit state free energy conversion barrier to be increased in order to engineer a more tightly regulated switch. The thiol bond formation along with the Jα helix unfolding is thermally reversible. Various LOV2 domain orthologs have different lit state to dark state reversion times, with the LOV2 domain from *Avena sativa* having a half time of 27 seconds (111). Other LOV domains, such as that from the *A. thalia* FKF1 protein have much longer half lives (118). FAD containing LOV domains, such as the fungal protein VVD, undergo thermal reversion that have half lives in the range of hours(119).

Mutations in the LOV domain are able to shift the half life of thermal reversion. Mutations V416I L496I lengthen the thermal reversion lifetime of *Avena sativa* LOV from 81 s to 1,009 s, a 12-fold increase (119). These mutation are theorized to affect this change by decreasing the size of a solvent accessible channel in the LOV2 domain core, thus minimizing the accessibility of water molecules to the FMN pocket, which are a critical component to the formation of a reversion intermediate needed for full reversion to occur (119). Conversely, increasing the size of the solvent accessible channel is theorized to decrease the half life of thermal reversion.

The mutation I427V decreases the size of the solvent accessible area around the FMN and also decreases half life of *A. sativa* LOV2 from 27 s to 4 s (120). Imidazole base molecules have a similar effect, decreasing the half life of thermal reversion by deprotonating a nitrogen critical to the thiol reversion intermediate formation (119).

Mutations have been used to mimic the two states of the LOV2 domain: dark, inactivated and lit state, activated. Mutating the cysteine residue required for thiol bond formation to alanine or serine inhibits formation of the lit state thiol adduct (111; 112). This renders the protein unable to undergo a dark state to lit state conformational change, and hence in a permanently dark, or dark mimetic state. Mutations have been shown to destabilize the Jα helix, thus rendering it unfolded and in a permanently lit or lit mimetic state (121). The mutation I539E in the full length phot1 protein of *A. sativa* abolishes the LOV2 dark state inhibition of the phot1 kinase domain, rendering it constitutively active. Mutations I532E and A536E individually partially activate the phot1 kinase domain in the dark.

1.5 Photoswitches that have made use of the LOV2 domain

The large conformation change that occurs within the G528A LOV2 Jα helix has been harnessed to create a photoswitchable transcriptional repressor and a photoactivatable DHFR enzyme. Both of these switches use LOV2 domain from the *Avena sativa* organism.

Strickland *et. al.* linked the TrpR transcriptional repressor *E. coli* protein to LOV2, thus designing the LOV-TAP switch (122). The linkage was made by connecting the C-terminus of the Jα helix to the N-terminal helix of TrpR, creating a large, shared, end-to end helix between the two proteins. The light switching mechanism of LOV-TAP proposed that the shared helix is docked to the LOV2 domain when in the dark, leaving TrpR sterically blocked from binding DNA. Irradiation with blue light undocked the helix from the LOV2 domain, wherein it docked to TrpR and relieved the steric block between the transcriptional repressor and DNA, allowing for binding and subsequent transcription repression. The LOV-TAP switch was shown to under go only a 5-fold dynamic range, or increase in affinity from dark state to lit state binding of DNA. In order to increase the dynamic range of the LOV-TAP switch,

mutations were engineered into the LOV2 domain. These mutations, G528A and N538E, were chosen for their helical propensity and stabilizing electrostatic properties (123). The reasoning behind the introduction of these mutations was to stabilize the Jα so that it would remain docked to LOV2, and raise the energy barrier of the lit state to dark state transition. Indeed, introduction of the two mutation into LOV-TAP increased the dynamic range of the switch from 5-fold to 70-fold (123).

The LOV2 domain was also used to photoactivate the enzyme dihydrofolate reductase (DHFR). DHFR catalyzes a step in the folate metabolism pathway. It contains a nicotinamide adenine dinucleotide phosphate (NADPH) cofactor that is used to catalyze the reduction of of 7,8-dihydrofolate (H2F) to 5,6,7,8-tetrahydrofolate (124; 125). Lee *et al.* used statistical coupling analysis to pinpoint areas where the LOV2 conformational change would lead to allosteric regulation of DHFR (124). Statistical coupling analysis quantifies areas of evolutionary sequence changes within a protein family allowing for identification of correlated areas of structural significance. The entire LOV2 domain, including Jα helix, was inserted into the βF-βbG loop of DHFR, close to the active site of the enzyme. The enzymatic, hydride transfer activity of the enzyme was reduced by about one-thousand fold in the dark state due to the insertion. Low levels of enzyme activity were seen upon light activation, a two-fold increase from the dark state activity.

This dissertation was embarked upon with the goal of expanding the ability to use naturally occurring proteins as genetically encoded caging agents. We sought to design photoswitches in a manner that could be be readily generalized to cage multiple proteins in varied systems. With this goal in mind, designing protein-protein interactions that can be switched on using light was a reasonable step to generalizing such interactions, allowing for signaling network activation in this manner. Due to its well characterized photo-switching mechanism, its small, easily expressible size, and multiple available crystal structures, the LOV2 domain was chosen as the principle protein caging agent in this work. The work describes the significant progress that was achieved toward being able to photactivate two classes of proteins, and using those proteins as tools to manipulate biological systems.

In Chapter 2, the caging of small, globular GTPase proteins is discussed. The photoacti-

vatable protein PA-Rac was created by caging the globular small GTPase Rac1 through the use of the LOV2 domain. This photoswitch was able to induce membrane ruffling, protrusions, and directed cell movement upon blue light irradiation at the leading edge of mammalian cells. Its use has resulted in deeper understanding of the role of Rac1 in mammalian cell motility. The modeling and characterization of PA-Rac was critical in understanding its mechanism of photoswitching. The knowledge gained from elucidating this mechanism was used to cage the small GTPase Cdc42, thus extending the ability to cage an entire class of proteins.

Chapter 3 describes the design and charactrization of LOV-ipaA, a photoactivatable peptide. The peptide ipaA, which naturally binds vinculin, was caged by creating a large, chimeric Jα-ipaA helix. As a model case, LOV-ipaA demonstrated the ability to alter the sequence of Jα helix of LOV2 while maintaining its photoswitching capacity in order to introduce new functionality into the helix.

In Chapter 4, the use of the LOV-ipaA-vinculin photoactivatable binding interaction *in vivo* is demonstrated. LOV-ipaA light activated heterodimerization to vinculin is used as tool for light induced transcription in yeast. This tool allowed for photoactivatable transcription of proteins Ste4 and Gpa1, critical in the yeast pheromone mating pathway.

In the concluding Chapter 5, the future directions of photoactivation are discussed. In particular, novel information gained from the use of PA-Rac in fruit files, zebrafish, and single cell studies is touched upon. The evolving, novel uses of LOV-ipaA, as well as its contribution to the creation of other photoactivatable peptides are detailed.

1.6 The molecular modeling program Rosetta as a tool for designing genetically encoded, caged proteins

The Rosetta program for for macromolecular modeling, prediction and design was used both to model PA-Rac function and to design LOV-ipaA. This program in an important tool for protein structure prediction and design. Rosetta is composed of three principle components that sample changes in the conformation of a protein, analyze the energy of the sampled protein, and sort changes as favorable or unfavorable in order to yield a protein structure prediction.

In order to sample the changes in the structure of a protein, Rosetta uses a combination of

side chain as well as backbone movement (126). Backbone perturbations consist of either small changes in phi and psi angles of up to five residues such as small moves and shear moves, or insertion of small backbone fragments from experimentally determined structures. Side chains which increase in energy upon backbone perturbation are repacked, and rotamers are sampled in these spots for their ability to optimize energy. An energy minimization step then alters backbone torsion angles (phi and psi) within ten residues of the initial perturbation in order to relive any clashes (127).

Rosetta uses a scoring function to evaluate the energy of sampled protein structures. This function is made of knowledge-based as well as atom-based terms which describe the likelihood and the favorability of a structure. Van der Waals attraction and repulsion interactions are calculated using the atom-based The Lennard-Jones potential (128). Another atom based term, the Lazaridis and Karplus implicit model (129), measures solvation energies of structures. Hydrogen bond energies are calculated through a secondary structure and orientation dependent model which is obtained from analyzing hydrogen bonds in experimentally determined crystal structures (130; 131). One energy term derives favorable Ramachadran torsion angles for amino acids based in part on probabilities of seeing those angles in experimentally determined structures (132). Similarly, amino acid side chain energies are based on the probability of finding a particular conformation in experimentally determined structures (133). Pairwise interactions, such as electrostatics and disulfides, are calculated using a knowledge-based term (128). A reference term describing the energy of the unfolded state of an amino acid is also included (128).

The scores generated by Rosetta's potential energy function and its terms are evaluated according to the Metropolis Monte Carlo criterion (134). Using this criterion, a change such as particular shear or small move which lowers the energy of the protein is accepted while a move that increases the protein's free enery is rejected. Once in a while, as determined by a random number generator, an unfavorable move will be accepted, so that the protein conformation can escape local energy minima.

In order to model PA-Rac (Chapter 2), both the protein backbone as well as protein sidechains were optimized. A protocol that combined both of these elements, domain assembly,

was utilized. The protein was initially modeled in low-resolution, centroid form, and small moves of the backbone phi and psi angles connecting LOV2 to Rac1 were imposed. In the next round of design, when modeled to full-atom resolution, flexible backbone small moves on linking amino acids were iterated with side chain optimizations on residues on and around the linker.

For the design of LOV-ipaA (Chapter 3), only fixed backbone operations were conducted. Due to this, only optimization of residue side chains was used, and at atomic level resolution. Sampling for Rosetta's side chain optimization with design protocol involves sampling side chains of all amino acids except for cysteine at the position to be designed. Side chain conformations are chosen from a backbone-dependent rotamer library, minus those rotamers rarely seen in nature (133; 128). In this way, Rosetta enabled design of photoswitches.

REFERENCES

1. Schreiber, S. (2003) The small-molecule approach to biology. Chem. Eng. News **81**, 51–61

2. Milligan, G. (2003) Constitutive activity and inverse agonists of G protein-coupled receptors: a current perspective. Molecular pharmacology **64**, 1271

3. Rao, K. (2001) MAP kinase activation in macrophages. Journal of Leukocyte Biology **69**, 3

4. Sussman, M., Welch, S., Walker, A., Klevitsky, R., Hewett, T., Price, R., Schaefer, E., and Yager, K. (2000) Altered focal adhesion regulation correlates with cardiomyopathy in mice expressing constitutively active rac1. Journal of Clinical Investigation **105**, 875–896

5. Xu, W., Baribault, H., and Adamson, E. (1998) Vinculin knockout results in heart and brain defects during embryonic development. Development **125**, 327

6. Lewandoski, M. (2001) Conditional control of gene expression in the mouse. Nature Reviews Genetics **2**, 743–755

7. Buskirk, A. and Liu, D. (2005) Creating small-molecule-dependent switches to modulate biological functions. Chemistry & biology **12**, 151–161

8. Young, D. and Deiters, A. (2007) Photochemical control of biological processes. Organic & Biomolecular Chemistry **5**, 999–1005

9. Lawrence, D. (2005) The preparation and in vivo applications of caged peptides and proteins. Current Oopinion in Chemical Biology **9**, 570–575

10. Walker, J., Gilbert, S., Drummond, R., Yamada, M., Sreekumar, R., Carraway, R., Ikebe, M., and Fay, F. (1998) Signaling pathways underlying eosinophil cell motility revealed by using caged peptides. Proceedings of the National Academy of Sciences **95**, 1568

11. Nguyen, A., Rothman, D., Stehn, J., Imperiali, B., and Yaffe, M. (2004) Caged phos-

phopeptides reveal a temporal role for 14-3-3 in G1 arrest and S-phase checkpoint function. Nature Biotechnology **22**, 993–1000

12. Gautier, A., Nguyen, D., Lusic, H., An, W., Deiters, A., and Chin, J. (2010) Genetically encoded photocontrol of protein localization in mammalian cells. Journal of the American Chemical Society **132**, 4086–4088

13. Hahn, M. and Muir, T. (2004) Photocontrol of Smad2, a multiphosphorylated cell-signaling protein, through caging of activating phosphoserines. Angewandte Chemie **116**, 5924–5927

14. Mendel, D., Ellman, J., and Schultz, P. (1991) Construction of a light-activated protein by unnatural amino acid mutagenesis. Journal of the American Chemical Society **113**, 2758–2760

15. Philipson, K., Gallivan, J., Brandt, G., Dougherty, D., and Lester, H. (2001) Incorporation of caged cysteine and caged tyrosine into a transmembrane segment of the nicotinic ACh receptor. American Journal of Physiology-Cell Physiology **281**, C195

16. Beene, D., Dougherty, D., and Lester, H. (2003) Unnatural amino acid mutagenesis in mapping ion channel function. Current Opinion in Neurobiology **13**, 264–270

17. Cropp, T. and Schultz, P. (2004) An expanding genetic code. TRENDS in Genetics **20**, 625–630

18. Deiters, A., Groff, D., Ryu, Y., Xie, J., and Schultz, P. (2006) A genetically encoded photocaged tyrosine. Angewandte Chemie **118**, 2794–2797

19. Wu, N., Deiters, A., Cropp, T., King, D., and Schultz, P. (2004) A genetically encoded photocaged amino acid. Journal of the American Chemical Society **126**, 14306–14307

20. Lemke, E., Summerer, D., Geierstanger, B., Brittain, S., and Schultz, P. (2007) Control of protein phosphorylation with a genetically encoded photocaged amino acid. Nature Chemical Biology **3**, 769–772

21. Ghosh, M., Ichetovkin, I., Song, X., Condeelis, J., and Lawrence, D. (2002) A new strategy for caging proteins regulated by kinases. Journal of the American Chemical Society **124**, 2440–2441

22. Ghosh, M., Song, X., Mouneimne, G., Sidani, M., Lawrence, D., and Condeelis, J.

(2004) Cofilin promotes actin polymerization and defines the direction of cell motility. Science **304**, 743

23. Chou, C., Young, D., and Deiters, A. (2009) A light-activated DNA polymerase. Angewandte Chemie **121**, 6064–6067

24. Chou, C., Young, D., and Deiters, A. (2010) Photocaged T7 RNA polymerase for the light activation of transcription and gene function in pro-and eukaryotic cells. ChemBioChem **11**, 972–977

25. Chou, C. and Deiters, A. (2011) Light-activated gene editing with a photocaged zinc-finger nuclease. Angewandte Chemie

26. Young, D., Lively, M., and Deiters, A. (2010) Activation and deactivation of DNAzyme and antisense function with light for the photochemical regulation of gene expression in mammalian cells. Journal of the American Chemical Society **132**, 6183–6193

27. Karginov, A., Zou, Y., Shirvanyants, D., Kota, P., Dokholyan, N., Young, D., Hahn, K., and Deiters, A. (2011) Light regulation of protein dimerization and kinase activity in living cells using photocaged rapamycin and engineered fkbp. Journal of the American Chemical Society

28. Gautier, A., Deiters, A., and Chin, J. (2011) Light-activated kinases enable temporal dissection of signaling networks in living cells. Journal of the American Chemical Society

29. Shimizu-Sato, S., Huq, E., Tepperman, J., and Quail, P. (2002) A light-switchable gene promoter system. Nature biotechnology **20**, 1041–1044

30. Zhang, F., Wang, L., Brauner, M., Liewald, J., Kay, K., Watzke, N., Wood, P., Bamberg, E., Nagel, G., Gottschalk, A., et al. (2007) Multimodal fast optical interrogation of neural circuitry. Nature **446**, 633–639

31. Zhang, F., Wang, L., Boyden, E., and Deisseroth, K. (2006) Channelrhodopsin-2 and optical control of excitable cells. Nature methods **3**, 785

32. Ahmad, M., Grancher, N., Heil, M., Black, R., Giovani, B., Galland, P., and Lardemer, D. (2002) Action spectrum for cryptochrome-dependent hypocotyl growth inhibition in Arabidopsis. Plant physiology **129**, 774

33. Imamoto, Y. and Kataoka, M. (2007) Structure and photoreaction of photoactive yellow protein, a structural prototype of the PAS domain superfamily. Photochemistry and photobiology **83**, 40–49

34. Kumauchi, M., Hara, M., Stalcup, P., Xie, A., and Hoff, W. (2008) Identification of six new photoactive yellow proteinsdiversity and structure–function relationships in a bacterial blue light photoreceptor. Photochemistry and photobiology **84**, 956–969

35. Yazawa, M., Sadaghiani, A., Hsueh, B., and Dolmetsch, R. (2009) Induction of protein-protein interactions in live cells using light. Nature biotechnology **27**, 941–945

36. Bogomolni, R. and Spudich, J. (1982) Identification of a third rhodopsin-like pigment in phototactic Halobacterium halobium. Proceedings of the National Academy of Sciences **79**, 6250

37. Nagel, G., Szellas, T., Huhn, W., Kateriya, S., Adeishvili, N., Berthold, P., Ollig, D., Hegemann, P., and Bamberg, E. (2003) Channelrhodopsin-2, a directly light-gated cation-selective membrane channel. Proceedings of the National Academy of Sciences **100**, 13940

38. Holland, E., Braun, F., Nonnengässer, C., Harz, H., and Hegemann, P. (1996) The nature of rhodopsin-triggered photocurrents in Chlamydomonas. I. kinetics and influence of divalent ions. Biophysical journal **70**, 924–931

39. Luecke, H., Schobert, B., Richter, H., Cartailler, J., and Lanyi, J. (1999) Structural changes in bacteriorhodopsin during ion transport at 2 angstrom resolution. Science **286**, 255

40. Douglass, A., Kraves, S., Deisseroth, K., Schier, A., and Engert, F. (2008) Escape behavior elicited by single, channelrhodopsin-2-evoked spikes in zebrafish somatosensory neurons. Current Biology **18**, 1133–1137

41. Alilain, W., Li, X., Horn, K., Dhingra, R., Dick, T., Herlitze, S., and Silver, J. (2008) Light-induced rescue of breathing after spinal cord injury. The Journal of Neuroscience **28**, 11862

42. Arenkiel, B. and Peca, J. (2009) Using light to reinstate respiratory plasticity. Journal of neurophysiology **101**, 1695

43. Han, X. and Boyden, E. (2007) Multiple-color optical activation, silencing, and desyn-

chronization of neural activity, with single-spike temporal resolution. PLoS One **2**, e299

44. Arrenberg, A., Del Bene, F., and Baier, H. (2009) Optical control of zebrafish behavior with halorhodopsin. Proceedings of the National Academy of Sciences **106**, 17968

45. Arrenberg, A., Stainier, D., Baier, H., and Huisken, J. (2010) Optogenetic control of cardiac function. Science **330**, 971

46. Chen, M., Chory, J., and Fankhauser, C. (2004) Light signal transduction in higher plants. Annual Review of Genetics **38**, 87

47. Davis, S., Vener, A., and Vierstra, R. (1999) Bacteriophytochromes: Phytochrome-like photoreceptors from nonphotosynthetic eubacteria. Science **286**, 2517

48. Hughes, J. and Lamparter, T. (1999) Prokaryotes and phytochrome. the connection to chromophores and signaling. Plant physiology **121**, 1059

49. Rockwell, N. and Lagarias, J. (2010) A brief history of phytochromes. ChemPhysChem **11**, 1172–1180

50. Rockwell, N., Su, Y., and Lagarias, J. (2006) Phytochrome sructure and signaling mechanisms. Annual review of plant biology **57**, 837

51. Essen, L., Mailliet, J., and Hughes, J. (2008) The structure of a complete phytochrome sensory module in the Pr ground state. Proceedings of the National Academy of Sciences **105**, 14709

52. Wagner, J., Brunzelle, J., Forest, K., and Vierstra, R. (2005) A light-sensing knot revealed by the structure of the chromophore-binding domain of phytochrome. Nature **438**, 325–331

53. Yang, X., Kuk, J., and Moffat, K. (2008) Crystal structure of Pseudomonas aeruginosa bacteriophytochrome: Photoconversion and signal transduction. Proceedings of the National Academy of Sciences **105**, 14715

54. Ni, M., Tepperman, J., and Quail, P. (1999) Binding of phytochrome b to its nuclear signalling partner pif3 is reversibly induced by light. Nature **400**, 781–784

55. Tyszkiewicz, A. and Muir, T. (2008) Activation of protein splicing with light in yeast. Nature Methods **5**, 303–305

56. Mootz, H. and Muir, T. (2002) Protein splicing triggered by a small molecule. Journal of the American Chemical Society **124**, 9044–9045

57. Leung, D., Otomo, C., Chory, J., and Rosen, M. (2008) Genetically encoded photoswitching of actin assembly through the Cdc42-WASP-Arp2/3 complex pathway. Proceedings of the National Academy of Sciences **105**, 12797

58. Levskaya, A., Weiner, O., Lim, W., and Voigt, C. (2009) Spatiotemporal control of cell signalling using a light-switchable protein interaction. Nature **461**, 997–1001

59. Higgs, H. and Pollard, T. (2001) Regulation of actin filament network formation through ARP2/3 complex: Activation by a diverse array of proteins 1. Annual review of biochemistry **70**, 649–676

60. Ridley, A. (2006) Rho gtpases and actin dynamics in membrane protrusions and vesicle trafficking. Trends in cell biology **16**, 522–529

61. Kim, A., Kakalis, L., Abdul-Manan, N., Liu, G., and Rosen, M. (2000) Autoinhibition and activation mechanisms of the wiskott–aldrich syndrome protein. Nature **404**, 151–158

62. Rohatgi, R., Ma, L., Miki, H., Lopez, M., Kirchhausen, T., Takenawa, T., and Kirschner, M. (1999) The interaction between N-WASP and the Arp2/3 complex links Cdc42-dependent signals to actin assembly. Cell **97**, 221–231

63. Inoue, T., Heo, W., Grimley, J., Wandless, T., and Meyer, T. (2005) An inducible translocation strategy to rapidly activate and inhibit small gtpase signaling pathways. Nat. Methods **2**, 415–418

64. Castellano, F., Montcourrier, P., Guillemot, J., Gouin, E., Machesky, L., Cossart, P., and Chavrier, P. (1999) Inducible recruitment of Cdc42 or WASP to a cell-surface receptor triggers actin polymerization and filopodium formation. Current biology **9**, 351–361

65. Yeh, K., Wu, S., Murphy, J., and Lagarias, J. (1997) A cyanobacterial phytochrome two-component light sensory system. Science **277**, 1505

66. Levskaya, A., Chevalier, A., Tabor, J., Simpson, Z., Lavery, L., Levy, M., Davidson, E., Scouras, A., Ellington, A., Marcotte, E., et al. (2005) Synthetic biology: engineering Escherichia coli to see light. Nature **438**, 441–442

67. Utsumi, R., Brissette, R., Rampersaud, A., Forst, S., Oosawa, K., and Inouye, M. (1989) Activation of bacterial porin gene expression by a chimeric signal transducer in response to aspartate. Science **245**, 1246

68. Ahmad, M. and Cashmore, A. (1993) HY4 gene of A. thaliana encodes a protein with characteristics of a blue-light photoreceptor. Nature **366**, 162

69. Brudler, R., Hitomi, K., Daiyasu, H., Toh, H., Kucho, K., Ishiura, M., Kanehisa, M., Roberts, V., Todo, T., Tainer, J., et al. (2003) Identification of a new cryptochrome class: Structure, function, and evolution. Molecular cell **11**, 59–67

70. Gauger, M. and Sancar, A. (2005) Cryptochrome, circadian cycle, cell cycle checkpoints, and cancer. Cancer research **65**, 6828

71. Lin, C. and Shalitin, D. (2003) Cryptochrome structure and signal transduction. Annual Review of Plant Biology **54**, 469–496

72. Lin, C. and Todo, T. (2005) The cryptochromes. Genome Biology **6**, 220

73. Müller, M. and Carell, T. (2009) Structural biology of DNA photolyases and cryptochromes. Current opinion in structural biology **19**, 277–285

74. Li, Q. and Yang, H. (2007) Cryptochrome signaling in plants. Photochemistry and photobiology **83**, 94–101

75. Shalitin, D., Yang, H., Mockler, T., Maymon, M., Guo, H., Whitelam, G., and Lin, C. (1966) Regulation of Arabidopsis cryptochrome 2 by blue-light-dependent phosphorylation. J. Med **41**, 815–830

76. Brautigam, C., Smith, B., Ma, Z., Palnitkar, M., Tomchick, D., Machius, M., and Deisenhofer, J. (2004) Structure of the photolyase-like domain of cryptochrome 1 from Arabidopsis thaliana. Proceedings of the National Academy of Sciences of the United States of America **101**, 12142

77. Kennedy, M., Hughes, R., Peteya, L., Schwartz, J., Ehlers, M., and Tucker, C. (2010) Rapid blue-light-mediated induction of protein interactions in living cells. Nature

Methods

78. Liu, H., Yu, X., Li, K., Klejnot, J., Yang, H., Lisiero, D., and Lin, C. (2008) Photoexcited CRY2 interacts with CIB1 to regulate transcription and floral initiation in arabidopsis. Science **322**, 1535

79. Moglich, A., Yang, X., Ayers, R., and Moffat, K. (2010) Structure and function of plant photoreceptors. Annual Review of Plant Biology **61**, 21–47

80. Morgan, S., Al-Abdul-Wahid, S., and Woolley, G. (2010) Structure-based design of a photocontrolled DNA binding protein. Journal of Molecular Biology **399**, 94–112

81. Morgan, S. and Woolley, G. (2010) A photoswitchable DNA-binding protein based on a truncated GCN4-photoactive yellow protein chimera. Photochem. Photobiol. Sci. **9**, 1320–1326

82. Fan, H., Morgan, S., Brechun, K., Chen, Y., Jaikaran, A., and Woolley, G. (2011) Improving a designed photo-controlled DNA-binding protein. Biochemistry

83. Borgstahl, G., Williams, D., and Getzoff, E. (1995) 1.4. ANG. structure of photoactive yellow protein, a cytosolic photoreceptor: Unusual fold, active site, and chromophore. Biochemistry **34**, 6278–6287

84. Getzoff, E., Gutwin, K., and Genick, U. (2003) Anticipatory active-site motions and chromophore distortion prime photoreceptor PYP for light activation. Nature Structural & Molecular Biology **10**, 663–668

85. Kamikubo, H., Shimizu, N., Harigai, M., Yamazaki, Y., Imamoto, Y., and Kataoka, M. (2007) Characterization of the solution structure of the M intermediate of photoactive yellow protein using high-angle solution x-ray scattering. Biophysical journal **92**, 3633–3642

86. Baca, M., Borgstahl, G., Boissinot, M., Burke, P., Williams, D., Slater, K., and Getzoff, E. (1994) Complete chemical structure of photoactive yellow protein: novel thioester-linked 4-hydroxycinnamyl chromophore and photocycle chemistry. Biochemistry **33**, 14369–14377

87. Ramachandran, P., Lovett, J., Carl, P., Cammarata, M., Lee, J., Jung, Y., Ihee, H., Timmel, C., and van Thor, J. (2011) The short-lived signaling state of the photoactive yellow protein photoreceptor revealed by combined structural probes.

Journal of the American Chemical Society

88. Anderson, S., Crosson, S., and Moffat, K. (2004) Short hydrogen bonds in photoactive yellow protein. Acta Crystallographica Section D: Biological Crystallography **60**, 1008–1016

89. Bernard, C., Houben, K., Derix, N., Marks, D., van der Horst, M., Hellingwerf, K., Boelens, R., Kaptein, R., and van Nuland, N. (2005) The solution structure of a transient photoreceptor intermediate: Δ25 photoactive yellow protein. Structure **13**, 953–962

90. Xia, Y. and Karin, M. (2004) The control of cell motility and epithelial morphogenesis by Jun kinases. Trends in cell biology **14**, 94–101

91. van Dam, H. and Castellazzi, M. (2001) Distinct roles of jun: Fos and jun: ATF dimers in oncogenesis. Oncogene **20**, 2453–2464

92. Josselyn, S. and Nguyen, P. (2005) CREB, synapses and memory disorders: past progress and future challenges. Current drug targets. CNS and neurological disorders **4**, 481–497

93. Christie, J. (2007) Phototropin blue-light receptors. Annu. Rev. Plant Biol. **58**, 21–45

94. Christie, J., Reymond, P., Powell, G., Bernasconi, P., Raibekas, A., Liscum, E., and Briggs, W. (1998) Arabidopsis NPH1: a flavoprotein with the properties of a photoreceptor for phototropism. Science **282**, 1698

95. Demarsy, E. and Fankhauser, C. (2009) Higher plants use LOV to perceive blue light. Current opinion in plant biology **12**, 69–74

96. Nelson, D., Lasswell, J., Rogg, L., Cohen, M., and Bartel, B. (2000) FKF1, a clock-controlled gene that regulates the transition to flowering in arabidopsis. Cell **101**, 331–340

97. Takahashi, F., Yamagata, D., Ishikawa, M., Fukamatsu, Y., Ogura, Y., Kasahara, M., Kiyosue, T., Kikuyama, M., Wada, M., and Kataoka, H. (2007) AUREOCHROME, a photoreceptor required for photomorphogenesis in stramenopiles. Proceedings of the National Academy of Sciences **104**, 19625

98. Hefti, M., Françoijs, K., De Vries, S., Dixon, R., and Vervoort, J. (2004) The PAS fold.

European Journal of Biochemistry **271**, 1198–1208

99. Sawa, M., Nusinow, D., Kay, S., and Imaizumi, T. (2007) FKF1 and GIGANTEA complex formation is required for day-length measurement in arabidopsis. Science **318**, 261

100. Giniger, E., Varnum, S., and Ptashne, M. (1985) Specific DNA binding of GAL4, a positive regulatory protein of yeast. Cell **40**, 767–774

101. Sadowski, I., Ma, J., Triezenberg, S., and Ptashne, M. (1988) GAL4-VP16 is an unusually potent transcriptional activator. Nature **335**, 563–564

102. Möglich, A., Ayers, R., and Moffat, K. (2009) Design and signaling mechanism of light-regulated histidine kinases. Journal of molecular biology **385**, 1433–1444

103. Gilles-Gonzalez, M., Ditta, G., and Helinski, D. (1991) A haemoprotein with kinase activity encoded by the oxygen sensor of Rhizobium meliloti

104. Gilles-Gonzalez, M., Gonzalez, G., Perutz, M., Kiger, L., Marden, M., and Poyart, C. (1994) Heme-based sensors, exemplified by the kinase fixl, are a new class of heme protein with distinctive ligand binding and autoxidation. Biochemistry **33**, 8067–8073

105. Russo, F. and Silhavy, T. (1993) The essential tension: opposed reactions in bacterial two-component regulatory systems. Trends in Microbiology **1**, 306–310

106. Huala, E., Oeller, P., Liscum, E., Han, I., Larsen, E., and Briggs, W. (1997) Arabidopsis NPH1: a protein kinase with a putative redox-sensing domain. Science **278**, 2120

107. Briggs, W. and Christie, J. (2002) Phototropins 1 and 2: versatile plant blue-light receptors. Trends in plant science **7**, 204–210

108. Crosson, S. and Moffat, K. (2001) Structure of a flavin-binding plant photoreceptor domain: insights into light-mediated signal transduction. Proceedings of the National Academy of Sciences **98**, 2995

109. Halavaty, A. and Moffat, K. (2007) N-and C-terminal flanking regions modulate light-induced signal transduction in the LOV2 domain of the blue light sensor phototropin 1 from Avena sativa. Biochemistry **46**, 14001–14009

110. Losi, A. (2007) Flavin-based blue-light photosensors: A photobiophysics update. Photochemistry and photobiology **83**, 1283–1300

111. Salomon, M., Christie, J., Knieb, E., Lempert, U., and Briggs, W. (2000) Photochemical and mutational analysis of the FMN-binding domains of the plant blue light receptor, phototropin. Biochemistry **39**, 9401–9410

112. Swartz, T., Corchnoy, S., Christie, J., Lewis, J., Szundi, I., Briggs, W., and Bogomolni, R. (2001) The photocycle of a flavin-binding domain of the blue light photoreceptor phototropin. Journal of Biological Chemistry **276**, 36493

113. Nash, A., Ko, W., Harper, S., and Gardner, K. (2008) A conserved glutamine plays a central role in lov domain signal transmission and its duration. Biochemistry **47**, 13842–13849

114. Harper, S., Neil, L., and Gardner, K. (2003) Structural basis of a phototropin light switch. Science **301**, 1541

115. Harper, S., Neil, L., Day, I., Hore, P., and Gardner, K. (2004) Conformational changes in a photosensory LOV domain monitored by time-resolved NMR spectroscopy. Journal of the American Chemical Society **126**, 3390–3391

116. Iwata, T., Yamamoto, A., Tokutomi, S., and Kandori, H. (2007) Hydration and temperature similarly affect light-induced protein structural changes in the chromophoric domain of phototropin. Biochemistry **46**, 7016–7021

117. Yao, X., Rosen, M., and Gardner, K. (2008) Estimation of the available free energy in a LOV2-Jα photoswitch. Nature Chemical Biology **4**, 491–497

118. Imaizumi, T., Tran, H., Swartz, T., Briggs, W., and Kay, S. (2003) Fkf1 is essential for photoperiodic-specific light signalling in Arabidopsis. Nature **426**, 302–306

119. Zoltowski, B., Vaccaro, B., and Crane, B. (2009) Mechanism-based tuning of a LOV domain photoreceptor. Nature Chemical Biology **5**, 827–834

120. Christie, J., Corchnoy, S., Swartz, T., Hokenson, M., Han, I., Briggs, W., and Bogomolni, R. (2007) Steric interactions stabilize the signaling state of the LOV2 domain of phototropin 1. Biochemistry **46**, 9310–9319

121. Harper, S., Christie, J., and Gardner, K. (2004) Disruption of the LOV-Jα helix inter-

action activates phototropin kinase activity. Biochemistry **43**, 16184–16192

122. Strickland, D., Moffat, K., and Sosnick, T. (2008) Light-activated DNA binding in a designed allosteric protein. Proceedings of the National Academy of Sciences **105**, 10709

123. Strickland, D., Yao, X., Gawlak, G., Rosen, M., Gardner, K., and Sosnick, T. (2010) Rationally improving LOV domain-based photoswitches. Nature methods **7**, 623–626

124. Lee, J., Natarajan, M., Nashine, V., Socolich, M., Vo, T., Russ, W., Benkovic, S., and Ranganathan, R. (2008) Surface sites for engineering allosteric control in proteins. Science **322**, 438

125. Rajagopalan, P., Lutz, S., and Benkovic, S. (2002) Coupling interactions of distal residues enhance dihydrofolate reductase catalysis: mutational effects on hydride transfer rates. Biochemistry **41**, 12618–12628

126. Rohl, C., Strauss, C., Misura, K., and Baker, D. (2004) Protein structure prediction using rosetta. Methods in enzymology **383**, 66–93

127. Butterfoss, G. and Kuhlman, B. (2006) Computer-based design of novel protein structures. Annu. Rev. Biophys. Biomol. Struct. **35**, 49–65

128. Kuhlman, B. and Baker, D. (2000) Native protein sequences are close to optimal for their structures. Proceedings of the National Academy of Sciences **97**, 10383

129. Lazaridis, T. and Karplus, M. (1999) Effective energy function for proteins in solution. Proteins: Structure, Function, and Bioinformatics **35**, 133–152

130. Kortemme, T., Morozov, A., and Baker, D. (2003) An orientation-dependent hydrogen bonding potential improves prediction of specificity and structure for proteins and protein-protein complexes. Journal of molecular biology **326**, 1239–1259

131. Wedemeyer, W. and Baker, D. (2003) Efficient minimization of angle-dependent potentials for polypeptides in internal coordinates. Proteins: Structure, Function, and Bioinformatics **53**, 262–272

132. Gunn, J. (1997) Sampling protein conformations using segment libraries and a genetic algorithm. The Journal of chemical physics **106**, 4270

133. Dunbrack Jr, R. and Cohen, F. (1997) Bayesian statistical analysis of protein side-chain rotamer preferences. Protein Science **6**, 1661–1681

134. Meteopolis, N. and Ulam, S. (1949) The monte carlo method. Journal of the American Statistical Association **44**, 335–341

CHAPTER 2

A GENETICALLY ENCODED PHOTOACTIVATABLE RAC CONTROLS THE MOTILITY OF LIVING CELLS

2.1 Summary

The precise spatio-temporal dynamics of protein activity are often critical in determining cell behaviour, yet for most proteins they remain poorly understood; it remains difficult to manipulate protein activity at precise times and places within living cells. Protein activity has been controlled by light, through protein derivatization with photocleavable moieties (1) or using photoreactive small-molecule ligands (2). However, this requires use of toxic ultraviolet wavelengths, activation is irreversible, and/or cell loading is accomplished via disruption of the cell membrane (for example, through microinjection). Here we have developed a new approach to produce genetically encoded photoactivatable derivatives of Rac1, a key GTPase regulating actin cytoskeletal dynamics in metazoan cells (3; 4). Rac1 mutants were fused to the photoreactive LOV (light oxygen voltage) domain from phototropin1 (5; 6), sterically blocking Rac1 interactions with effector PAK1 until irradiation unwound a helix linking LOV to Rac1. Rac1 interactions with PAK1 under dark and lit state conditions were quantified using Isothermal Titration Calorimetry. Photoactivatable Rac1 (PA-Rac1) could be reversibly and repeatedly activated using 458- or 473-nm light to generate precisely localized cell protrusions and ruffling. We used molecular modeling to probe the mechanism of Rac caging in the dark. We show that the interface formed between loops of the LOV2 domain and the effector binding region of Rac1 block interaction between Rac1 and PAK1 in the dark, thus leading to Rac1 caging. Introduction of a similar interface between LOV2 and Cdc42 led to the dark state caging of the Cdc42 small GTPase.

2.2 Introduction

NMR studies have revealed the mechanism of a protein light switch in *Avena sativa* phototropin1 (6; 7): a flavin-binding LOV2 domain interacts with a carboxy-terminal helical extension (Jα) in the dark. Photon absorption leads to formation of a covalent bond between Cys 450 and the flavin chromophore, causing conformational changes that result in dissociation and unwinding of the Jα helix.

We fused the complete LOV2-Jα sequence (404-547) to the amino terminus of a constitutively active Rac1, anticipating that the LOV domain in its closed conformation would block the binding of effectors to Rac1, and that light-induced unwinding of the Jα helix would release steric inhibition, leading to Rac1 activation. Sampling of different junctional sequences in pull-down assays revealed that connecting Leu 546 of LOV2-Jα to Ile 4 of Rac1 led to substantial reduction in Rac1 binding to its effector PAK. To ensure that the photoactivatable Rac1 would induce no dominant-negative effects and that its activity would not be subject to upstream regulation, mutations were introduced to abolish GTP hydrolysis (Q61L) and diminish interactions with nucleotide exchange factors, guanine nucleotide dissociation inhibitors and GTPase activating proteins (E91H and N92H). This resulted in the photoactivatable analogue of Rac1 (PA-Rac1) used in the following studies. Pull-down assays showed that PA-Rac1 has greatly reduced affinity for its effector protein PAK in the dark, as does a PA-Rac1 construct containing a light-insensitive LOV2 mutation (C450A) (8). Effector binding was restored in a PA-Rac1 construct containing a LOV2 mutant (I539E) (9) which mimics the unfolded lit state.

Activation of PA-Rac1 was examined in HeLa cells expressing a YFP fusion of PA-Rac1 to gauge expression level. The cells remained quiescent when illuminated with wavelengths longer than flavin absorbance but within seconds after switching to 458nm, lamellipodial protrusions and membrane ruffles appeared around the cell edges. To show that this effect was due to PA-Rac1, kymograms were used to quantify maximum protrusion length; irradiation of PA-Rac1 elicited protrusions that were four times as long as those seen in cells expressing either LOV domain alone or the light-insensitive PA-Rac1(C450A) mutant. An important advantage of

PA-Rac1 is its ability to control precisely the subcellular location of Rac activation. We first examined this in mouse embryo fibroblasts (MEFs) stably expressing PA-Rac1, and cultured without serum to minimize cell activity before irradiation. Irradiation of 20-mm spots at the cell edge generated large protrusions clearly localized next to the point of irradiation. Repeated irradiation led first to ruffles and then to protrusion. Movement of a laser spot to different positions led to cessation of ruffling or protrusion at the initial irradiation position and new activities appearing where the laser spot was brought to rest, demonstrating reversible activation. In MEF cells, more prone to movement than HeLa cells, complex shape changes were produced by painting the cell with the laser spot).

We sought to understand how PA-Rac1 drives such a large phenotypic change in live cells. In order to do so, we studied how Rac1 is maintained in a caged conformation in the dark state, thus inhibiting binding to its effector PAK1; and at what affinity PAK1 binds PA-Rac1 in both the lit and dark states. PAK1 drives actin polymerization and formation of cell protrusions at the leading edge of motility (10; 11). We modeled the construct of PA-Rac1 that inhibited binding of Rac1 to PAK1 in the dark (546-4) in pull-down assays, along with the constructs of PA-Rac1 connecting Glu 545 of LOV2-Jα to Ile 4 of Rac1 (545-4) that was too short to inhibit binding of Rac1 to PAK1 in the dark, and the constructs of PA-Rac1 connecting Pro 547 of LOV2-Jα to Ile 4 of Rac1 (547-4) that was too long to inhibit binding of Rac1 to PAK1 in the dark. Isothermal titration calorimetry experiments were conducted to quantify the affinity of that PA-Rac1 dark and lit state mutants to the CRIB domain of PAK1.

The crystal structure of PA-Rac1 was later solved. Models of PA-Rac1 were compared to this structure. The Crystal structure was then used to model a PA-Cdc42 photoswitch.

2.3 Methods

2.3.1 Rosetta domain assembly protocol

The Rosetta program (12; 13) was used to predict the dark state structure of LOV2-Rac1 based on the solved crystal structures of dark state LOV2 (PBD code 2V0U) (14) and Rac1(PBD code 1MH1) (15). Structure prediction simulations were performed on LOV2-Rac1

545-4, 546-4, and 547-4 constructs. In these simulations, the torsion angles of the residues connecting the two proteins were optimized with Monte Carlo sampling. Using the Rosetta domain assembly protocol (16), we first applied 1000 Φ and Ψ backbone torsion angle movements of up to 180° each to three residues connecting LOV2 to Rac1 in a low resolution representation. Small backbone torsion angle moves of up to 4° were then performed on a high-resolution representation of LOV2-Rac1, followed by a global repacking of all sidechain rotamers. After every 15 cycles of small moves and repacking, further repacking was restricted to the rotamers at the interface and next to the LOV2-Rac1 linkers. This sequence of refinement was repeated for a total of 150 cycles. Next, we adopted a series of small moves, global rotamer repacking, as well as backbone minimization within 5 residues of the LOV2-Rac1 linker for high-resolution optimization cycles. After every ten cycles, only rotamers at the interface and next to the LOV2-Rac1 linkers were repacked. A total of 100 such high resolution optimizations were used to generate models, which were further scored using Rosetta's energy function. One thousand models, each representing a different folding trajectory, were generated per construct from simulations using the domain assembly protocol.

2.3.2 Modeling of Rac binding to CRIB

The complex structure of Rac3 and the CRIB domain of PAK4 (PBD code 2OV2) was used to model the interaction of CRIB-containing effectors with LOV2-Rac1 constructs. The crystal structure of Rac1 (1MH1) (15) was superimposed onto the complex structure by mapping the Cα atoms of Rac1 onto those of Rac3. This derived complex structure was then superimposed onto the LOV2-Rac1 models to create model-CRIB complexes. Side chain rotamers at the interface of each complex were optimized using rotamer repacking (17). These complexes were scored using the Rosetta energy function. A low-scoring model-CRIB complex indicated the model could bind CRIB, while a high-scoring model-CRIB complex indicated clashes between atoms of the model and the CRIB domain, resulting in reduced binding.

2.3.3 Clustering of models

Models generated in a simulation were grouped into clusters according to their pairwise root mean square deviation (RMSD). The RMSD (in $\mathring{A}$) of the Cα atom positions of each model from all other models in the simulation was calculated. Those models falling within a radius of 3 $\mathring{A}$ RMSD from each other were grouped into a cluster. A cluster member representing the center of each cluster was chosen.

2.3.4 Cloning and protein purification

Dark and lit state mimetics of PA-Rac1, C450A and I539E, were cloned into a pTriEx4 vector with an N terminal six Histidine tag. Residues 65-150 of PAK1, comprising the extended CRIB domain, were cloned into a pET23 vector, with a C-terminal 6 Histidine tag. All proteins were expressed in *E.coli* strain BL21(DE3) cells(Stratagene) at 16°C overnight in the dark. Cells were lysed in 50 mM sodium phosphate pH 7.0, 300 mM NaCl, and 5 mM $MgCl_2$. Proteins were purified under yellow light using TALON Metal Affinity Resin (Clontech) and eluted with 150 mM Imidazole at pH 7.0. The proteins were dialyzed against 50 mM sodium phosphate, 150 mM NaCl, 7.15 mM 2-mercaptoethanol, 5 mM $MgCl_2$, and 1% glycerol.

2.3.5 Isothermal titration calorimetry

ITC experiments were performed by injecting the dark state mutant C450A of PA-Rac1 (0.14 mM) or the lit state mutant I539E (0.13 mM) into the CRIB domain of PAK1 (10 μM) using a Microcal VP-ITC calorimeter at 25°C. Each titration consisted of 29 injections of 10 μL of mutants of PA-Rac1. The baseline of each titration was determined and subtracted from all of the data points. Titration data for the heat change per injection were fitted to a one-site binding model using Origin software (OriginLab).

2.4 Results

2.4.1 Structure prediction of LOV2-Rac1 constructs

One striking result from our study is that the caging of Rac1 is very sensitive to the length of the linker that connects Rac1 to LOV2. Adding or removing a single residue from the linker disrupts caging. To determine the physical basis for this length dependence we performed structure prediction simulations with the Rosetta molecular modeling program on three of the constructs (545-4, 546-4, 547-4) used in the dark state pull down experiments. The most prevalent conformation of 546-4 was similar to the crystal structure of 546-4 and contains an extensive interface between Rac1 and LOV2 that is predicted to occlude CRIB binding. A similar interface was not observed in the low energy conformations predicted for 545-4 and 547-4, and the binding site for CRIB is predicted to be accessible in the majority of the low energy conformations.

Models of the dark state 546-4 structure showed a marked difference in quaternary structure from models of 545-4 and 547-4, and importantly, were similar to the crystal structure of PA-Rac1 (Figure 2.1). Our lowest RMSD model was 1.7 $\mathring{A}$ away from the solved crystal structure. Furthermore, the largest cluster of 546-4 models was on average 4.5 $\mathring{A}$ RMSD away from the solved crystal structure. As in the crystal structure, a well-packed binding interface was formed between the two domains (Figure 2.2, Table 2.1). Residues Leu422, Pro423, Ile428, Tyr508, Leu546 from LOV2 as well as Phe37 and Trp56 of the beta sheet from Rac1 created hydrophobic contacts across the LOV2-Rac1 interface. Residues Asp419 and Trp56 also made a hydrogen bond across the interface. The tight packing of the Rac1 β-strand against LOV2 occluded the strand addition binding of CRIB to the Rac1 β-sheet.

An interface did not form in models of the 545-4 construct. In these models, Rac1 orients away from the LOV2 domain, and thus CRIB is not occluded from binding LOV2-Rac1 (Figure 2.3, Table 2.2). Also, a LOV2-Rac1 interface did not form in most of the models of the 547-4 construct. Clusters generated using the 547-4 simulations contained less models per cluster than all other simulations (Table 2.2). Because of the longer linker, 547-4 could sample more conformational space (Figure 2.3). In the majority of conformations the Rac1 β-sheet was

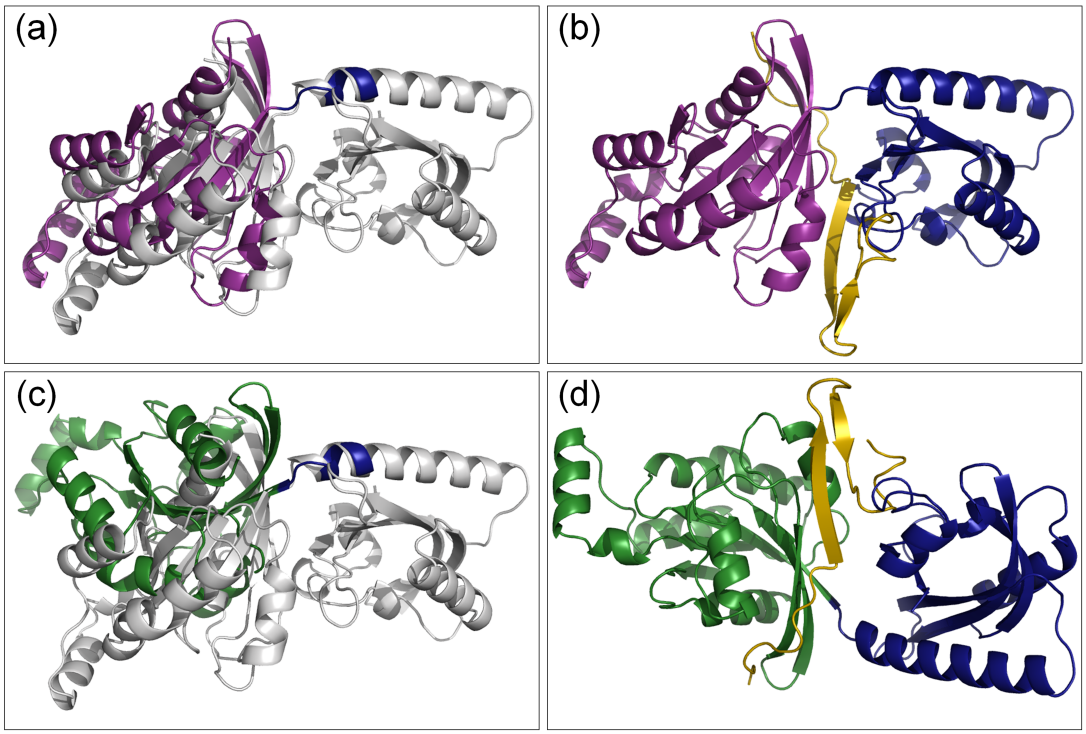

Figure 2.1: Comparison of PA-Rac models to X-ray crystal structure. (a) Superposition of X-ray structure of PA-Rac1 (white) and the 546-4 model with the lowest RMSD to the X-ray structure. LOV2 is in blue, Rac1 in purple. (b) The model with the lowest RMSD to the PA-Rac1 X-ray structure is unable to bind PAK4 CRIB (yellow). (c) Superposition of X-ray structure of PA-Rac1 (white) and the best-scoring 546-4 model. LOV2 is in blue, Rac1 in green. (d) The model with best Rosetta score is unable to bind PAK4 CRIB (yellow).

not adjacent to the LOV2 domain and the CRIB domain binding site was predicted to be accessible.

2.4.2 Binding of LOV2-Rac1 to CRIB

Isothermal titration experiments were performed to analyze the ability of lit as well as dark state 546-4 to bind the CRIB domain of PAK1. The lit state mimetic, I539E, of 546-4 bound to PAK1 CRIB with an affinity of 220-280 nM. In contrast, the dark state C450A 546-4 mimetic bound PAK1 CRIB with a ten-fold weaker affinity of 2.3-3.1 μM (Figure 2.5, Table 4.1).

Table 2.1: Simulation of the LOV2-Rac1 546-4 construct. The five most populated model clusters are listed, along with their Rosetta score. Rosetta scores listed are averages of the best 10% scoring models in each cluster. The center member of each cluster was analyzed for its RMSD to the X-ray structure of PA-Rac1 and its ability to bind the CRIB domain of p-21 activated kinase 4 (PAK4). Of the 1000 models generated during the simulations, 813 were unable to bind PAK4 CRIB.

Cluster Number	Members	Score	RMSD from X-ray (in $\AA$)	Binds CRIB?
1	566	-512	4.5	No
2	151	-512	2.1	No
3	62	-513	7.6	Yes
4	60	-506	4.5	No
5	54	-503	9.0	Yes

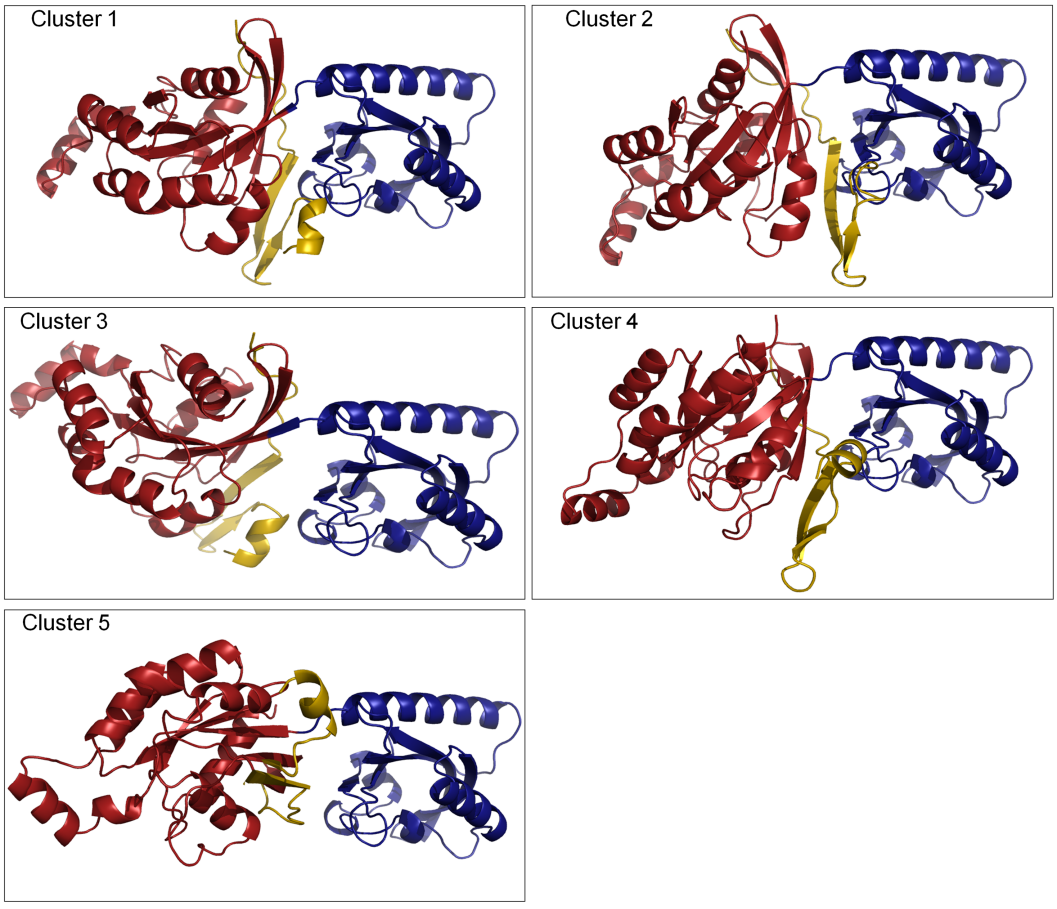

Figure 2.2: Models of the LOV2-Rac1 546-4 construct. The model representing the center member of the five most populated clusters is pictured. LOV2 is in blue, and Rac1 is in red, and PAK4 CRIB is in yellow.

Table 2.2: Simulations of LOV2-Rac1 545-4 construct. The five most populated model clusters are listed, along with their Rosetta score. Rosetta scores listed are averages of the best 10% scoring models in each cluster. The center member of each cluster was analyzed for its ability to bind the CRIB domain of PAK4. All 1000 models generated from the simulations were able to bind PAK4.

Cluster Number	Members	Score	Binds CRIB?
1	553	-509	Yes
2	178	-509	Yes
3	107	-507	Yes
4	46	-508	Yes
5	43	-509	Yes

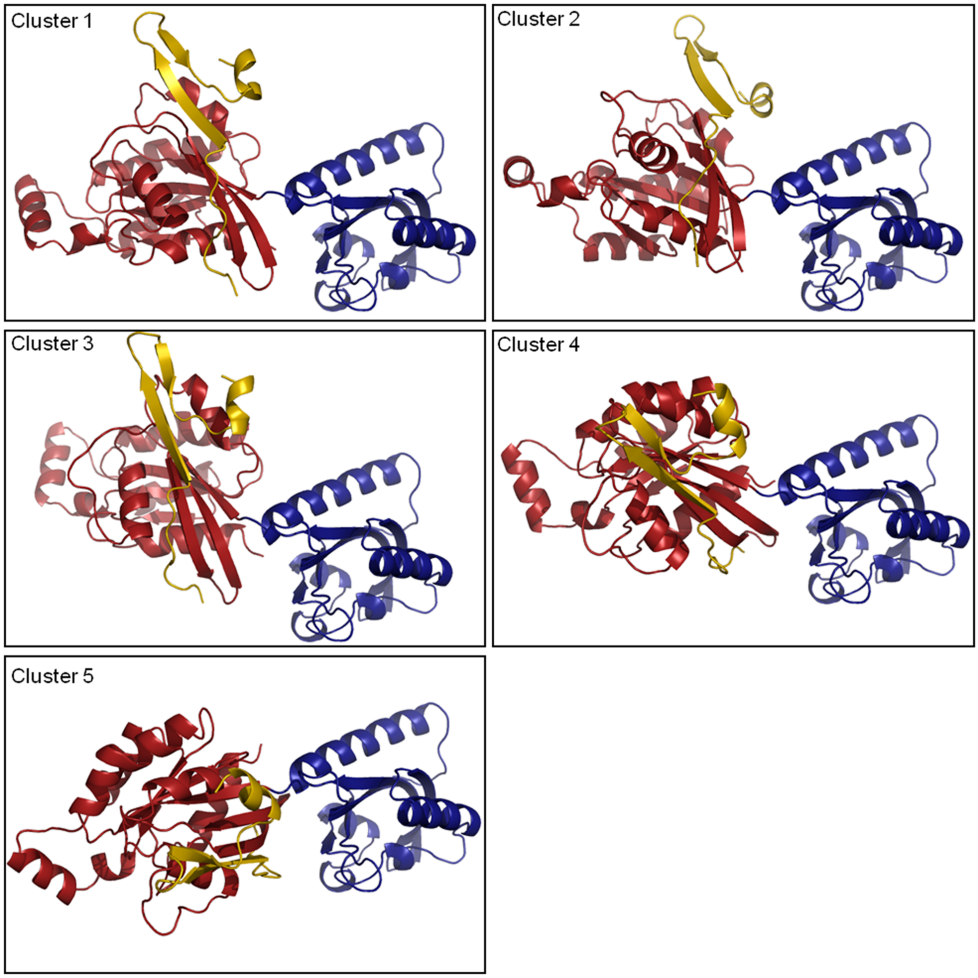

Figure 2.3: Models of the LOV2-Rac1 545-4 construct. The model representing the center member of the five most populated clusters is pictured. LOV2 is in blue, and Rac1 is in red, and PAK4 CRIB is in yellow.

Table 2.3: Simulations of LOV2-Rac1 547-4 construct. The five most populated clusters are listed, along with their Rosetta score. Rosetta scores listed are averages of the best 10% scoring models in each cluster. The center member of each cluster was analyzed for its ability to bind the CRIB domain of PAK4. Of the 1000 models generated during the simulations, 967 were able to bind PAK4 CRIB.

Cluster Number	Members	Score	Binds CRIB?
1	337	-507	Yes
2	115	-500	Yes
3	104	-508	Yes
4	100	-508	Yes
5	63	-491	Yes

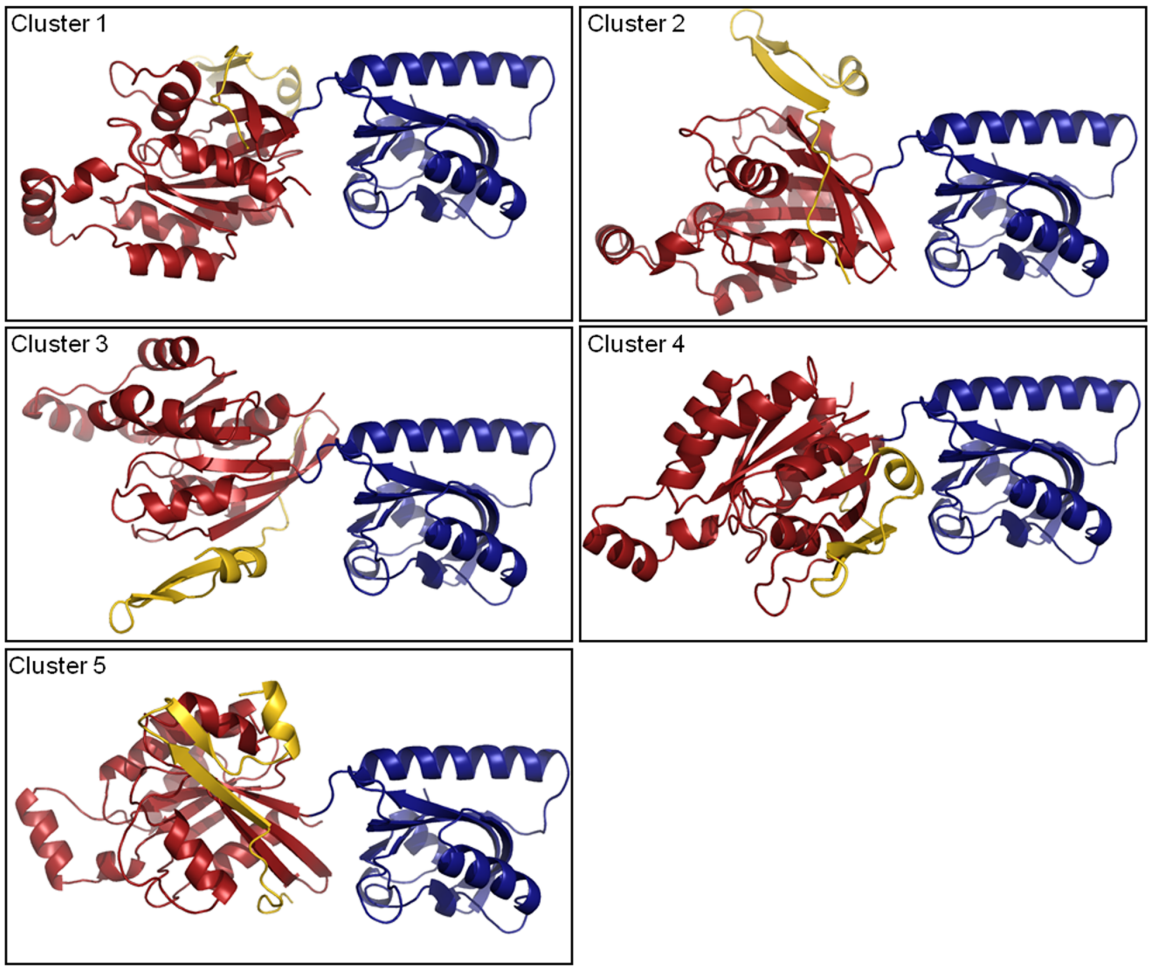

Figure 2.4: Models of the LOV2-Rac1 547-4 construct. The model representing the center member of the five most populated clusters is pictured. LOV2 is in blue, and Rac1 is in red, and PAK4 CRIB is in yellow.

PA-Rac Mutant	K_D (μM)	ΔH (Kcal mol^{-1})	ΔS (Kcal mol^{-1} K^{-1})	N
C450A	2.3 ± 0.36	-7.0 ± 0.49 $\times 10^3$	2.6	1.0 ± 0.051
dark state	3.1 ± 0.90	-5.6 ± 1.9 $\times 10^3$	6.6	0.64 ± 0.18
I539E	2.2 ± 0.14 $\times 10^{-1}$	-1.8 ± 0.016 $\times 10^4$	-30.0	0.95 ± 0.0057
lit state	2.8 ± 0.51 $\times 10^{-1}$	-1.8 ± 0.036 $\times 10^4$	-31	0.95 ± 0.013

Table 2.4: Binding affinities of PA-Rac1 mutants to the PAK1 CRIB domain. Values measured by ITC for binding affinity, enthalpy, entropy, and molar ratio are listed. Two experiments are shown per mutant.

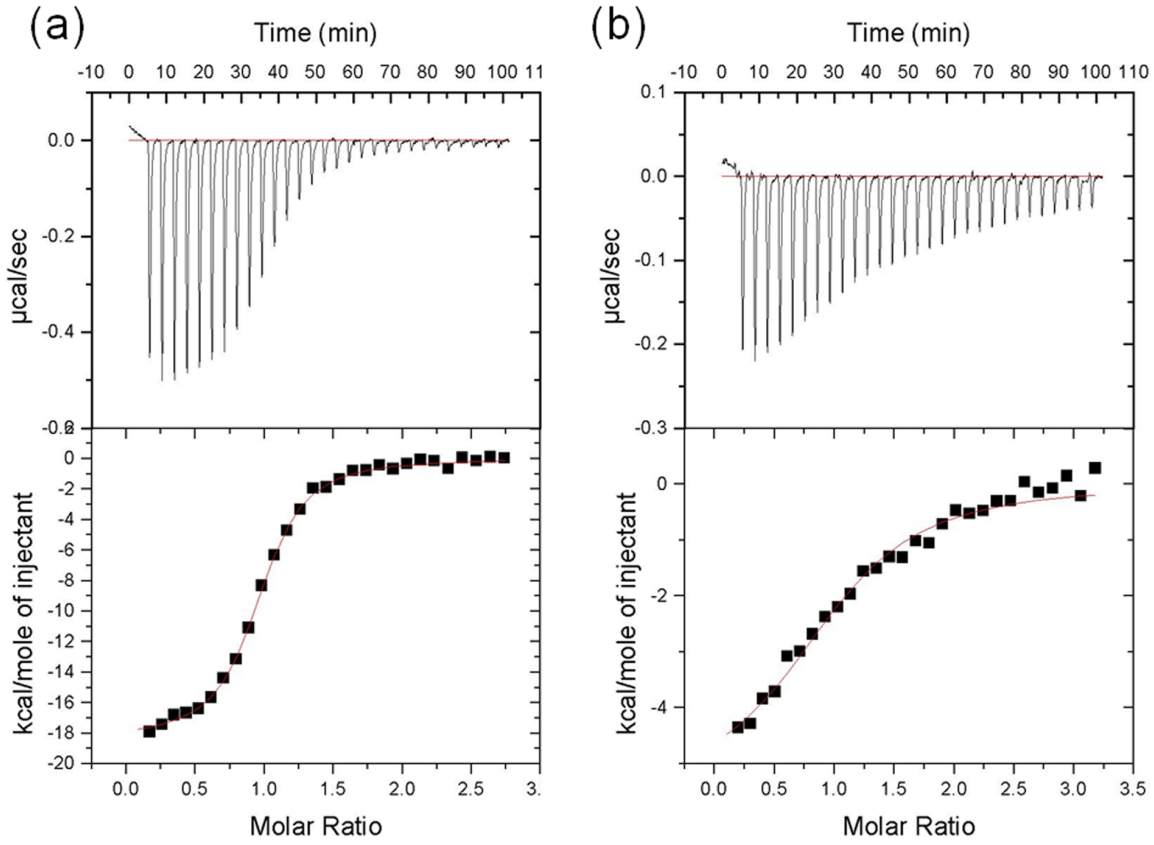

Figure 2.5: Isothermal titration calorimetry experiment measuring binding of PAK1 CRIB to PA-Rac1. Measruements of (a) Pa-Rac1 lit state (I539E) and (b) dark state (C450A) binding to CRIB are shown. The raw data of heat generated per injection is shown in the top panels, and integrated data of heat output per mole of injected PA-Rac1 versus molar ratio of PA-Rac1 to CRIB is shown at the bottom.

2.4.3 Application of modelling to PA-Cdc42 interface

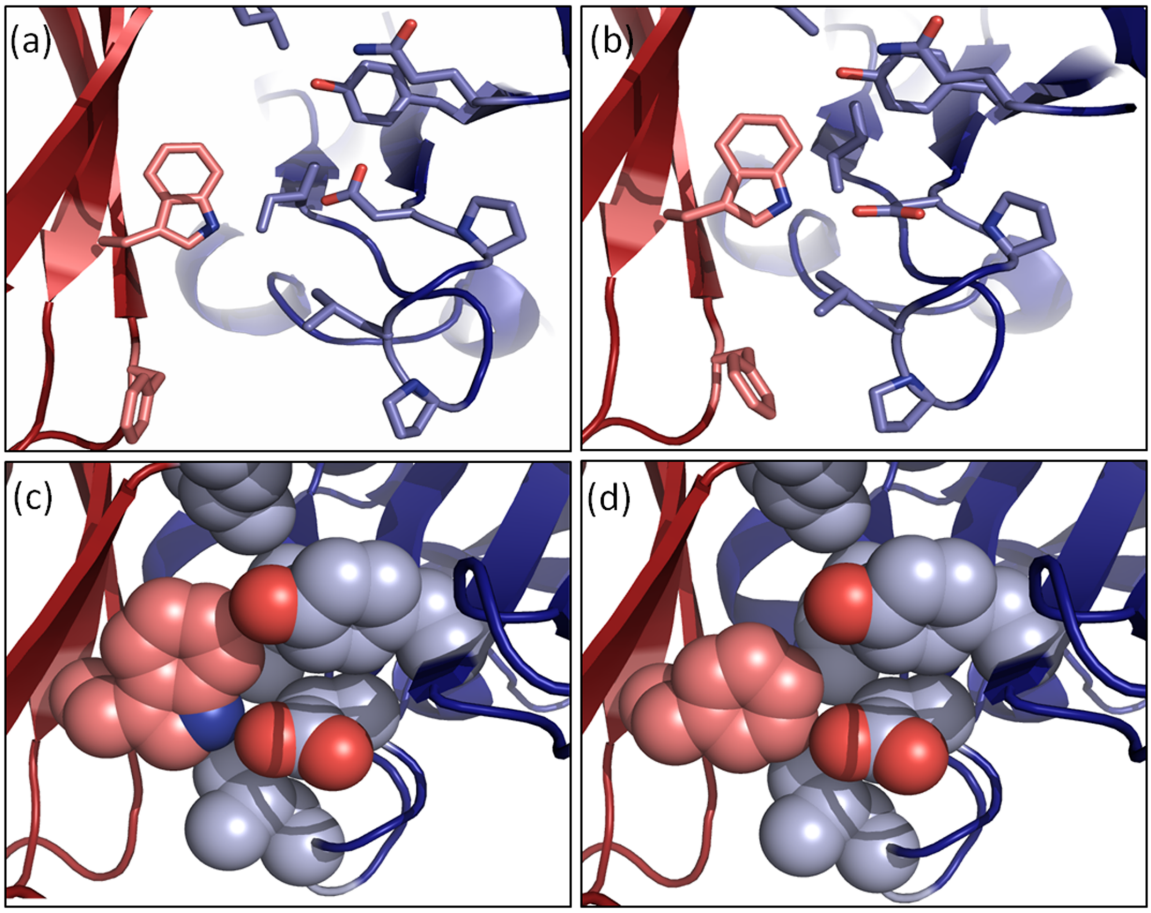

Figure 2.6: PA-Rac1 and predicted Pa-Cdc42 interfaces. (a) The interface between LOV2 and Rac1 of Pa-Rac1 546-4 construct Rosetta predicted model. (b) The interface between LOV2 and Rac1 in the Pa-Rac1 solved crystal structure (PDB code 2WKP) in stick representation and (c) in space filling representation. (d) The Rosetta predicted PA-Cdc42 interface.

The Rosetta models as well as the crystal structure of PA-Rac1 were used to create a caged Cdc42 construct. When examining the models and crystal structure of PA-Rac1, it became evident that the interface between LOV2 and Rac1 played a critical role in inhibiting PAK1-CRIB binding to Rac1 while in the dark. We sought to expand on this knowledge to cage Cdc42.

Cdc42 is a protein that has large sequence and structure identity to Rac1. About 70% of residues are shared between the two proteins (18). The effector binding region of both proteins

is located in the same place within their structures, ad Cdc42 also binds the CRIB domain of proteins such as PAK1 and WASP. While Rac1 is thought to control membrane ruffling and cell protrusion, overexpression of Cdc42 leads to cell polarization, and the formation of spike-like cell structures termed filipodia. Cdc42 is, thus, also a critical protein in cell motility.

While a large sequence identity existed between Rac1 and Cdc42, initial efforts to cage Cdc42 in the same manner as Rac1 failed. Upon examining a model of PA-Cdc42 having sequence of Cdc42 threaded onto the Rac1 portion of the PA-Rac1 crystal structure, we were able to determine why this was the case. A tryptophan residue in Rac1 (W56) forms a large hydrophobic patch with the loops of LOV2. That residue, however, is a phenylalanine in Cdc42 (Figure 2.6). The hydrophobic patch formed at the interface of Cdc42 and LOV2 is therefore smaller and less well-packed, thus lessening the inhibition of Cdc42 binding to CRIB in the dark. When a tryptophan was substituted for phenylalanine in PA-Cdc42, the interaction between Cdc42 and CRIB was better inhibited in the dark, as seen in pull-down assays of PA-Cdc42 binding PAK1-CRIB.

2.5 Discussion

Through the use of the domain assembly protocol in the Rosetta molecular modeling program, we were able to model the structure of PA-Rac1 constructs. The Crystal structure of PA-Rac1 was within 4.5 $\mathring{A}$ RMSD of the model, indicating close structural similarity between the two. The domain assembly protocol can be used as a tool to create other photoactivatable proteins, by modeling how the LOV2 domain could act as a dark state cage. The domain assembly protocol may also act as a tool to model the structures of multidomain proteins wherein the individual domains have known structures and are linked together through various linkages (16). Such a tool could serve a powerful function in predicting structures of large multidomain proteins where conformational changes play an important role in function, such as FRET biosensors.

PA-Rac1 had a tenfold tighter binding affinity for its effector CRIB in the lit versus the dark state. While this is seems a small difference in affinity, or dynamic range, it mimics the

binding of Rac1 to it effector in the GTP versus the GDP bound states (19). When in the GTP bound state, Rac1 binds CRIB with an affinity of 90 nM; PA-Rac1 lit state binds CRIB with an affinity of about 200 nM. When in the GDP bound state, Rac1 binds CRIB with an affinity of 4 μM; PA-Rac1 dark state binds CRIB with an affinity of about 2-3 μM. So, even though the dynamic range of the photoswitch is small, it straddles the binding affinties where Rac1 has maximal *in vivo* effect on CRIB binding. Photoswitches for other proteins might have to be engineered take into account their lit state and dark state effective ranges. Caged proteins might have to be engineered in two ways, by shifting their affinities to effectors either by weakening or tightening the interaction, and by changing the dynamic range, or the difference in affinity the switch achieves in the dark versus the lit state. In this way photoactivatable proteins could be fine-tuned to have the maximal effect on protein-protein interactions.

Using models and a crystal structure of PA-Rac1, we were able to create a caged version of PA-Cdc42. By introducing a tryptophan mutation into Cdc42 (F56W), we were able to make an interface between Cdc42 and LOV2 similar to that found between LOV2 and Rac1 in PA-Rac1. This mutation, however, is in the effector binding region of Cdc42 (20). Such a mutation has the potential to alter the avidity of Cdc42 for its effectors, increasing its affinity for some, while decreasing affinity for others. Due to these changes, PA-Cdc42 F56W as it is currently designed might not be ideal for *in vivo* cell motility studies. Other strategies must be tested. Most promisingly, the interface on the LOV2 side of PA-Cdc42 is being evolved to compensate for the loss of hydrophobic surface area on Cdc42.

REFERENCES

1. Goeldner, M. and Givens, R. (2005) Dynamic studies in biology: phototriggers, photoswitches and caged biomolecules. Vch Verlagsgesellschaft Mbh

2. Fortin, D., Banghart, M., Dunn, T., Borges, K., Wagenaar, D., Gaudry, Q., Karakossian, M., Otis, T., Kristan, W., Trauner, D., et al. (2008) Photochemical control of endogenous ion channels and cellular excitability. Nature Methods **5**, 331–338

3. Raftopoulou, M. and Hall, A. (2004) Cell migration: Rho GTPases lead the way. Developmental Biology **265**, 23–32

4. Ridley, A., Schwartz, M., Burridge, K., Firtel, R., Ginsberg, M., Borisy, G., Parsons, J., and Horwitz, A. (2003) Cell migration: integrating signals from front to back. Science **302**, 1704

5. Christie, J., Salomon, M., Nozue, K., Wada, M., and Briggs, W. (1999) LOV (light, oxygen, or voltage) domains of the blue-light photoreceptor phototropin (nph1): binding sites for the chromophore flavin mononucleotide. Proceedings of the National Academy of Sciences **96**, 8779

6. Harper, S., Neil, L., and Gardner, K. (2003) Structural basis of a phototropin light switch. Science **301**, 1541

7. Yao, X., Rosen, M., and Gardner, K. (2008) Estimation of the available free energy in a LOV2-Jα photoswitch. Nature Chemical Biology **4**, 491–497

8. Salomon, M., Christie, J., Knieb, E., Lempert, U., and Briggs, W. (2000) Photochemical and mutational analysis of the FMN-binding domains of the plant blue light receptor, phototropin. Biochemistry **39**, 9401–9410

9. Harper, S., Christie, J., and Gardner, K. (2004) Disruption of the LOV-Jα helix interaction activates phototropin kinase activity. Biochemistry **43**, 16184–16192

10. Parrini, M., Matsuda, M., and de Gunzburg, J. (2005) Spatiotemporal regulation of the Pak1 kinase. Biochemical Society Transactions **33**, 646

11. Maruta, H., Nheu, T., He, H., and Hirokawa, Y. (2003) Rho family-associated kinases

PAK1 and rock. Progress in Cell Cycle Research **5**, 203

12. Rohl, C., Strauss, C., Misura, K., and Baker, D. (2004) Protein structure prediction using Rosetta. Methods in enzymology **383**, 66–93

13. Das, R. and Baker, D. (2008) Macromolecular modeling with rosetta. Annu. Rev. Biochem. **77**, 363–382

14. Halavaty, A. and Moffat, K. (2007) N-and C-terminal flanking regions modulate light-induced signal transduction in the LOV2 domain of the blue light sensor phototropin 1 from Avena sativa. Biochemistry **46**, 14001–14009

15. Hirshberg, M., Stockley, R., Dodson, G., and Webb, M. (1997) The crystal structure of human rac1, a member of the rho-family complexed with a GTP analogue. Nature Structural & Molecular Biology **4**, 147–152

16. Wollacott, A., Zanghellini, A., Murphy, P., and Baker, D. (2007) Prediction of structures of multidomain proteins from structures of the individual domains. Protein Science **16**, 165–175

17. Kuhlman, B. and Baker, D. (2000) Native protein sequences are close to optimal for their structures. Proceedings of the National Academy of Sciences **97**, 10383

18. Nassar, N., Hoffman, G., Manor, D., Clardy, J., and Cerione, R. (1998) Structures of Cdc42 bound to the active and catalytically compromised forms of Cdc42GAP. Nature Structural & Molecular Biology **5**, 1047–1052

19. Thompson, G., Owen, D., Peter, A., and Lowe, P. (1998) Delineation of the Cdc42/Rac-binding domain of p21-activated kinase. Biochemistry **37**, 7885–7891

20. Zhao, Z., Manser, E., Chen, X., Chong, C., Leung, T., and Lim, L. (1998) A conserved negative regulatory region in alpha PAK: inhibition of PAK kinases reveals their morphological roles downstream of Cdc42 and Rac1. Molecular and CellularBiology **18**, 2153

CHAPTER 3

DESIGN OF A PHOTOACTIVATABLE VINCULIN BINDER

3.1 Summary

Photocontrol of protein binding interactions is a powerful tool for studying cell signaling networks, allowing for precise spatial and temporal control of cellular functions. We have created a light switchable peptide that binds vinculin with enhanced affinity under blue light using the photoactivatable LOV2 domain. The peptide, ipaA, binds with low nanomolar affinity to vinculin, a protein critical to inside-out and outside-in signaling at focal adhesions and adherens junctions. The photoswitch, termed LOV-ipaA, embeds the functionality of ipaA into the sequence of LOV2. In the switch, ipaA-vinculin binding is sterically blocked when in the dark, and the inhibition is relieved upon blue light activation. We show that the LOV-ipaA protein can be photoactivated by blue light and undergoes spectral and secondary structural changes from a lit/active to a dark/inactive state. Through the use of a novel fluorescence polarization competition assay, we report the on and off rates, as well as the binding affinities, of the LOV-ipaA photoswitch binding to vinculin under dark or blue light conditions. We show LOV-ipaA binds the vinculin D1 subdomain with a 25-fold tighter affinity in the lit than in the dark state. Mutations on the LOV2 domain have extended the dynamic range of this photoswitch to 48-fold. The LOV-ipaA switch is able to control binding of full-length vinculin to actin, releasing the auto-inhibition between the head and actin-binding tail of vinculin. This indicates that LOV-ipaA is a physiologically relevant switch that may be used to control vinculin signaling through actin binding *in vivo*.

3.2 Introduction

Photocontrol of protein-protein interactions is a powerful approach to studying signaling networks (1; 2; 3; 4). Using light to activate these networks allows for precise spatial and temporal control of cell functions. Unlike chemical activators of signaling, proteins allow for specific control of desired interactions and quick reversibility (5). Naturally-occurring photoactivatable proteins are ideal for use in designed light switches due to their specificity, reversibility, and ease of use as genetically encoded effectors (6).

The LOV2 domain has been used to photocontrol protein-protein interactions (3; 7; 8). Found in higher plants (9), it is part of the PAS superfamily of domains (10), and contains a flavin mononucleotide (FMN) co-factor located in the center of the PAS fold, as well as a large α-helical region C-terminal to the fold, termed the Jα helix (11; 12). Upon irradiation with a photon of blue light, a covalent adduct is formed between a cysteine side chain in the PAS fold and a carbon atom of the FMN (13; 14). NMR and spectroscopic studies indicate this leads to a larger overall conformational change in the domain wherein the Jα helix cooperatively unfolds (15; 16). Reversion of the thiol bond and conformational change back into the dark state occurs spontaneously within seconds to hours, depending on the LOV2 domain ortholog (17).

The large conformation change that occurs within the Jα helix has been previously harnessed to create a photoswitchable GTPase, PA-Rac (3); a transcriptional repressor, LOV-TAP (7; 18); and a photoactivatable DHFR enzyme (8). In PA-Rac, constitutively active Rac1 was linked to the C-termius of LOV2 and the Jα helix in such a way as to occlude the binding site of Rac1 to its effector, PAK1, in the dark. Upon blue light irradiation, unfolding of the Jα helix relieves steric blocking of the PAK1 binding site on Rac1, and allows Rac1 to interact with its downstream effectors. PA-Rac exhibits a 10-fold dynamic range in its ability to inhibit Rac1-effector interactions in the dark versus under blue light irradiation conditions. PA-Rac has been used to study cell motility in single cells (3) as well as in whole organisms. In the LOV-TAP switch, Strickland *et. al.* linked the TrpR transcriptional repressor *E. coli* protein through its N-terminal helix to the C- terminus of the Jα helix, creating a large end-to end

helix that is shared by the two proteins (7). The reaction mechanism of this switch proposes that the helix remains docked to the LOV domain in the dark, sterically blocking interaction between TrpR and DNA binding. Upon irradiation with blue light, the helix undocks from the LOV2 domain and the steric block is relieved, allowing for binding between TrpR and DNA and subsequent transcription repression. Although important as a proof of concept, LOV-TAP was calculated to undergo only a small change in binding affinity to DNA between lit and dark states, a dynamic range of 5-fold. Recently, the dynamic range of this switch was improved through the introduction of 2 mutations into the Jα helix, G528A and N538E, which stabilized the structure of the helix in the dark state (18). The LOV2 domain was also used to photoactivate the enzyme dihydrofolate reductase (DHFR) (8). Using statistical coupling analysis to pinpoint areas where LOV2 conformational change would lead to allosteric regulation of DHFR, the entire LOV2 domain and Jα helix were inserted into an active site loop of the DHFR enzyme. Low levels of enzyme activity were seen upon light activation.

All three of the previously designed switches based on the LOV2 domain were constructed by simple fusions or domain insertions. An alternative design approach is to embed the desired functionality within the conformational switch. For instance, redesign the Jα helix so that it still folds against the rest of the LOV2 domain in the dark but can bind another protein when released from the LOV2 domain in the light. This strategy was recently used to cage a coiled-coil interaction by creating a chimeric sequence of a leucine zipper and the N-terminus of the photoactivable yellow protein (PYP) (19). Like the Jα helix from LOV2, the N-terminus of PYP docks more tightly with the rest of the protein in the dark. One challenge of this approach is that a linear stretch of sequence must be created that it is compatible with alternative conformations and binding events. A potential advantage of this approach is greater caging capacity as the target functionality is more tightly embedded within the switch protein.

We have used the LOV2 domain to create LOV-ipaA, a photoactivatable switch that binds to vinculin with enhanced affinity in the light (20). Vinculin is a critical protein in forming focal adhesions and adherens junctions (21; 22). It is composed of 3 domains; the head domain, containing 5 4-helix bundles D1-D5, a proline rich neck region, and the tail domain (23; 24). Integrin signaling proteins talin and α-actinin bind vinculin through a helix

addition mechanism in a groove in the D1 head domain bundle, while the tail domain binds polymerized F-actin (25; 26). The F-actin binding site on the tail domain is autoinhibited through an interaction between the head and tail domains (27). Interaction between high-affinity vinculin binding sites (VBS) in proteins such as talin with the D1 subdomain in the presence of F-actin releases autoinhibition between the head domain and the actin-binding site of the tail (28). This allows vinculin to form a tensile bridge linking integrin binding proteins to the actin cytoskeleton (29) The invasin protein ipaA from the *Shigella flexneri* bacterium contains a VBS that binds to the D1 groove with a much tighter affinity than those from talin or α-actinin, thus out-competing naturally occurring interactions in epithelial cells and activating vinculin- F-actin binding (20). Selectively photo controlling the binding of ipaA to vinculin through the LOV-ipaA photoswitch could render it useful as a dominant negative inhibitor of vinculin in mammalian cells, and an integral tool for studying the role of vinculin dynamics in cell motility.

We have designed LOV-ipaA using the Rosetta molecular modeling program so that the functionality of the ipaA VBS peptide is embedded within the LOV2 Jα helix (30). The last ten residues of the Jα helix and the first ten residues of ipaA form a chimeric sequence. We were able to maintain LOV2 reversibility in the FMN thiol bond formation and the Jα helix conformational change using the chimeric sequence. Under dark conditions, the LOV2 domain in LOV-ipaA reduces the binding affinity of the ipaA sequence for vinculin; upon blue light irradiation, the Jα helix unfolds, the LOV2 steric block is relieved, and LOV-ipaA is able to bind vinculin with high affinity. This conformational switching leads to a 20-fold change in binding affinity for vinculinD1. Mutations designed on the LOV domain extended this dynamic range to almost 50-fold. These changes in dynamic range between lit and dark states of LOV-ipaA to the vinculin subdomain translated into large changes in apparent binding affinity of LOV-ipaA to full-length vinculin between lit and dark states. The LOV-ipaA switch was able to control binding of full-length vinculin to actin, releasing the auto-inhibition between the head and actin-binding tail of vinculin. This indicates the photoswitch could be used to control vinculin signaling through actin binding *in vivo*. Mutations in the LOV2 domain that lengthened or shortened the reversibility time of the LOV2 domain were also tested in the

LOV-ipaA system. Kinetics measurements indicate these mutations have a small effect on binding between ipaA and vinculinD1.

3.3 Methods

3.3.1 Cloning

The LOV-ipaA gene was synthesized with a 6 histidine N-terminal tag (Genscript) and cloned into the pET21b vector. Mutations on LOV-ipaA were performed using site-directed mutagenesis. VinculinD1 subdomain (residues 1-258) and full-length vinculin (residues 1-1066) cloned into a pET15b vector were a gift from the Craig lab at Johns Hopkins University.

3.3.2 Protein expression and purification

LOV-ipaA WT and mutants were expressed in *E.coli* strain BL21(DE3) cells (Genese) at 16°C overnight in the dark. Cells were lysed in buffer containing 50 mM sodium phosphate pH 7.5, 150 mM NaCl and 5 mM 2-mercaptoethanol. Proteins were purified by affinity chromatography over HiTrap HisTrap columns (GE) and eluted with 150 mM Imidazole at pH 7.5. The proteins were further purified through size exclusion chromatography over a Sephadex S75 column (GE) equilibrated with 50 mM sodium phosphate, 150 mM NaCl and 5 mM 2-mercaptoethanol. VinculinD1 subdomain was expressed in *E.coli* strain BL21(DE3) cells (Stratagene) at 16°C overnight. Cells were lysed in buffer containing 50 mM Tris-HCl pH 8.0, 500 mM NaCl and 5 mM 2-mercaptoethanol. The protein was purified by affinity chromatography over HiTrap HisTrap columns (GE) and eluted with 500 mM Imidazole at pH 8.0. The protein was further purified by ion exchange chromatography using a HiTrap Q column (GE) eluted with a NaCl gradient. VinculinD1 was stored in 20 mM Tris-HCl with 2 mm DTT and 2 mM EDTA.

Vinculin full-length protein was expressed in *E.coli* strain BL21(DE3) cells (Genese) at 37°C for four hours. Cells were lysed in buffer containing 50 mM Tris-HCl pH 8.0, 500 mM NaCl and 5 mM 2-mercaptoethanol. The protein was purified by affinity chromatography over

HiTrap HisTrap columns (GE) and eluted with 500 mM Imidazole at pH 8.0. The protein was then purified by ion exchange chromatography using a HiTrap Q column (GE) eluted with a NaCl gradient. Vinculin was further purified through size exclusion chromatography over a Sephadex S200 column (GE) equilibrated with 50 mM sodium phosphate, 150 mM NaCl and 5 mM 2-mercaptoethanol.

Protein concentrations for LOV-ipaA and vinculinD1 were determined using Bradford assays (Thermo). Protein concentrations for full-length vinculin were determined using absorbance at 280 nm measurements with an extinction coefficient of 62,000 M^{-1} cm^{-1}.

3.3.3 Peptide synthesis

Peptides containing the sequence TANNIIKAAKDATTSLSKVLKNIN, TANNIIKAAKDATTSASKVLNIN and TANNIIKAAKDATTSLSKALKNIN were synthesized by the Strahl Lab at UNC-Chapel Hill and amine labeled using 5-(and-6)-Carboxytetramethylrhodamine TAMRA dye (Anaspec). Peptide concentration was determined by measuring absorbance of the TAMRA dye at 555 nm using 65,000 M^{-1} cm^{-1} extinction coefficient.

3.3.4 Illumination

LOV-ipaA WT and mutants were irradiated using a collimated blue LED with maximum emission wavelength of 455 nm (ThorLabs). Illumination power was measured to be 6.8 mW cm^{-2}

3.3.5 Spectrophotometry

All spectrophotometry experiments were carried out using a Cary 50 UV-Vis spectrophotometer (Varian). LOV-ipaA WT and mutant spectra were determined by irradiating samples in a 1 cm path-length cuvette for 1 min and measuring absorbance from 285 to 525 nm every 4 nm. Irradiation was subsequently turned off and the spectrum was measured at 30 s or 5 min (for the V416I L496I mutant) intervals until no change in absorbance at 450 nm was observed.

Kinetics of adduct recovery were determined by irradiation of a LOV-ipaA sample for 1 min to saturate the protein in the lit state. Irradiation was then turned off and absorbance at 450 nm was measured over 2 s or 30 s intervals. Recovery kinetics were fit in Prism software using a first order exponential decay equation to determine FMN adduct recovery half-life.

3.3.6 Circular dichroism

All Circular Dichroism experiments were carried out using a Jasco J600 circular dichroism spectrometer. All proteins were dialyzed into 50 mM potassium phosphate buffer pH 7.5. LOV-ipaA WT and mutant residue molar ellipticity was determined by irradiating samples in a 0.1 cm path-length cuvette for 1 min to saturate the protein in the lit state. Irradiation was turned off and absorbance at 207 nm and 222 nm was measured over 2 s or 30 s intervals. Recovery kinetics were fit in Prism software using a first order exponential decay equation to determine Jα helix re-folding half-life.

3.3.7 Fluorescence polarization competition experiments

All fluorescence polarization experiments were conducted usinga Jobin Yvon Horiba FluoroMax3 fluorescence spectrometer. All proteins were dialyzed into 50 mM sodium phosphate pH 7.5 150 mM NaCl, 5 mM 2-mercaptoethanol, and 0.01% triton X100 buffer. TAMRA labeled peptides were excited with polarized light at 555 nm and the polarization of emitted light was measured at 583 nm.

The binding affinity of synthesized TAMRA-labeled ipaA peptide to vinculinD1 was determined by titrating increasing concentrations of vinculinD1 into 2 nM TAMRA labeled ipaA peptide and measuring fluorescence polarization at the emission wavelength of TAMRA, 583 nm. The curve was fit using a one site binding model in Sigma Plot software.

The off rate of TAMRA-labeled ipaA peptide binding to vinculinD1 was determined by using 50 nM TAMRA-ipaA peptide 85 bound to vinculinD1 in a 0.3 cm path length cuvette. A 30-fold excess of unlabeled ipaA peptide was then added to the reaction. The reaction was allowed to proceed for 3 hours at 25°C, with polarization of TAMRA dye emission measured

at intervals of 5 min and was fit to a one phase exponential decay equation to determine the first order rate constant.

Competition assays were conducted using 50 nM TAMRA-ipaA peptide and a concentration of vinculin appropriate for binding 85% of the TAMRA-ipaA peptide, as determined from the previously measured dissociation constant for TAMRA-ipaA and vinculin. Varying concentrations of LOV-ipaA were then added to the reaction. The reaction was allowed to proceed for 3 hours at 25°C, with polarization of TAMRA dye emission measured at intervals of 5 min. Competition curves were fit using a first order exponential decay equation to determine the polarization at time point zero. The fraction of TAMRA-ipaA bound to vinculin was determined by normalizing each curve using the time point zero as the calculated 85% bound point and the polarization of TAMRA-ipaA alone as the zero fraction bound point in the dark. In the light, each curve was normalized with a zero fraction bound point determined by mixing TAMRA-ipaA and LOV-ipaA at the concentration used in the titration under blue light and setting the resulting polarization as the zero fraction bound point. Normalized curves were fit for k_{on} and K_D rates using a numerical integration script in Matlab. Six curves were used per fit, and two fits were averaged for each kinetic measurement.

3.3.8 Surface plasmon resonance

Surface plasmon resonance experiments were conducted using a Biacore 2000 machine (GE). VinculinD1 was immobilized through amine coupling to the surface of a CM5 chip (GE) Different concentrations of LOV-ipaA were flown over the immobilized protein and the change in response units over time was recorded. Data were fit simultaneously for k_{on} and k_{off} to a pseudo-first order binding model.

3.3.9 Actin co-sedimentation assays

Purified rabbit actin (invitrogen) was polymerized for 30 min at room temperature in 10 mM Tris-HCl pH 7.5 containing 100 mM KCl, 2 mM $MgCl_2$, 2 mM DTT and 1 mM ATP. 2 mM vinculin and either ipaA peptide or LOV-ipaA mutants were mixed for vinculin:ipaA ratios

of 1:0, 1:1, 1:2.5, 1:5, 1:10, 1:20, or 1:50 per sample. 12 mM polymerized actin was added per sample, within a volume of 45 μL per sample. Samples were incubated at room temperature for 1 hour. They were then centrifuged in a TLA-100 rotor in a Beckman Coulter Optimax XP ultracentrifuge at an acceleration of 150,000 g for 30 min cooled to 20°C. Samples were split into supernatant and pellet fractions. Pellets were resuspended into 45 μL 2x tris-glycine SDS buffer. All fractions were denatured and run onto an 8 SDS-page polyacrylamide gel. Gels were comassie stained and analyzed using ImageJ software to determine the fraction of vinculin present in the pellet versus total vinculin in each sample. Apparent binding affinity of ipaA or LOV-ipaA to vinculin was determined by plotting the fraction of vinculin bound to actin versus concentration of LOV-ipaA and fitting the curve to the equation below using Prism software. A total of 3 gels were quantified and averaged for each binding affinity measurement (31).

$$F = a + (b - a) \times \left[\frac{(K + X_0 + V_0) - \sqrt{(K + X_0 + V_0)^2 - 4(X_0 V_0)}}{2V_0} \right]$$

F is the fraction of vinculin bound to actin in the pellet, a is the minimum fraction bound, b is the plateu for fraction bound (set to 0.39), K is the binding affinity, X_0 is the concentration of ipaA or LOV-ipaA added to the reaction, and V_0 is concentration of vinculin in the reaction (set to 2 μM).

3.4 Results

3.4.1 Design of LOV-ipaA

The ipaA VBS1 helical peptide was identified as good a candidate for caging with the LOV2 domain by performing a search of the protein data bank for protein-binding peptides with sequences similar to the LOV2 Jα helix. The first ten residues of the ipaA helix were identified as a good match to the last ten residues of the Jα helix. In addition to having strong sequence similarity, 5 of the 10 positions are identical, and the hydrophobic residues on the Jα helix that make critical contacts with the LOV2 domain β-sheet (539, 542, 543) are conserved in the alignment with ipaA. Additionally, residues in the ipaA sequence that make extensive

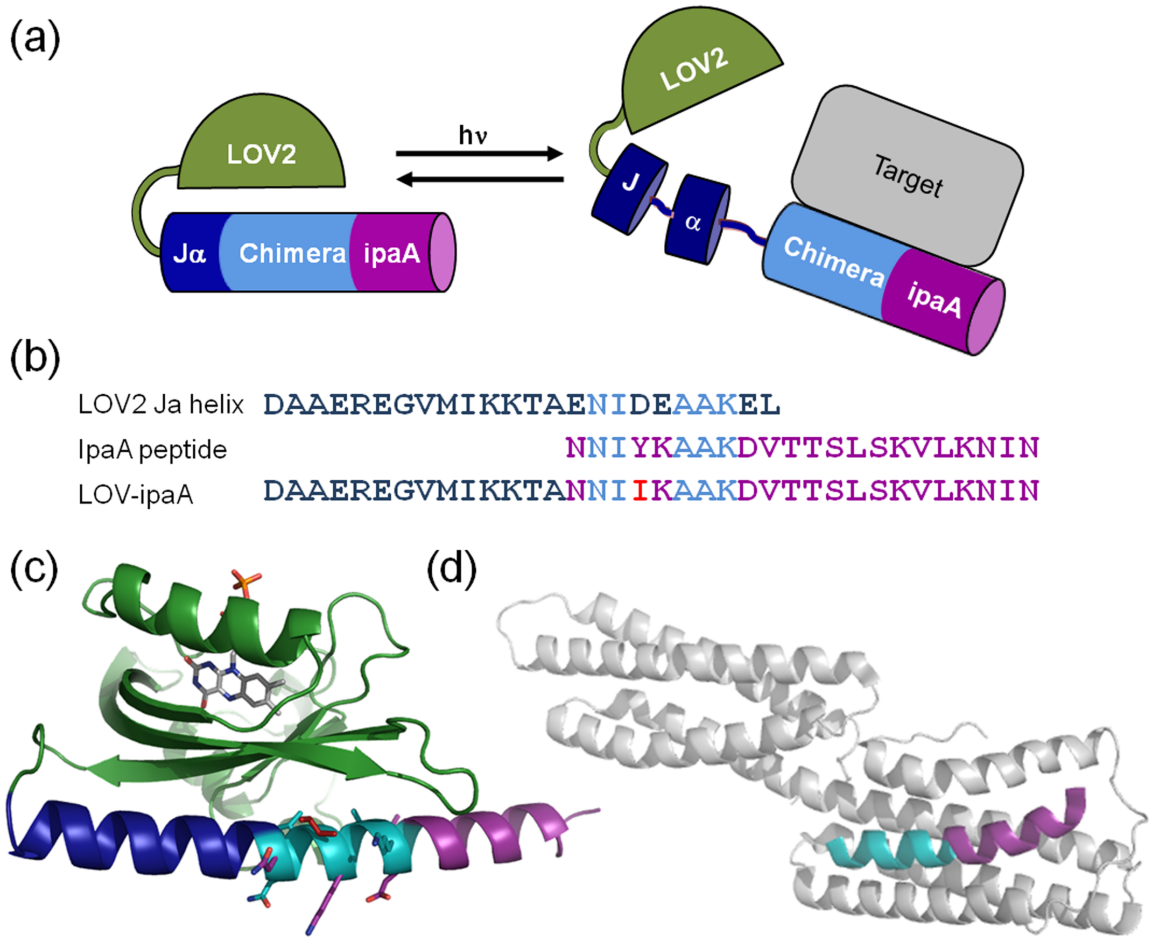

Figure 3.1: LOV-ipaA design (a) The LOV-ipaA switch was designed as a chimera between the LOV2 Jα helix and ipaA VBS peptide. Upon irradiation with blue light, the Jα helix unfolds and ipaA can bind effector vinculin. (b) Sequence alignment of LOV2-Jα, ipaA, and LOV-ipaA. Jα sequence (blue) ipaA sequence (purple), chimera sequence (cyan), and designed residues (red) are indicated. (c) Model of LOV-ipaA with residues colored as in (b). (d) Crystal structure of ipaA in complex with vinculin, PDB code 2GWW.

contacts with vinculin are conserved in the alignment (Ile 612, Ala 615, Ala 616, and Val 619 in ipaA). The number, placement, and identity of polar residues are also very similar in both sequences. The close similarty of these two sequences suggested that it may be possible to create a chimera sequence that could dock against the LOV2 domain in the dark, but then bind to vinculin when the Jα helix is released by light activation.

To further evaluate the viability of the proposed chimera sequence we used the Rosetta molecular modeling program to assess the impact of altering the LOV2-Jα and vinculin-ipaA

Design Residue	LOV2 -Jα ΔScore	Vinculin -ipaA ΔScore
540 Y	+3.4	0 (native sequence)
540 D	-1.9	-0.20
540 I	-2.5	+2.1

Table 3.1: Rostta energies for LOV-ipaA designed residues. Change in Rosetta Energy Units of native minus designed sequences is given. Designed sequences incorporate all ipaA residues into the Jα helix or ipaA peptide, with the exception of position 540, which is designed to the residue listed.

complex sequences. Side chain optimization simulations were used to thread the first ten residues of ipaA onto the last ten residues of the Jα helix. The protein backbone was held fixed during the simulations, but side chains on the Jα helix and the neighboring β-sheet were allowed to adopt alternative conformations. The Rosetta scores of individual residues were examined to determine if particular residues in the IpaA sequence packed unfavorably against the LOV2 domain β-sheet. A single position showed unfavorable scores, the mutation of aspartic acid 540 to tyrosine. This mutation, D540Y, led to a high Van der Waals repulsive energy for the residue, indicating a clash between side chain atoms of Y540 and the LOV2 β-sheet. To search for an alternative amino acid to place at this position, Rosetta was used to perform a sequence optimization simulation in which position 540 was allowed to adopt alternative identities and neighboring side chains were free to adopt new side chain conformations. One of the best scoring residues in the 540 position on the Jα helix was isoleucine. The designed LOV2-Jα structure containing this sequence improved protein stability by 2.5 Rosetta energy units (Table 3.1). When designed onto vinculin-ipaA, the isoleucine mutation was predicted to destabilize the protein complex by 2.1 Rosetta energy units. This was considered a desirable outcome since the binding affinity of ipaA to vinculin had previously been reported to be a staggeringly tight 110 pM. Destabilizing the vinculin-ipaA complex could lead to a slightly lower binding affinity, enabling easier working conditions for assays. In contrast to the isoleucine mutation, retaining aspadric acid, the Jα helix native amino acid, and incorporating it into both the Jα helix and ipaA would have slightly stabilized both LOV2-Jα and the vinculin-ipaA complex. Incorporating Tyrosine along with all 10 other residues of ipaA onto the last ten residues of

Jα would have destabilized LOV2-Jα by a substantial amount, while maintaining the same stability for vinculin-ipaA. A working model for LOV-ipaA was then created by using the threaded LOV2-Jα design and adding the remaining 11 residues of ipaA onto the C-terminal end of Jα using the fragment insertion capability of Rosetta's domain assembly protocol.

3.4.2 LOV-ipaA photoswiching characterization

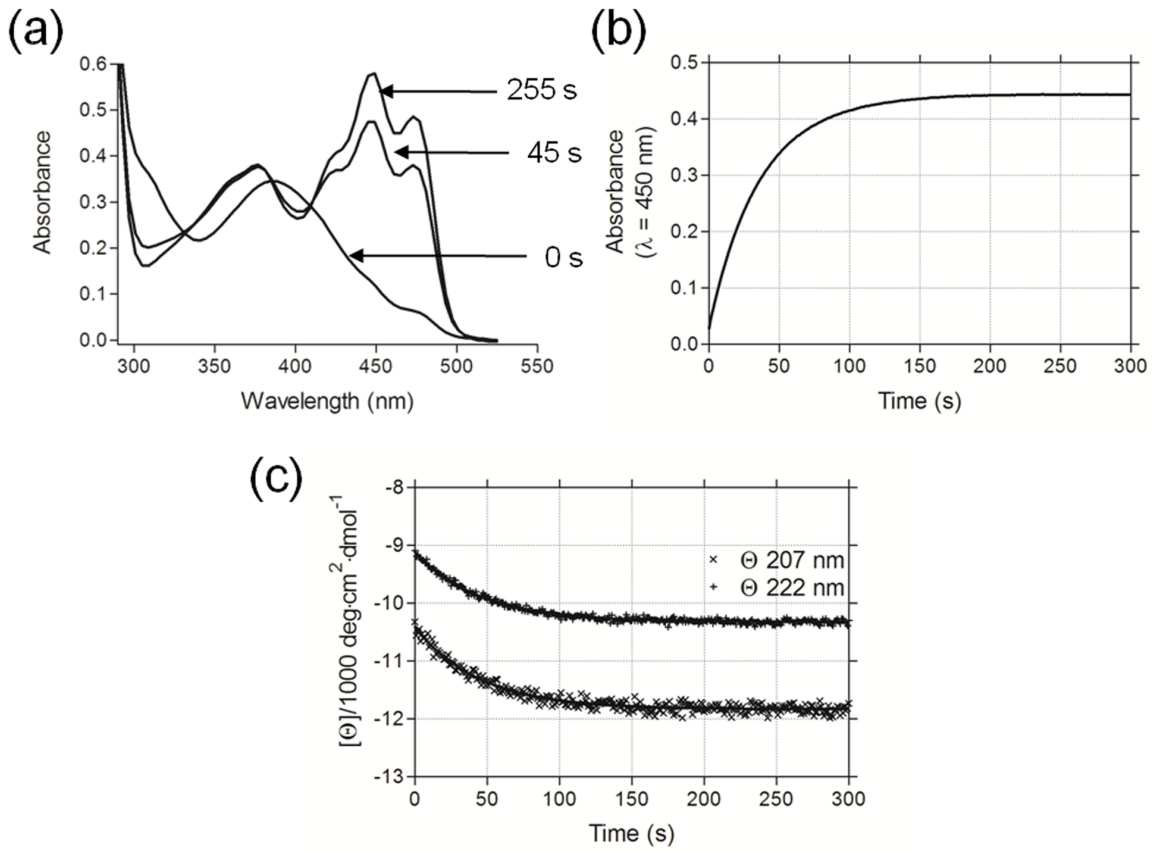

Figure 3.2: Spectrophotometric and circular dichroism characterization of LOV-ipaA photoswitching. (a) LOV-ipaA FMN absorbance vs. wavelength spectrum as LOV-ipaA reverts from lit state (0 s) to dark state (255 s). (b) LOV-ipaA FMN absorbance at 450 nm over time as LOV-ipaA reverts from lit state to dark state (c). LOV-ipaA residue molar ellipticity at 207 nm and 222 nm over time as LOV-ipaA reverts from lit state to dark state.

Spectrophotometric and circular dichrochorism experiments were performed to measure the photoswitching ability of LOV-ipaA. The Absorption spectrum of FMN within LOV-ipaA was measured in both the lit and dark states. Upon irradiation with blue light, a thiol bond

forms between cysteine 450 of *Avena sativa* LOV2 and FMN. This creates an absorbance spectrum from the FMN with a peak at a wavelength of 378 nm. Upon reversion to dark state, the thiol bond is broken, and the FMN has two peaks of absorption at 447 nm and 478 nm (32; 13). The absorption spectrum of LOV-ipaA in both the blue light and in the dark state remains the same as that of the wildtype LOV2 domain, with LOV-ipaA showing a 378 nm peak absorbance under blue light irradiation conditions. When the protein is then placed in the dark, the absorption shifts to dark state with peaks at 447 nm and 478 nm over the course of about 250 s, indicating that LOV-ipaA also retains the wildtype LOV2 domain ability to shift from lit to dark state (Figure 3.2).

We measured the time required for LOV-ipaA to revert from lit state to dark state after blue light irradiation by following the protein's increasing absorption at of 450 nm wavelength light (Figure 3.2). As it reverted from lit stare to dark state, the 450 nm absorbance peak increased. Fitting the subsequent absorbance trace over time to an equation for first order exponential decay, we measured the half life of LOV-ipaA lit state to dark state reversion as being 25 s, similar to the reported wildtype LOV2 domain rate of 27 s (32).

We also took circular dichroism measurements of the lit state to dark state conversion of LOV-ipaA. By following the residue molar ellipticity at 207 nm and 222 nm over time, we observed an increase in helical content of LOV-ipaA (Figure 3.2). Fitting to a first order exponential decay equation, we calculated the change in helical content to have a half life of 31 s for absorption of both 207 nm and 222 nm. This indicated that LOV-ipaA gained more helical structure as it converted from lit state to dark state, most likely from the Jα helix unfolding under blue light conditions, then re-folding in the dark.

3.4.3 Dark and lit state binding between LOV-ipaA and vinculinD1

We developed a fluorescence polarization competition assay to measure the binding affinity of LOV-ipaA to the vinculinD1 subdomain under dark as well as blue light irradiation conditions. We first labeled an ipaA peptide with fluorescent 5-(and-6)-Carboxytetramethylrhodamine (TAMRA) and measured its binding affinity to the vinulinD1 subdomain by measuring its fluo-

rescence polarization emission at 583 nm. The assay was then designed with the TAMRA-ipaA peptide 85% bound to vinculinD1, yielding a high fluorescence polarization signal readout. Increasing concentrations of LOV-ipaA would be titrated into the complex, competing vinculinD1 off and decreasing the fluorescence polarization as an increasing amount of free TAMRA-ipaA peptide was generated. The titration curves would be generated for LOV-ipaA in both dark and blue light conditions, and fit for binding affinity under steady state conditions. After attempting a test titration, we observed that the dissociation of TAMRA-ipaA-vinculinD1 and formation of the LOV-ipaA-vinculinD1 complex did not reach equilibrium for at least 3 hours, making titration measurements under steady state conditions less practical. Instead, kinetic measurements were measured for the competition assay. First, the off rate for TAMRA-ipaA dissociation from the TAMRA-ipaA-vinculinD1 complex was measured. Then, LOV-ipaA was added to the TAMRA-ipaA-viculinD1 reaction, and the dissociation of vinculinD1 from TAMRA-ipaA-vinculinD1 along with the formation of the LOV-ipaA-vinculinD1 complex was observed over time through the decrease of fluorescence polar. The experiment was repeated with six different concentrations of LOV-ipaA. Experiments were fit simultaneously for the on rate and binding affinity of LOV-ipaA to vinculinD1 in Matlab using a numerical integration protocol.

The same concentrations of LOV-ipaA under either blue light irradiation or dark state conditions yielded very different kinetic curves. The figure below illustrates a global fit for LOV-ipaA WT under dark and blue light conditions, respectively. Plots of the fraction of TAMRA-ipaA bound to vinculinD1 over time are shown (Figure 3.3). Five to ten times more LOV-ipaA WT was used under dark conditions than under blue light to reach roughly the same fraction of TAMRA-ipaA peptide bound to vinculinD1. These results were globally fit to determine on rates, off rates and binding affinities (Table 3.2). The binding affinity of LOV-ipaA WT in the light is 3.5 nM, while it is 69 nM in the dark, a 19-fold change. Interestingly, the on rate of binding is extremely slow under both dark and blue light conditions, on the order of 1×10^{3} or 1×10^{4} M^{-1} s^{-1}. The slow k_{on} rates require hours of reaction time for the competition assay to reach steady state, indicating why it was challenging for us to measure these rates under steady state conditions. The off rates of the reactions seem to be unchanged

between lit and dark state measurements, remaining around 5×10^{-5} s^{-1} to 9×10^{-5} s^{-1}. In fact, most of the change in the binding affinity between lit and dark states seems to be contributed by an order of magnitude change in the reaction k_{on} rates of the two states, slowing from

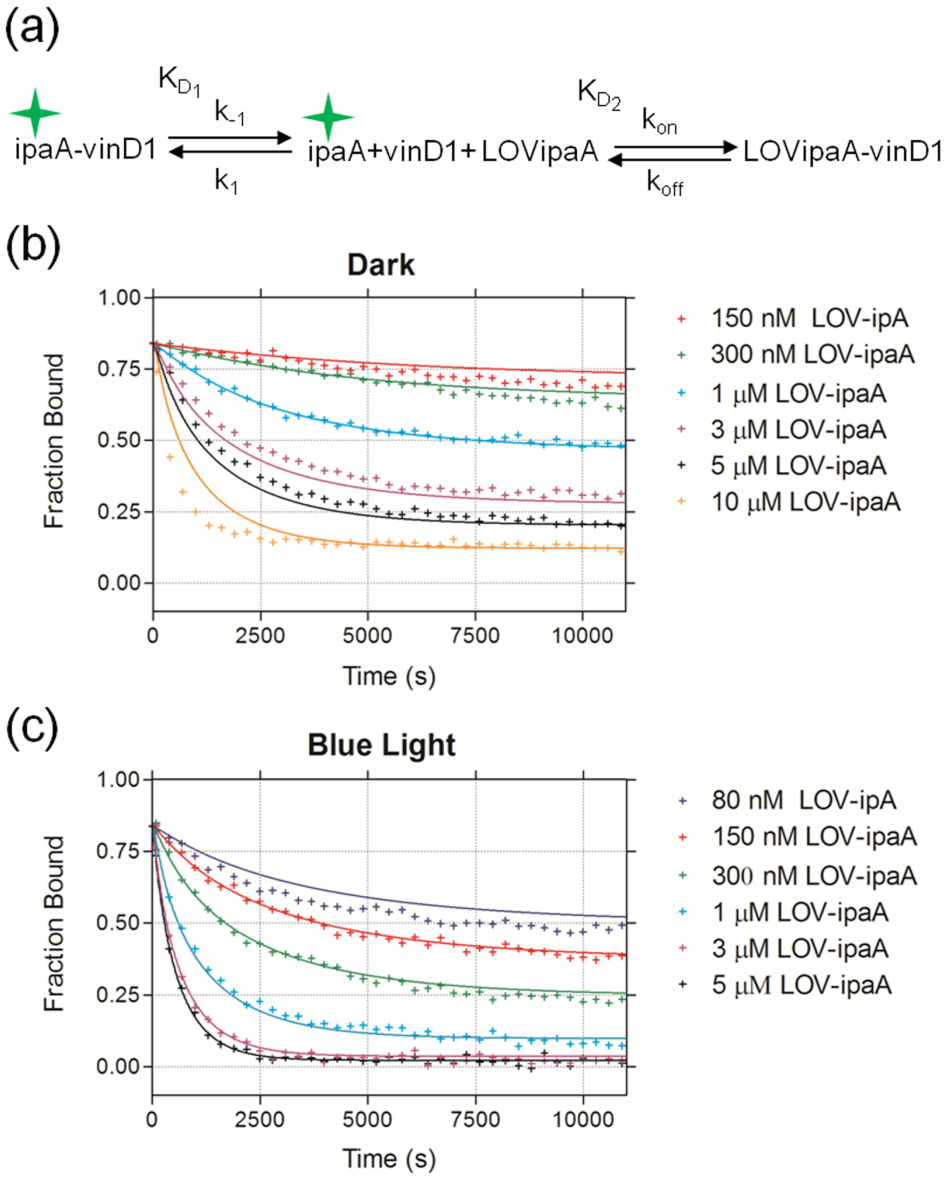

Figure 3.3: Fluorescence polarization competition assay (a) TAMRA labeled ipaA (ipaA*) is bound to vinculinD1 subdomain (vinD1). Vinculin dissociates from the complex with rates k_{-1}, k_1 and binding affinity K_{D1}. LOV-ipaA (LOVipaA) binds vinculin with rates k_{on}, k_{off} and affinity K_{D2}. Fluorescence polarization decreases as the fraction of TAMRA-ipaA bound to vinculin decreases. (b) Fraction of TAMRA-ipaA bound to vinculin over time with varying concentrations of LOV-ipaA titrated in the dark and (c) under blue light.

around 1×10^4 M^{-1} s^{-1} in the lit state to 1×10^3 M^{-1} s^{-1} in the dark state. This was seen for both LOV-ipa WT protein under dark and blue light conditions as well as for LOV-ipaA mutants that either abolish FMN-thiol bond formation (C450A) and lead to a pseudo dark state (32) or mutants that destabilized the Jα helix (A532E I536E), causing a pseudo lit state conformation (33).

Next, we tested two sets of mutations predicted to change the dynamic range of the LOV-ipa photoswitch. The first set, L514K L531E was designed using the interactive protein folding game FoldIt (34). This set of mutations replaces two hydrophobic residues, one in the Jα helix, and the other on the β-sheet contacting the Jα helix, with a salt bridge. The design is meant to stabilize interactions between the β-sheet and Jα helix and so lead to a more tightly bound helix within the protein dark state. Indeed, the binding affinity of LOV-ipaA L514K L531E to vinculinD1 in the dark state weakened to 245 nM, while the lit state affinity increased only slightly, to 5 nM (Table 3.2). This set of mutations makes LOV-ipaA a photoswitch with a 49-fold dynamic range between lit state and dark state effector binding. The second set of mutations we tested were designed by Strickland *et al.* to stabilize the helical structure of Jα (18). The mutations, G528A and N538E, increased the dynamic range of the LOV-TAP photoswitch for its effector from 5-fold to 70-fold. When used in the LOV-ipaA system, the mutations did have a large effect on LOV-ipaA dark state binding to vinculinD1, decreasing affinity more that 7-fold to 475 nM (Table 3.2). However, the mutations also weakened lit state binding affinity over 10-fold, to 110 nM. The net effect of the G528A and N538E mutations in LOV-ipaA then, was a decrease in the photoswitching dynamic range of the protein.

To independently validate results from the florescence polarization competition assay, surface plasmon resonance experiments were conducted (Figure 3.4). The on rate, off rate, and binding affinity of vinculinD1 to LOV-ipaA L514K L531E was measured using this method. Since light cannot be controlled in the Biacore 2000 surface plasmon resonance machine (SPR), LOV-ipaA L514K L531E pseudo lit (A532E I536E) and pseudo dark (C450A) states were used. Pseudo-dark state LOV-ipaA L514K L531E was able to bind vinculinD1 with an on rate of 4.5×10^2 M^{-1} s^{-1} and an off rate of 2.9×10^{-5} s^{-1}. A binding affinity of 64 nM was calculated from the kinetic data. The on rate was identical to that measured for LOV-ipaA L514K L531E un-

LOV-ipaA Construct	k_{on} M^{-1} s^{-1}	k_{off} s^{-1}	K_D (nM)
Dark Mimetic (C450A)	$1.3 \pm 0.3 \times 10^3$	$8.0 \pm 0.7 \times 10^{-5}$	64 ± 9.5
WT Dark	$1.4 \pm 0.1 \times 10^3$	$9.6 \pm 0.1 \times 10^{-5}$	69 ± 0.5
Lit Mimetic (A532E I536E)	$2.9 \pm 0.2 \times 10^4$	$8.5 \pm 0.3 \times 10^{-5}$	3.0 ± 1.0
WT Blue Light	$1.3 \pm 0.3 \times 10^4$	$4.5 \pm 1.2 \times 10^{-5}$	3.5 ± 0.5
L514K L531E Dark	$4.5 \pm 1.5 \times 10^2$	$1.1 \pm 0.4 \times 10^{-4}$	245 ± 5.0
L514K L531E Blue Light	$2.5 \pm 0.1 \times 10^3$	$1.3 \pm 0.1 \times 10^{-5}$	5.0 ± 0.1
G528A N538E Dark	$1.8 \pm 0.3 \times 10^2$	$8.2 \pm 0.2 \times 10^{-5}$	475 ± 75
G528A N538E Blue Light	$8.0 \pm 2.0 \times 10^2$	$1.2 \pm 0.1 \times 10^{-4}$	160 ± 40

Table 3.2: Kinetic rates and binding affinities of LOV-ipaA binding to vinculinD1. k_{on} k_{off}, and K_D rates of varying LOV-ipaA mutants binding vinculinD1 were measured using a fluorescence polarization competition assay.

der dark state condition using the fluorescence polarization assay. The off rate varied slightly, leading to a 4-fold difference in binding affinity between the two measurements. In part, the discrepancy might be due to the fact that it is quite difficult to fit an off rate that is so slow. Measuring the LOV-ipaA L514K L531E pseudo lit photoswitch binding to vinculinD1, an on rate of 3.8×10^4 M^{-1} s^{-1} and an off rate of 8.7×10^{-5} s^{-1} were obtained. The binding affinity was fit to be 2.3 nM. These numbers corresponded well to the kinetic rates measured for LOV-ipaA lit mimetic using the fluorescence polarization assay. SPR data, then, confirmed kinetic measurements obtained from the fluorescence polarization competition assay.

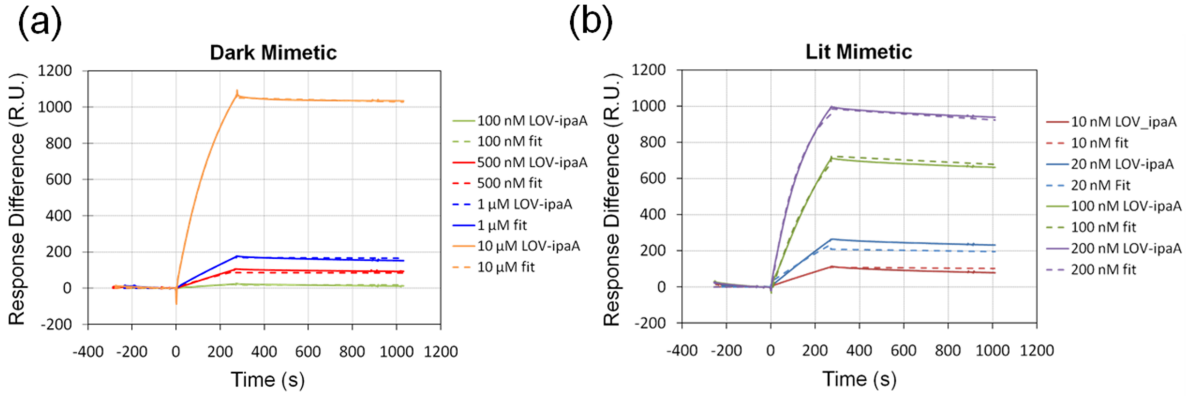

Figure 3.4: Surface plasmon resonance measurements and fits of vinculinD1 binding to (a) LOV-ipaA L514K L531E C450A pseudo-dark and (b) LOV-ipaA L514K L531E A532E I53E pseudo-lit mutants.

3.4.4 Binding to full-length Vinculin: actin co-sedimentation assays

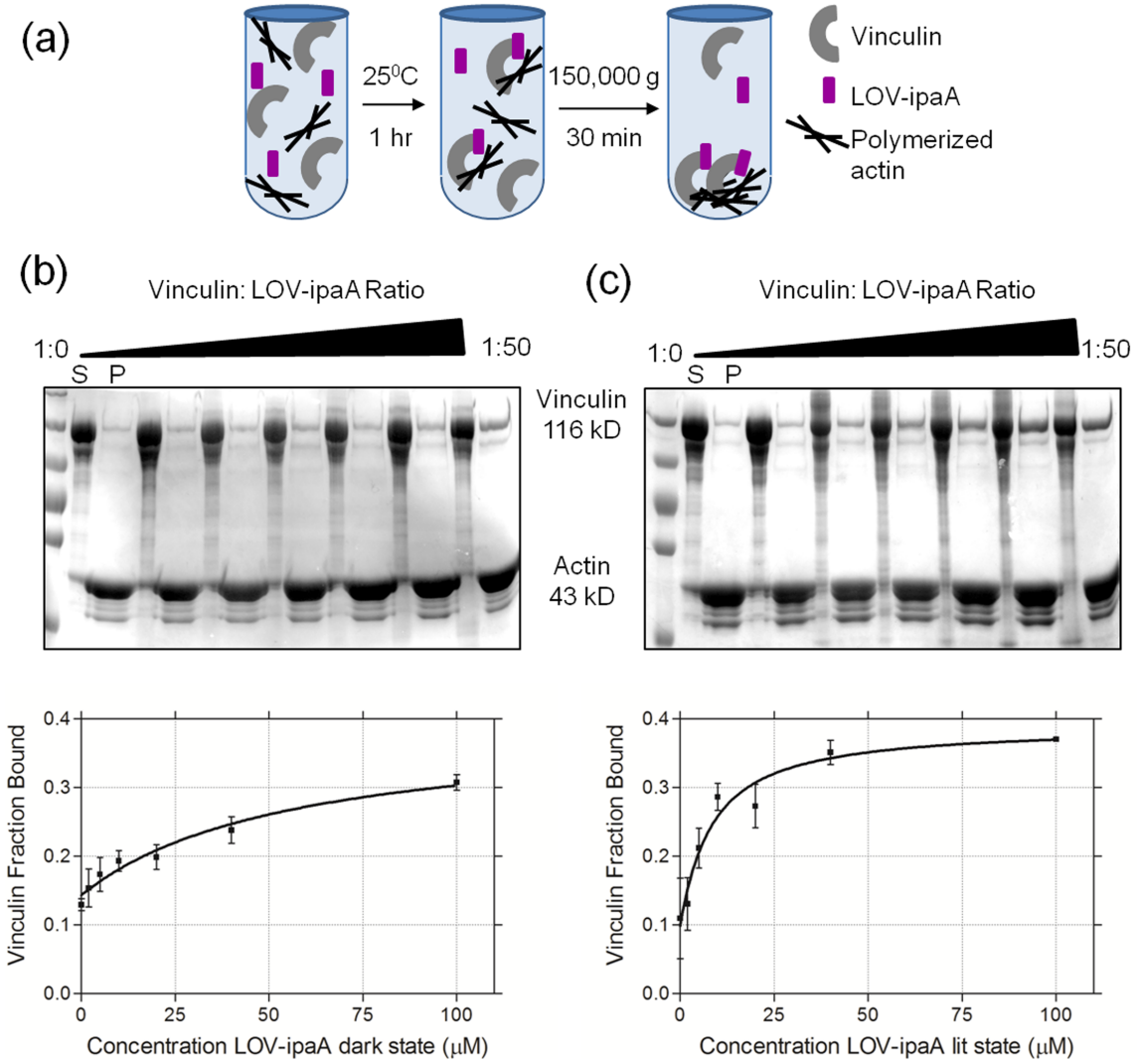

Figure 3.5: Actin co-sedimentation assay (a) Full-length vinculin, LOV-ipaA, and polymerized actin are incubated 1 hr at room temperature. Vinculin that is bound to LOV-ipaA will bind polymerized actin. The mixture is centrifuged at 150,000 g, pelleting polymerized actin and all vinculin bound to it out of solution. (b) SDS-page gel of LOV-ipaA C450A and (c) LOV-ipaA A532E I536E actin co-sedimentation assay with vinculin. Molar ratios from 1:0 to 1:50 vinculin:LOV-ipaA were used. Supernatant (S) and pellet (P) fractions are shown side by side. Apparent binding affinity curves of fraction of vinculin bound to actin v. concentration of LOV-ipaA are plotted below.

Actin co-sedimentation assays were performed to measure the apparent binding affinity of LOV-ipaA to full-length vinculin. Full-length vinculin is able to interact through its head

domain to bind ipaA; this releases the vinculin tail domain to bind with polymerized f-actin. In the actin co-sedimentation assay, polymerized actin, vinculin, and LOV-ipaA were incubated together (Figure 3.5). Only vinculin that has bound to LOV-ipaA should be able to interact and bind to f-actin. The resulting mix of bound and unbound vinculin was centrifuged at high speeds, resulting in fractionation of f-actin polymers out of solution, along with the vinculin-LOV-ipaA complexes that had bound to them. By measuring on an SDS-page gel the amount of vinculin that fractionated out of solution along with f-actin versus the total concentration of vinculin, we obtained the fraction of full-length vinculin bound to LOV-ipaA. By repeating the assay with increasing concentrations of LOV-ipaA, a binding curve of vinculin fraction bound to LOV-ipaA versus concentration of LOV-ipaA was plotted. The figure below illustrates the SDS-page gel of an assay with concentrations of LOV-ipaA pseudo dark mutant C450A added in molar ratios from 1:0 to 1:50 of vinculin:LOV-ipaA. Supernatant (S) and pellet (P) fractions of each molar ratio sample are side by side. The resulting binding curve and plot is drawn below the gel. The co-sedimentation assay performed with LOV-ipaA C450A pseudo dark state mimetic mutant, contrasts greatly with the gel and analysis of a co-sedimentation assay performed with LOV-ipaA A532E I536E, the pseudo lit state mutant. Gels clearly show more vinculin in the pellet fractions of the LOV-ipaA A532E I536E as the molar ratio of vinculin to lov-ipaA increased. The binding curves for the two mutants show these differences.

LOV-ipaA Mutant	K_D (μM)	Error (μM)
IpaA Peptide	7.8	1.3
Dark Mimetic (C450A)	54	12
Lit Mimetic (A532E I536E)	7.4	2.3
L514K L531E Dark Mmetic	116	34
L514K L531E Lit Mimetic	8.15	2.1
G528A N538E Dark Mimetic	315	81
G528A N538E Lit Mimetic	12	2.1

Table 3.3: Apparent binding affinity of LOV-ipaA to full-length vinculin. Binding affinities determined from actin co-sedimentation assays are listed.

We fit the binding curves generated from SDS-page gels to calculate apparent binding affinities of full-length vinculin to LOV-ipaA mutants (Table 3.3). The equation chosen to fit

the curves relates vinculin binding affinity to fraction of vinculin bound to LOV-ipaA. LOV-ipaA pseudo lit state, LOV-ipaA L514K L531E pseudo lit state as well as ipaA peptide all have similar apparent biniding affinities to full-length vinculin, about 8 μM. In contrast, all dark state mimetic mutants bound vinculin with an affinity of at least 50 μM, 6-fold weaker, indicating the difference between dark state and lit state binding held for full-length vinculin as well as for assays involving the D1 domain alone. The binding of vinculin to ipaA in the presence of polymerized actin also gives us a window into the reactions that occur *in vivo*, where full-length vinculin must be bound both by ipaA and by f-actin. The difference in binding affinity between lit and dark states of LOV-ipaA to full-length vinculin in the presence of polymerized actin suggests that LOV-ipaA may have photoswitching abilities *in vivo*.

3.4.5 LOV-ipaA fast and slow reversion mutations

Mutations that slow down or speed up the reversion from lit state to dark state in the LOV2 domain were also tested in the LOV-ipaA photoswitch (Figure 3.6). These mutations, I427V and V416I L496I were previously designed and characterized within the LOV2 domain (35; 17). The mutation I427V was found to decrease LOV2 reversion half life from 27 s to 4 s. Indeed, when tested within the LOV-ipaA photoswitch, spectrophotometric experiments indicated the FMN absorption spectrum changes from the initial lit state to dark state within 45 s. When measuring absorbance at 450 nm, we found that the FMN-thiol bond breaks and is reverted with a half-life of 4 s. Circular dichroism data on the mutant also indicated that the helical structure increased as the protein reverted from dark state to lit state. Both 207 nm and 222 nm absorbance spectra indicated a half-life for the helix reversion of 4 s, consistent with the FMN-thiol bond reversion experiments. Mutations V416I L496I in the LOV2 domain were previously reported to lengthen the FMN lit state to dark state reversion lifetime. When the mutations were made in LOV-ipaA, the lit state and dark state spectra maintained the same peaks as LOV-ipaA WT. The reversion half life was measured to be 10 minutes.

While the lit state to dark state reversion lifetimes for the I427V and V416I L496I mutations in the LOV2 domain had been previously reported, no work has been done on identifying how

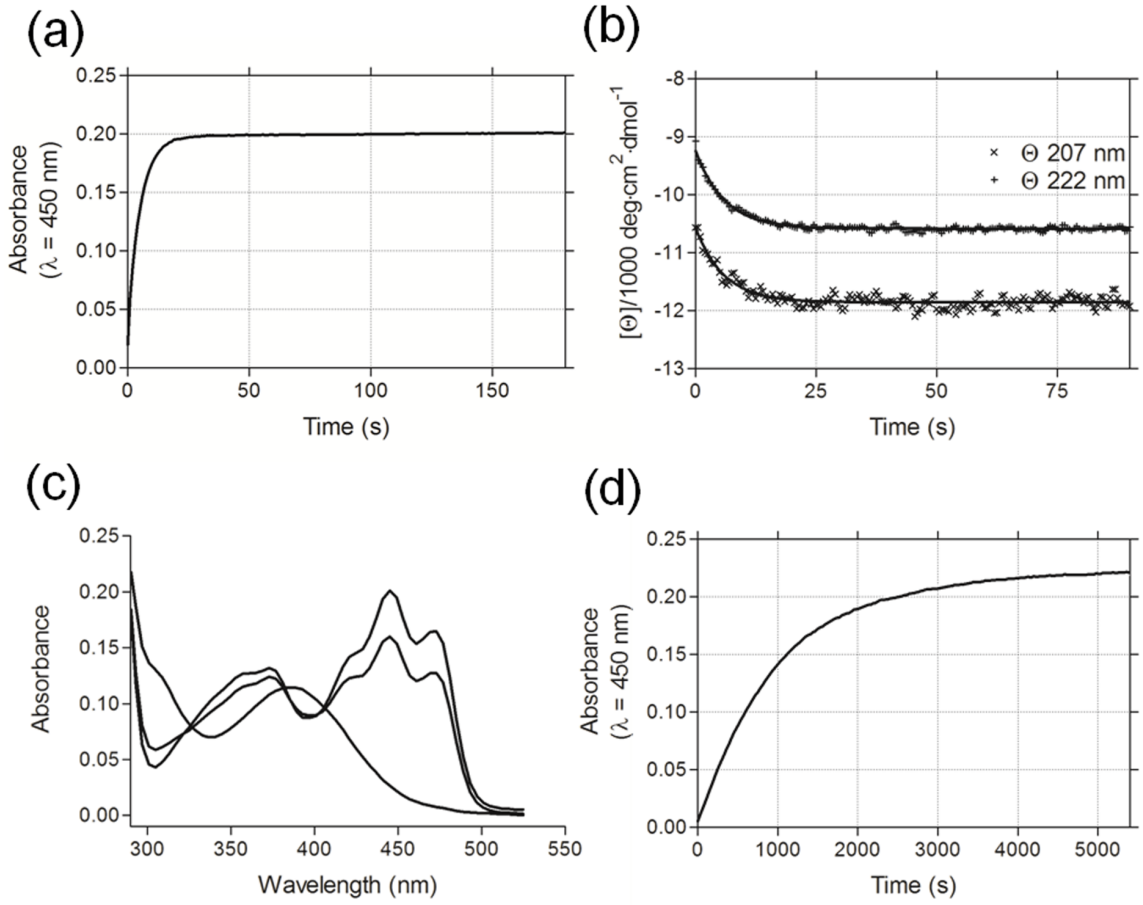

Figure 3.6: Photoswitching characterization of LOV-ipaA I427V and V416I L496I (Photoswitching characterization of LOV-ipaA V416I L496I. (a) LOV-ipaA I427V FMN absorbance at 450 nm over time as LOV-ipaA reverts from lit state to dark state. Reversion half-life was measured to be 4 s (b). LOV-ipaA I427V residue molar ellipticity at 207 nm and 222 nm over time as LOV-ipaA reverts from lit state to dark state. Half-life was measured to be 4 s (c) LOV-ipaA V416I L496I FMN absorbance v. wavelength spectrum as LOV-ipaA reverts from lit state (0 s) to dark state (5400 s). (d) LOV-ipaA V416I L496I FMN absorbance at 450 nm over time as LOV-ipaA reverts from lit state to dark state. Reversion half-life was measured to be 10 min.

these mutations change the dynamic range of LOV2. In order to do so, we examined the binding affinity and kinetics of LOV-ipaA fast reversion (I427V) and slow reversion (V416I L496I) mutants to vinculinD1 (Table 3.4). For both mutants, the off rate was on the order of 1×10^{-4} s^{-1} in both the dark and lit states, similar to LOV-ipaA WT. The on rates stayed around 1×10^{3} M^{-1} s^{-1} in the dark state and 1×10^{4} M^{-1} s^{-1} in the lit state. Binding affinities for both mutants in the dark were close to those measured for WT LOV-ipaA in the dark.

LOV-ipaA Construct	k_{on} M^{-1} s^{-1}	k_{off} s^{-1}	K_D (nM)
I427V Dark	$1.6 \pm 0.3 \times 10^3$	$1.1 \pm 0.1 \times 10^{-4}$	78 ± 13
I427V Blue Light	$1.3 \pm 0.1 \times 10^4$	$1.2 \pm 0.1 \times 10^{-4}$	9.5 ± 1.5
V416I L496I Dark	$4.0 \pm 0.1 \times 10^3$	$2.0 \pm 0.4 \times 10^{-4}$	50 ± 10.0
V416I L496I Blue Light	$1.3 \pm 0.2 \times 10^4$	$1.2 \pm 0.1 \times 10^{-4}$	10.0 ± 0.5

Table 3.4: Kinetic parameters for LOV-ipaA altered lifetime mutations. k_{on} k_{off}, and K_D rates of varying LOV-ipaA mutants binding vinculinD1 were measured using a fluorescence polarization competition assay.

Binding affinities of both mutants under blue light to vinculinD1 were slightly weaker than those for LOV-ipaA WT under blue light, falling about 3-fold, from 3.5 nM to about 10 nM. This led to a slightly diminished dynamic range for the switches, from 19-fold to 5 to 8-fold for slow reversion and dark reversion mutations, respectively. These results indicate that the slow and fast reversion mutations on LOV2 can be used in photoswitches to regulate the amount of time the photoswitch is active while maintaining switching behavior.

3.5 Discussion

We have designed a photoswitchable peptide using the blue light switching properties of the LOV2 domain. The photoswitch, LOV-ipaA, incorporates both residues from the LOV2-Jα helix and ipaA peptide into a chimera helical sequence. This allows for enhanced binding of ipaA effector vinculinD1 subdomain under blue light conditions, while maintaining the LOV2 domain ability to photoconvert. LOV-ipaA binds vinculin with 20-fold enhanced affinity under blue light conditions than in the dark. Mutations L514K L531E on the LOV2 domain strengthened contacts between the Jα helix and PAS fold β-sheet through the addition of a salt bridge and enhanced the dynamic range of LOV-ipaA to binding to vinculinD1 to nearly 50-fold. Turning LOV-ipaA on also led to the activation of full-length vinculin, allowing full-length vinculin to bind polymerized actin, a biologically important event in cell motility. Mutations that altered the half-life of LOV-ipaA reversion from lit to dark state did not affect its binding kinetics to vinculinD1.

The kinetics of LOV-ipaA binding to the vinculinD1 subdomain were measured for both dark and blue light activating conditions. Interestingly, off rates for LOV-ipaA WT and

mutants binding vinculinD1 were measured to be around 1×10^{-4} s^{-1}, regardless of the LOV-ipaA activation state. This indicates the interaction between ipaA and vinculin is the main contributor to the slow off kinetics of the LOV-ipaA photoswitch. One reason the off rate for ipaA- vinculin interaction may be so slow is the nature of the binding that takes place between the two proteins. It is thought that ipaA and other vinculin binding proteins bind the D1 subdomain groove through a helix addition interaction, wherein the vinculinD1 4-helix bundle is rearranged into a 5-helix bundle through the addition of ipaA (36). The nature of this protein rearrangement may lead to less reversible vinculin-ipaA binding and hence, slow off rates. The on rates of LOV-ipaA binding to vinculin are, however, highly dependent on the photostate of the LOV2 domain. In the dark, these rates are as slow as 2×10^{2} M^{-1} s^{-1}, while under blue light conditions they are at least an order of magnitude faster. This indicates the principle mechanism of altered binding affinity for LOV-ipaA to vinculin in dark versus blue light states is through a slowdown of on rates when LOV-ipaA is in the dark state. When the LOV2 domain is attached and sterically occluding ipaA-vinculin binding, ipaA is simply available for binding vinculin less of the time in the dark than in the lit state, leading to slower on rates.

The difference in binding affinities between LOV-ipaA in the lit and dark state to vinculinD1 translated into differences in full-length vinculin activity. Through actin co-sedimentation assays, we saw large differences in the amount of LOV-ipaA bound to full-length vinculin in the dark or lit states. This, in turn, led to vinculin binding to full-length actin. This suggests that LOV-ipaA binding to the vinculinD1 subdomain causes a conformational change in vinculin that relieves the autoinhibition between the head and tail domains, thus allowing the tail domain to bind f-actin. Through such a mechanism, ipaA mimics native protein interactions with vinculin, and thus could be used in vivo to as a dominant negative inhibitor of vinculin.

Overall, the LOV-ipaA photoswitch illustrates how a peptide can be caged through direct threading onto the Jα helix. In this manner, LOV-ipaA is a good proof of principle for the caging of peptides. By incorporating the ipaA sequence onto the Ja helix, we can more tightly regulate photoswitching of the peptide. Whereas in engineering PA-Rac, the linkage of the Ja helix to Rac1 had to be fine tuned through many trials in order to achieve the exact orientation

to cage Rac1 in the dark, only the correct alignment of the ipaA and Jα helices were required for dark state caging of ipaA. Even so, the dynamic range of the PA-Rac switch was only 10-fold, whereas by directly harnessing the Jα conformational change, the LOV-ipaA switch had a dynamic range of at least 20-fold. Such a method of photoactivation could further be extended to cage other helical peptides.

By testing on and off rates as well as binding affinities of mutations that speed up or slow down lit state to dark state reversion lifetimes in the LOV2 domain within the LOV-ipaA system, we were able to ascertain how these mutations affect binding between LOV2 domain-based switches and their effectors. We saw that the rates of the photoswitch binding to vinculin in both the lit and dark remained unchanged in comparison to the 27 s half life LOV2 previously tested, indicating these mutations do not alter dynamic range of switches utilizing the LOV2 domain. This result has broader implications for all switches using the LOV2 domain, indicating the altered lifetime mutations could potentially be used in photoswitches for experiments where desired outcomes are on longer or shorter timescales than possible using the unaltered LOV2 domain without leading to deleterious decreases of the switches' dynamic range.

REFERENCES

1. Levskaya, A., Weiner, O., Lim, W., and Voigt, C. (2009) Spatiotemporal control of cell signalling using a light-switchable protein interaction. Nature **461**, 997–1001

2. Yazawa, M., Sadaghiani, A., Hsueh, B., and Dolmetsch, R. (2009) Induction of protein-protein interactions in live cells using light. Nature biotechnology **27**, 941–945

3. Wu, Y., Frey, D., Lungu, O., Jaehrig, A., Schlichting, I., Kuhlman, B., and Hahn, K. (2009) A genetically encoded photoactivatable rac controls the motility of living cells. Nature **461**, 104–108

4. Kennedy, M., Hughes, R., Peteya, L., Schwartz, J., Ehlers, M., and Tucker, C. (2010) Rapid blue-light-mediated induction of protein interactions in living cells. Nature Methods

5. Möglich, A. and Moffat, K. (2010) Engineered photoreceptors as novel optogenetic tools. Photochem. Photobiol. Sci.

6. Moglich, A., Yang, X., Ayers, R., and Moffat, K. (2010) Structure and function of plant photoreceptors. Annual Review of Plant Biology **61**, 21–47

7. Strickland, D., Moffat, K., and Sosnick, T. (2008) Light-activated dna binding in a designed allosteric protein. Proceedings of the National Academy of Sciences **105**, 10709

8. Lee, J., Natarajan, M., Nashine, V., Socolich, M., Vo, T., Russ, W., Benkovic, S., and Ranganathan, R. (2008) Surface sites for engineering allosteric control in proteins. Science **322**, 438

9. Huala, E., Oeller, P., Liscum, E., Han, I., Larsen, E., and Briggs, W. (1997) Arabidopsis NPH1: a protein kinase with a putative redox-sensing domain. Science **278**, 2120

10. Crosson, S. and Moffat, K. (2001) Structure of a flavin-binding plant photoreceptor domain: insights into light-mediated signal transduction. Proceedings of the National Academy of Sciences **98**, 2995

11. Harper, S., Neil, L., and Gardner, K. (2003) Structural basis of a phototropin light

switch. Science **301**, 1541

12. Halavaty, A. and Moffat, K. (2007) N-and C-terminal flanking regions modulate light-induced signal transduction in the LOV2 domain of the blue light sensor phototropin 1 from Avena sativa. Biochemistry **46**, 14001–14009

13. Swartz, T., Corchnoy, S., Christie, J., Lewis, J., Szundi, I., Briggs, W., and Bogomolni, R. (2001) The photocycle of a flavin-binding domain of the blue light photoreceptor phototropin. Journal of Biological Chemistry **276**, 36493

14. Crosson, S. and Moffat, K. (2002) Photoexcited structure of a plant photoreceptor domain reveals a light-driven molecular switch. The Plant Cell Online **14**, 1067

15. Swartz, T., Wenzel, P., Corchnoy, S., Briggs, W., and Bogomolni, R. (2002) Vibration spectroscopy reveals light-induced chromophore and protein structural changes in the lov2 domain of the plant blue-light receptor phototropin 1. Biochemistry **41**, 7183–7189

16. Harper, S., Neil, L., Day, I., Hore, P., and Gardner, K. (2004) Conformational changes in a photosensory LOV domain monitored by time-resolved NMR spectroscopy. Journal of the American Chemical Society **126**, 3390–3391

17. Zoltowski, B., Vaccaro, B., and Crane, B. (2009) Mechanism-based tuning of a LOV domain photoreceptor. Nature Chemical Biology **5**, 827–834

18. Strickland, D., Yao, X., Gawlak, G., Rosen, M., Gardner, K., and Sosnick, T. (2010) Rationally improving lov domain-based photoswitches. Nature methods **7**, 623–626

19. Fan, H., Morgan, S., Brechun, K., Chen, Y., Jaikaran, A., and Woolley, G. (2011) Improving a designed photo-controlled DNA-binding protein. Biochemistry

20. Izard, T., Tran Van Nhieu, G., and Bois, P. (2006) Shigella applies molecular mimicry to subvert vinculin and invade host cells. The Journal of cell biology **175**, 465

21. Saunders, R., Holt, M., Jennings, L., Sutton, D., Barsukov, I., Bobkov, A., Liddington, R., Adamson, E., Dunn, G., and Critchley, D. (2006) Role of vinculin in regulating focal adhesion turnover. European journal of cell biology **85**, 487–500

22. Carisey, A. and Ballestrem, C. (2010) Vinculin, an adapter protein in control of cell adhesion signalling. European Journal of Cell Biology

23. Borgon, R., Vonrhein, C., Bricogne, G., Bois, P., and Izard, T. (2004) Crystal structure of human vinculin. Structure **12**, 1189–1197

24. Bakolitsa, C., Cohen, D., Bankston, L., Bobkov, A., Cadwell, G., Jennings, L., Critchley, D., Craig, S., and Liddington, R. (2004) Structural basis for vinculin activation at sites of cell adhesion. Nature **430**, 583–586

25. Cohen, D., Kutscher, B., Chen, H., Murphy, D., and Craig, S. (2006) A conformational switch in vinculin drives formation and dynamics of a talin-vinculin complex at focal adhesions. Journal of Biological Chemistry **281**, 16006

26. Bois, P., Borgon, R., Vonrhein, C., and Izard, T. (2005) Structural dynamics of {alpha}-actinin-vinculin interactions. Molecular and cellular biology **25**, 6112

27. Ziegler, W., Liddington, R., and Critchley, D. (2006) The structure and regulation of vinculin. Trends in cell biology **16**, 453–460

28. Izard, T., Evans, G., Borgon, R., Rush, C., Bricogne, G., and Bois, P. (2003) Vinculin activation by talin through helical bundle conversion. Nature **427**, 171–175

29. Grashoff, C., Hoffman, B., Brenner, M., Zhou, R., Parsons, M., Yang, M., McLean, M., Sligar, S., Chen, C., Ha, T., et al. (2010) Measuring mechanical tension across vinculin reveals regulation of focal adhesion dynamics. Nature **466**, 263–266

30. Das, R. and Baker, D. (2008) Macromolecular modeling with rosetta. Annu. Rev. Biochem. **77**, 363–382

31. Le Clainche, C., Dwivedi, S., Didry, D., and Carlier, M. (2010) Vinculin is a dually regulated actin filament barbed end-capping and side-binding protein. Journal of Biological Chemistry **285**, 23420

32. Salomon, M., Christie, J., Knieb, E., Lempert, U., and Briggs, W. (2000) Photochemical and mutational analysis of the FMN-binding domains of the plant blue light receptor, phototropin. Biochemistry **39**, 9401–9410

33. Harper, S., Christie, J., and Gardner, K. (2004) Disruption of the LOV-Jα helix interaction activates phototropin kinase activity. Biochemistry **43**, 16184–16192

34. Cooper, S., Khatib, F., Treuille, A., Barbero, J., Lee, J., Beenen, M., Leaver-Fay, A., Baker, D., Popović, Z., et al. (2010) Predicting protein structures with a multiplayer

online game. Nature **466**, 756–760

35. Christie, J., Corchnoy, S., Swartz, T., Hokenson, M., Han, I., Briggs, W., and Bogomolni, R. (2007) Steric interactions stabilize the signaling state of the lov2 domain of phototropin 1. Biochemistry **46**, 9310–9319

36. Van Nhieu, G. and Izard, T. (2007) Vinculin binding in its closed conformation by a helix addition mechanism. The EMBO journal **26**, 4588–4596

CHAPTER 4

INDUCING PHOTOACTIVATABLE GENE EXPRESSION IN BUDDING YEAST USING LOV-IPAA

4.1 Summary

Photoactivation of protein-protein interactions is a powerful tool for manipulating signaling pathways and phenotypic responses. We demonstrate the use of the LOV-ipaA photoswitch to induce gene expression by blue light. LOV-ipaA binds the vinculinD1 subdomain with an enhanced affinity of 2.4 μM under blue light, allowing for light-induced heterodimerization of the two proteins. When introduced into a yeast-two hybrid system, this heterodimerization interaction brings together the GAL4 activation and binding domains, allowing for photoactivatable induction of yeast reporter gene expression. The light-inducible heterodimerization system was used to induce overexpression of Ste4 and Gpa1, two genes critical to yeast pheromone response pathway. Phenotypic and biochemical responses are obsereved as a result.

4.2 Introduction

Photoacivation of protein-protein interactions is a valuable tool for studying signaling networks in cells (1; 2; 3; 4). This technology allows one to perturb cellular processes in a precise spatial and temporal manner, thus enabling fine control over when and how a signaling cascade is activated (5). Naturally-occurring light-sensitive proteins have been successfully used for genetically encoded, reversible photoacivation of interactions in signaling networks (6).

One of the most predominant manners in which naturally occurring light-sensitive proteins

have been used to control cell signaling has been through light-induced heterodimerizaion of protein-protein interactions (2; 7; 8). In such heterodimerization photoswitches, A naturally occurring photosensitive protein is linked to a critical signaling protein, while its binding partner is linked to the effector target of the signaling protein. Light irradiation activates the photosensitive protein so that it may then bind its partner, thus bringing into proximity the signaling protein and its effector, enabling activation of a signaling cascade. Such as strategy has been used to photoactivate Rac1-induced ruffling in mammalian cells through the red light absorbing Pif-PhyB protein system (1). This strategy has also been used to photoactivate Cre-Lox DNA recombination using the blue light sensing Cryptochrome2 protein and its binding partner CIB1 (4). Both of these systems make use of large, difficult to express proteins as light sensing domains. Clear knowledge of their structures and light sensing systems is lacking, thus presenting challenges to their broader applicability.

In this work, we discuss use of the LOV2 domain for light-activated heterodimerizaion. To our knowledge, this is the first system that has used the LOV2 domain for such a purpose. The LOV2 domain is part of the PAS superfamily of domains (9) and is found in higher plants (10). A flavin mononucleotide (FMN) co-factor located in the center of the PAS fold absorbs photon of blue light, converting this energy into the formation of a covalent adduct between a cysteine side chain in the PAS fold and a carbon atom of the FMN (11; 12) A large helix extends C-terminal to the fold, termed the Jα helix (13; 14). NMR and spectroscopy studies indicate this leads to a large conformational change in the domain, including the unfolding of the Jα helix (15; 16). When irradiation ceases, reversion of the thiol bond and conformational change back into the dark state occurs spontaneously (17).

We have used the previously designed LOV-ipaA photoswitch to photoactivate gene expression in *S. cerevisiae* organisms. LOV-ipaA was previously characterized to bind the vinculin D1 subdomain (vinD1) with low nanomolar affinity under blue light irradiation, and high nanomolar affinity in dark conditions. We weakened the affinity of the LOV-ipaA photoswitch for vinD1 to 2.4 μM under blue light conditions, a 500-fold change. We then introduced LOV-ipaA and vinD1 as the two principle components of a photoactivatable heterodimerization system in yeast transcriptional activation. The LOV-ipaA photoswitch was linked to the

GAL4 activation domain, while vinD1 was linked to the GAL4 binding domain. Irradiation with blue light enabled activation of the GAL4 transcriptional activator, leading to expression of reporter genes controlled by the GAL promoter.

We applied light-induced gene transcriptional activation to overexpress two protein critical to the yeast pheromone mating response pathway, Ste4 and Gpa1. Overexpression of Ste4 leads to the activation of the pheromone mating response pathway, while overexpression of Gpa1 inhibits the pathway (18; 19; 20). Traditional methods to induce expression of yeast genes such as galactose induction, or nocodazole use to induce growth arrest, lead to a large stress responses in yeast, activating a substantial portion of the organisms' genomes (21), thus potentially altering responses of signalling networks. Additionally, use of α factor to activate the pheromone mating response pathway is costly. Light induction is an innocuous, cost-effective alternative to such harsh, less-isolated methods of gene expression. Light-induced gene expression has the potential to expand knowledge of yeast G protein signaling.

4.3 Methods

4.3.1 Cloning for *E. coli* expression

The LOV-ipaA gene was synthesized with a 6 histidine N-terminal tag (Genscript) and cloned into the pET21b vector. Mutations on LOV-ipaA were performed using site-directed mutagenesis. VinculinD1 subdomain (residues 1-258) cloned into a pET15b vector was a gift from the Craig lab at Johns Hopkins University.

4.3.2 Protein expression and purification

LOV-ipaA L623A lit mimetic (I532E A536E) and dark mimetic were expressed in *E.coli* strain BL21(DE3) cells (Genese) at 16°C overnight in the dark. Cells were lysed in buffer containing 50 mM sodium phosphate pH 7.5, 150 mM NaCl and 5 mM 2-mercaptoethanol. Proteins were purified by affinity chromatography over HiTrap HisTrap columns (GE) and eluted with 150 mM Imidazole at pH 7.5. The proteins were further purified through size

exclusion chromatography over a Sephadex S75 column (GE) equilibrated with 50 mM sodium phosphate, 150 mM NaCl and 5 mM 2-mercaptoethanol.

VinculinD1 subdomain was expressed in *E.coli* strain BL21(DE3) cells (Stratagene) at 16°C overnight. Cells were lysed in buffer containing 50 mM Tris-HCl pH 8.0, 500 mM NaCl and 5 mM 2-mercaptoethanol. The protein was purified by affinity chromatography over HiTrap HisTrap columns (GE) and eluted with 500 mM Imidazole at pH 8.0. The protein was further purified by ion exchange chromatography using a HiTrap Q column (GE) eluted with a NaCl gradient. VinculinD1 was stored in 20 mM Tris-HCl with 2 mm DTT and 2 mM EDTA.

Protein concentrations for LOV-ipaA and vinculinD1 were determined using Bradford assays (Thermo). Protein concentrations for full-length vinculin were determined using absorbance at 280 nm measurements with an extinction coefficient of 62,000 M^{-1} cm^{-1}.

4.3.3 Illumination

LOV-ipaA WT and mutants were irradiated using a collimated blue LED with maximum emission wavelength of 455 nm (ThorLabs). Illumination power was measured to be 6.8 mW cm^{-2}

4.3.4 Isothermal titration calorimetry

All ITC experiments were performed at UNC-Chapel Hill in the Macromolecular Interaction Facility using a MicroCal Auto-ITC200. Purified LOV-ipaA L623A lit state (A532E I536E), dark state (C450A) mimetics, and vinculinD1 were dialyzed for four hours in 50 mM sodium phosphate, 150 mM NaCl and 5 mM 2-mercaptoethanol buffer. ITC experiments were performed by injecting the dark state mutant C450A of LOV-ipaA L623A (50 μM) or the lit state mutant I532E A536E (50 μM) into vinculinD1 (970 μM) at 25°C. Each titration consisted of 19 injections of 2 μL of LOV-ipaA. The baseline of each titration was determined and subtracted from all of the data points. Titration data for the heat change per injection were fitted to a one-site binding model using Origin software (OriginLab)

4.3.5 Yeast strains and plasmids

LOV-ipaA L623A WT, lit state mutants, dark state mutants, LOV2 domain and ipaA were cloned into a pGADT7 vector (Clonetech), while the vinculinD1 subdomain was cloned into a pGBKT7 vector (Clonetech). Yeast two hybrid and Miller assays were conducted using pGADT7 constructs transformed into *S. cerevisiae* Y187 strain, and pGBKT7 constructs transformed into *S. cerevisiae* Y2Hgold strain (Clonetech). Empty vectors were also transformed into the appropriate strains. For Gpa1 and Ste4 assays, GAL1-Ste4 cloned into a pRS316 vector as well as GAL1-Gpa1 cloned into a pG1501 were a gift from the Dohlman lab at UNC-Chapel Hill. GAL1-Gpa1 or GAL1-Ste4 were triple transformed, along with constructs in pGADT7 and pGBKT7 vectors, into *S. cerevisiae* YPH499 strain for all GAL-Gpa1 and GAL-Ste4 transcription activation experiments.

4.3.6 Yeast two hybrid assays

Transformed colonies of Y2Hgold and Y187 yeast strains were mated at 30°C overnight and plated on synthetic dropout (SD) -Leu -Trp media. Mated colonies were serially diluted (1:5, from right to left on plates shown) and replica plated onto SD -Leu -Trp agar; SD -Leu -Trp agar with auerobasidin A and 5-bromo-4-chloro-3-indolyl-α-D-gactopyranoside (x-α-gal); SD -Leu -Trp -His agar with auerobasidin A and x-α-gal; and SD -Leu -Trp -His -Ade agar with auerobasidin A and x-α-gal. Plates were grown for 3 days at 30°C.

4.3.7 Miller assays

Mated aα colonies were picked and grown to saturation in SD -Leu -Trp media at 30°C. Saturated colonies were diluted to low-log phase and grown for 4 hours under dark or blue light conditions. Cells were lysed open and treated with Chlorophenol red-β-D-galactopyranoside (CPRG) substrate to determine β-galactosidase activity in Miller Units.

4.3.8 Plate growth assays

Transformed colonies were grown to saturation in SD -Leu -Trp -Ura media in the dark . Colonies were serially diluted (1:5) and replica plated onto SD -Leu -Trp -Ura and YPD media. Plates were grown for 3 days at 30°C in blue light or dark conditions. For galactose induction controls, colonies were serially diluted and replica plated onto SD -Leu -Trp -Ura medial containing 2% glucose or 2% galactose, and YPD media as a control. Plates were grown for 3 days at 30°C in dark conditions.

4.3.9 Microscopy

Transformed colonies of the YPH499 yeast strain were picked and grown to saturation in SD -Leu -Trp -Ura media at 30°C in the dark. For galactose induction, colonies were grown in SD 2% raffinose -Leu -Trp -Ura media. Cells were diluted to low-log phase and grown for 6 hours under blue light or dark conditions. Colonies grown in SD 2% raffinose were induced with the addition of 2% galactose. Samples were taken and imaged every hour for 6 hours.

4.3.10 Cell extract preparation and immuno-blotting

Transformed cells expressing AD-LOV-ipaA, BD-vinD1, and GAL-Ste4 were grown in SD -Leu -Trp -Ura media to mid-log phase. Cell cultures were divided in half, and treated with blue light or left in the dark over the course of 120 minutes. Transformed cells expressing AD-empty vector, BD-empty vector, and GAL-Ste4 were grown in SD -Leu -Trp -Ura 2% raffinose media to mid-log phase. Cell cultures were divided in half, and treated with galactose for 0 min or 120 min. Protein extracts were produced by glass bead lysis in trichloroacetic acid (TCA). Protein extract concentrations were determined through DC assays (Bio-Rad), and equal amounts of protein were resolved on 10% SDS-PAGE gels and immunoblotted with Phospho-p44/42 MAPK antibodies (Cell Signaling Technology) at 1:500. Immunoblotted proteins were visualized by chemiluminescent detection (PerkinElmer) of horseradish peroxidase-conjugated antibodies (Bio-Rad). Protein concentration was determined by DC protein assay

(Bio-Rad).

4.3.11 Pheromone halo assays

Transformed colonies of the YPH499 yeast strain were picked and grown to saturation in SD -Leu -Trp -Ura media at 30°C in the dark. Cells from saturation cultures were plated in a lawn of 0.5% top agar on SD -Leu -Trp -Ura plates. For galactose induction, cells were plated on SD 2% galactose -Leu -Trp -Ura plates. Four concentrations of α factor (1.5 μg, 4.5 μg, 15 μg, and 45 μg) were spotted in 15 μL drops on the solidified agar. Plates were grown for 2 days at 30°C in blue light or dark conditions.

4.4 Results

4.4.1 LOV-ipaA L623A Mutation

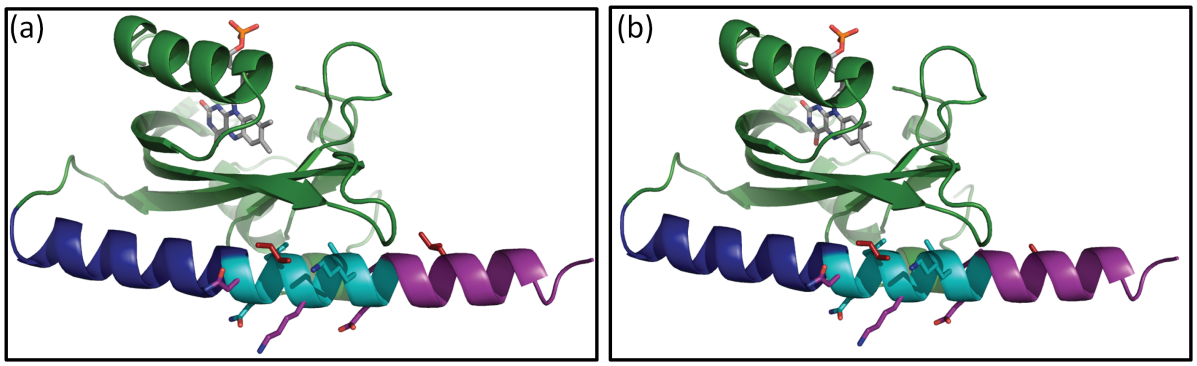

Figure 4.1: LOV-ipaA L623A mutation. (a) Model of LOV-ipaA. Jα residues (blue) ipaA residues (purple), chimera residues (cyan), and designed residues (red) are indicated. (b) Mutation L623A on LOV-ipaA is shown. Residues are colored as in (a).

Originally, the designed LOV-ipaA photoswitch had a dark state binding affinity for vinculinD1 of 65 nM. Mutations L514K L531E increased the dynamic range of the switch by deceasing its affinity for vinculinD1 to 245 nm. This is still a considerably tight affinity. For some applications, it may be useful to have a switch that has weaker binding affinity in the dark. To test if we could switch the range of affinities over which LOV-ipaA functions, we

made a mutation to LOV-ipaA that was predicted to reduce affinity for vinculin, but should have negligible effect on the interactions between the Jα helix and the LOV domain. The mutation, L623A, was located in the section of LOV-ipaA that only interacted with vinculin, and had no interactions with the LOV domain (Figure 4.1).

The L623A mutation weakened the affinity of the LOV-ipaA lit state mimetic (I532E A536E) for the vinculin D1 domain from 3 nM to 2.4 μM, an almost 1000-fold decrease in affinity (Figure 4.2 and Table 4.1). The dark state mimetic (C450A) had no detectable binding as monitored with isothermal titration calorimetry. Considering concentration of proteins used in the study, This suggested that binding in the dark was weaker than 40 μM. In this manner, we were able to dramatically shift the binding affinity of the photoswitch for vinculinD1.

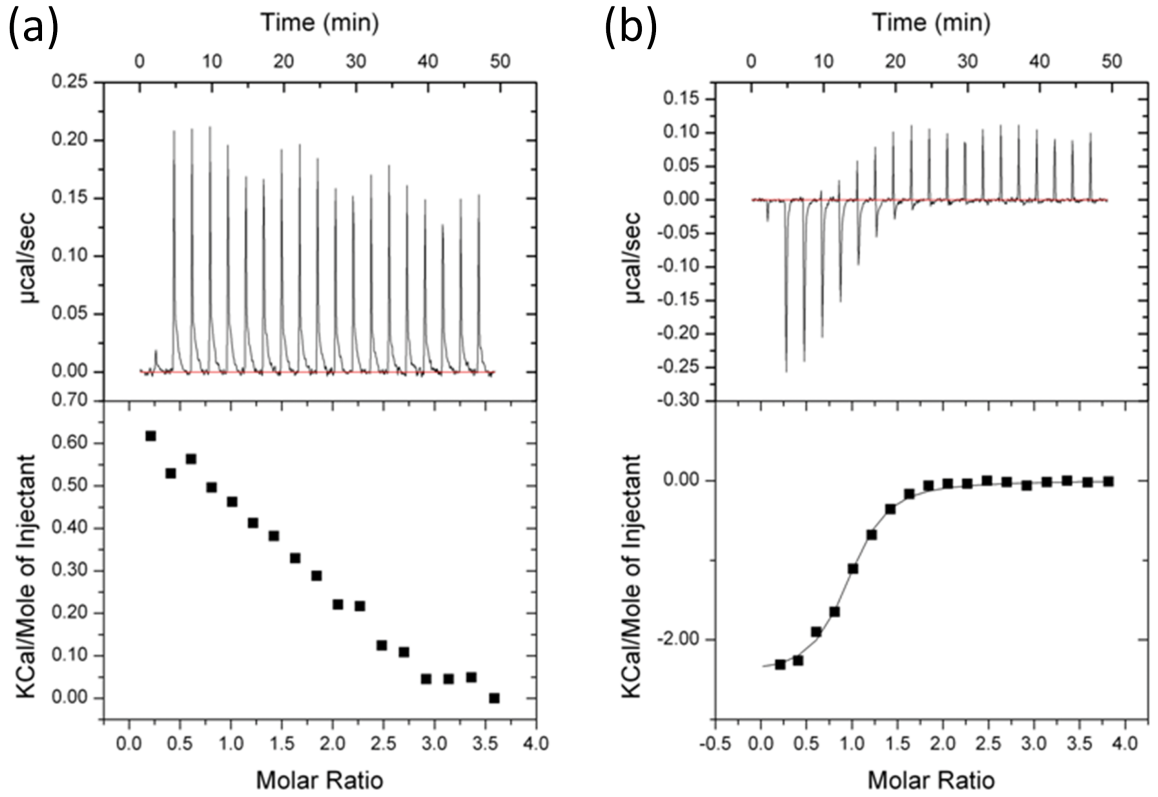

Figure 4.2: ITC of LOV-ipaA L623A mutation binding the vinculinD1 subdomain. (a) dark state LOV-ipaA (C450A) or (b) lit state LOV-ipaA (I532A I536E, right) binding vinculinD1. Both experiments were done with identical amounts and concentrations of protein. Binding affinity of dark state could was too weak to fit. Binding affinity of lit state was determined to be 2.4 μM

LOV-ipaA L623A Lit state mimetic	K_D (μM)	ΔH (Kcal mol^{-1})	ΔS (Kcal mol^{-1} K^{-1})	N
Titration 1	2.0 ± 0.32	-2.4 ± 0.059 $\times 10^3$	18	0.85 ± 0.051
Titration 2	2.4 ± 0.31	-2.5 ± 0.050 $\times 10^3$	17	0.92 ± 0.18

Table 4.1: Binding affinity of LOV-ipaA L623A lit mimetic mutant to vinculinD1. Values measured by ITC for binding affinity, enthalpy, entropy, and molar ratio are listed.

4.4.2 Light-induced yeast two-hybrid interactions

We wanted to test whether we could use the LOV-ipaA-vinculinD1 interaction for light-induced heterodimerization. We chose to do so in *S. cerevisiae*, as it is an orthogonal system, lacking proteins that would cross-react with the LOV-ipaA-vinculinD1 interaction. We linked LOV-ipaA L623A to the GAL4 activation domain (AD), while linking vinculinD1 (vinD1) to the GAL4 binding domain (BD), and monitored the GAL4-induced activation of the transcriptional GAL1 promoter through a yeast two-hybrid assay (Figure 4.3). This is a strategy that has been widely used to identify protein-protein interactions. In our case, LOV-ipaA and vinculinD1 should only interact upon irradiation with blue light, thus bringing the GAL4 AD and BD into proximity. The full GAL4 protein can then activate transcription of reporter genes downstream of the GAL promoter. We tested the ability to activate the reporter gene LacZ under both dark state and lit state conditions through quantification of β-galactosidase activity. We observed a modest activity of 6 Miller Units under blue light conditions, and an activity of 20 Miller Units with substantial activity using the LOV-ipaA L623A lit state mimetic (20 units) and the ipaA peptide as a positive control. Almost no activity (0.4 Miller Units) was seen under dark or dark state conditions, and no activity was seen in empty vector negative controls. We also tested activation of genes MEL1, HIS3, and ADE2 under dark and lit state conditions by replica plating BD-vindD1 colonies mated with AD-LOV-ipaA L623A lit state and dark state mimetic mutants or AD-LOV-ipaA L623A WT. We saw strong growth of colonies containing LOV-ipaA L623A lit mimetic or WT grown in blue light on plates lacking His as well as those lacking His and Ade, indicating transcription of both HIS3 and ADE2 genes. Furthermore, colonies were blue, indicating transcription of the MEL1 gene whose

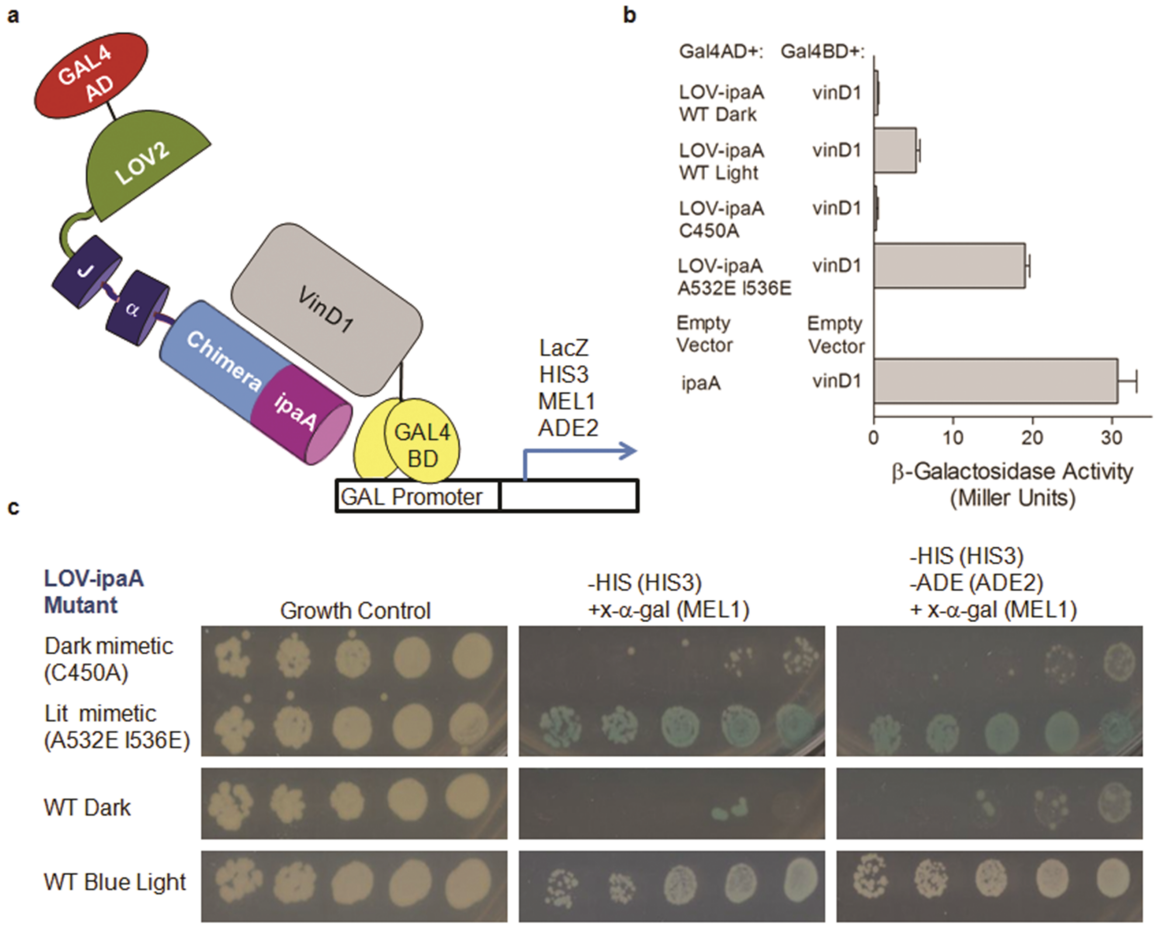

Figure 4.3: LOV-ipaA induces reporter gene transcription under lit state conditions. (a) LOV-ipaA L623A is linked to the GAL4 activation domain (AD), while vinculinD1 (vinD1) is linked to GAL4 binding domain (BD). Irradiation with blue light brings AD-LOV-ipaA into proximity to BD-vinD1, allowing for GAL-induced transcription of reporter genes LacZ, MEL1, HIS2, and ADE2. (b) LacZ transcription is quantified. β galactosidase activity of *S. cerevisiae* mated strains containing BD and AD linked proteins, as specified, is shown. (c) *S. cerevisiae* mated strains containing BD-vinD1 and AD-LOV-ipaA mutants, as indicated, are grown in dark or blue light conditions on SD plates. Difference in levels of transcription of MEL1, HIS3 and Ade2 in dark v. lit state conditions can be seen.

product, α-galactosidase, interacted with the x-α-gal substrate for blue screening. Colonies containing LOV-ipaA L623A dark mimetic or WT grown in the dark grew on control plates, but did not grow on plates lacking His or Ade, showing low to no transcription of HIS2, ADE2 or MEL1 genes. This indicates that LOV-ipaA-vinculinD1 heterodimerization can be used as a tool to photocontrol yeast transcription.

The LOV-ipaA L623A mutation was critical to achieving a lit state to dark state change

of phenotype in yeast transcription. When experiments for MEL1 and HIS3 were conducted using LOV-ipaA lacking this mutation, no observable growth change was seen between colonies containing lit state and dark state AD-LOV-ipaA mated with BD-vinD1. The binding affinity of LOV-ipaA to vinculinD1, was hence, so tight, even in the dark state, as to allow binding events and subsequently yeast transcription to occur. The L623A mutation shifted the binding affinity of LOV-ipaA to vinculinD1 to a range where there was no binding in the dark, but significant activation in the light. This result highlights the usefulness of being able to tune the switches for specific applications.

4.4.3 Photoactivation of Ste4 transcription

We applied the LOV-ipaA-vinculinD1 heterodimerization system in order to photoacitvate transcription of two yeast proteins, Gpa1 and Ste4. Both are part of the pheromone response mating pathway (22). Gpa1 is the α subunit of the yeast mating G protein, while Ste4 is the β subunit (23). In haploid yeast, stimulation of the Ste2 receptor by the peptide mating pheromone released by yeast of the opposite mating type leads the exchange of GDP for GTP in the Gα subunit, allowing for the dissociation of the α subunit (Gpa1) from the $\beta\gamma$ (Ste4 and Ste18, respectively) subunits (23). In yeast of MATa mating type, stimulation with the α-factor peptide WHWLQLKPGQPMY allows for this response to occur. The $\beta\gamma$ subunits may then go on to signal through a mitogen-activated protein kinase (MAPK) cascade encompassing Ste20, Ste11, Ste7, and Fus3 (24). The scaffolding protein Ste5 spatially directs this process by bringing together the three MAPKs Ste11, Ste7, and Fus3. Downstream activation of the MAPK pathway leads to activation of genes responsible for growth arrest in the G1 phase of the cell cycle, the formation of shmoo mating projections, and eventual fusion with MATa type yeast cells to produce diploid strains (25; 26). Inactivation of the pathway occurs as the Gα subunit slowly catalyzes hydrolysis of GTP back to inactive GDP (27).

Overexpression of Ste4 leads to pheromone-independent activation of the mating response pathway (18; 19; 20). This allows for continuous expression of the mating cascade and permanent growth arrest. Overexpression of Gpa1 leads to insensitivity to pheromone response.

Gpa1 sequesters the G β and γ subunits, thus inhibiting activation of the mating cascade.

We attempted to induce pheromone-independent activation of the yeast mating response pathway through blue light. In order to do so, we tested whether we could overexpress Ste4 through light-induced heterodimerization of AD-LOV-ipaA and BD-vinD1.

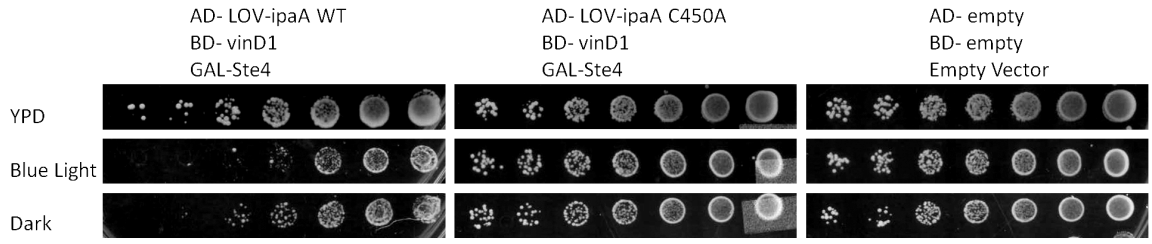

Figure 4.4: LOV-ipaA heterodimerization induces Ste4 expression under blue light. Budding yeast transformed with GAL-Ste4, BD-vinD1, and AD-LOV-ipaA WT or AD-LOV-ipaA C450A (Dark state) were grown under dark (non-inducing) and blue light (inducing) conditions. Resulting growth arrest is seen on serially diluted colonies (1:5, ascending concentrations from left to right). Empty pRS316 vector is used as a control.

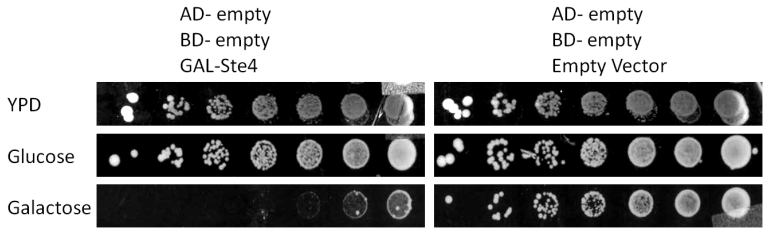

Figure 4.5: Galactose induction of Ste4 expression. Budding yeast transformed with GAL-Ste4 or empty pRS316 vector were grown under glucose (non-inducing) and galactose (inducing) conditions. Resulting growth arrest is seen on serially diluted colonies (1:5, ascending concentrations from left to right).

We tested phenotypic responses to light-induced overexpression of Ste4 through two separate assays. We first looked at the ability to induce growth arrest in yeast cells using blue light. *S. Cerevisiae* cells were transformed with GAL1-Ste4, BD-vinD1, and AD-LOV-ipaA genes, and grown under blue light (inducing) or dark state (non-inducing) conditions for two days. As a control, growth was compared to cells transformed with empty vector versions (pGADT7, pGBKT7, and pRS316) of the genes described. Cultures expressing AD-LOV-ipaA WT serially diluted and grown on plates under blue light conditions showed slightly less growth at the lowest dilutions than those grown under dark conditions (Figure 4.4). Both

colonies grown under dark as well as lit state conditions showed slight growth arrest at the lowest concentrations as compared to those cultures grown on YPD media, possibly indicating leaky expression of Ste4 in the dark state. We repeated the experiment using the AD-LOV-ipaA C450A mutated gene, rendering LOV-ipaA in a pseudo-dark state. We saw no difference in growth of replica plated colonies under YPD, dark, or blue light conditions, indicating no residual overexpression of Ste4 in the dark.

We compared our slight growth arrest to that seen by overexpression of GAL1-Ste4 through galactose induction. Colonies transformed with empty pGADT7 (AD), pGBKT7 (BD), and GAL1-Ste4 were serially diluted, replica plated, and grown on YPD, glucose (non-inducing), and galactose (inducing media) media (Figure 4.5) As a control, growth was compared to cells transformed with the empty vector version of GAL1-Ste4(pRS316). When grown on galactose, colones with containing the GAL1-Ste4 gene experienced substantial growth arrest as compared to those grown on glucose media. This indicated galactose induction of Ste4 overexpression was more robust than that achieved through blue light, either because the induction under blue light condition was dampened, or more transient than that seen under galactose induction.

We next looked at the ability of blue light to induce shmoo formation. Shmoos are elongated structures used for sexual mating. Cell exposed to pheromone will respond by enlarging and elongating in one direction, going from a round to a triangular shape. Yeast colonies transformed with GAL1-Ste4, BD-vinD1, and AD-LOV-ipaA genes were exposed to blue light and their shape was monitored over the course of five hours (Figure 4.6). As a control, cells espressing GAL1-Ste4 were induced by galactose, thus allowing side-by side comparison of the two induction conditions. No yeast colonies initially had the shmoo projectile shape. Over time, after about two hours, the shape became evident in both samples treated with blue light as well as galactose. The shmoo shape predominated in those samples by the end of 2 hrs. In contrast, colonies transformed with GAL1-Ste4, BD-vinD1, and AD-LOV-ipaA C450A lit mimetic genes and exposed to blue light showed no shmoo formation whatsoever. This indicated that shmoo formation was a result of LOV-ipaA-vinD1 heterodimerization interactions.

We also biochemically tested for overexpression of Ste4. Overexpression of Ste4 leads to activation of the mitogen activated protein kinase (MAPK) cascade. Activation of the cascade

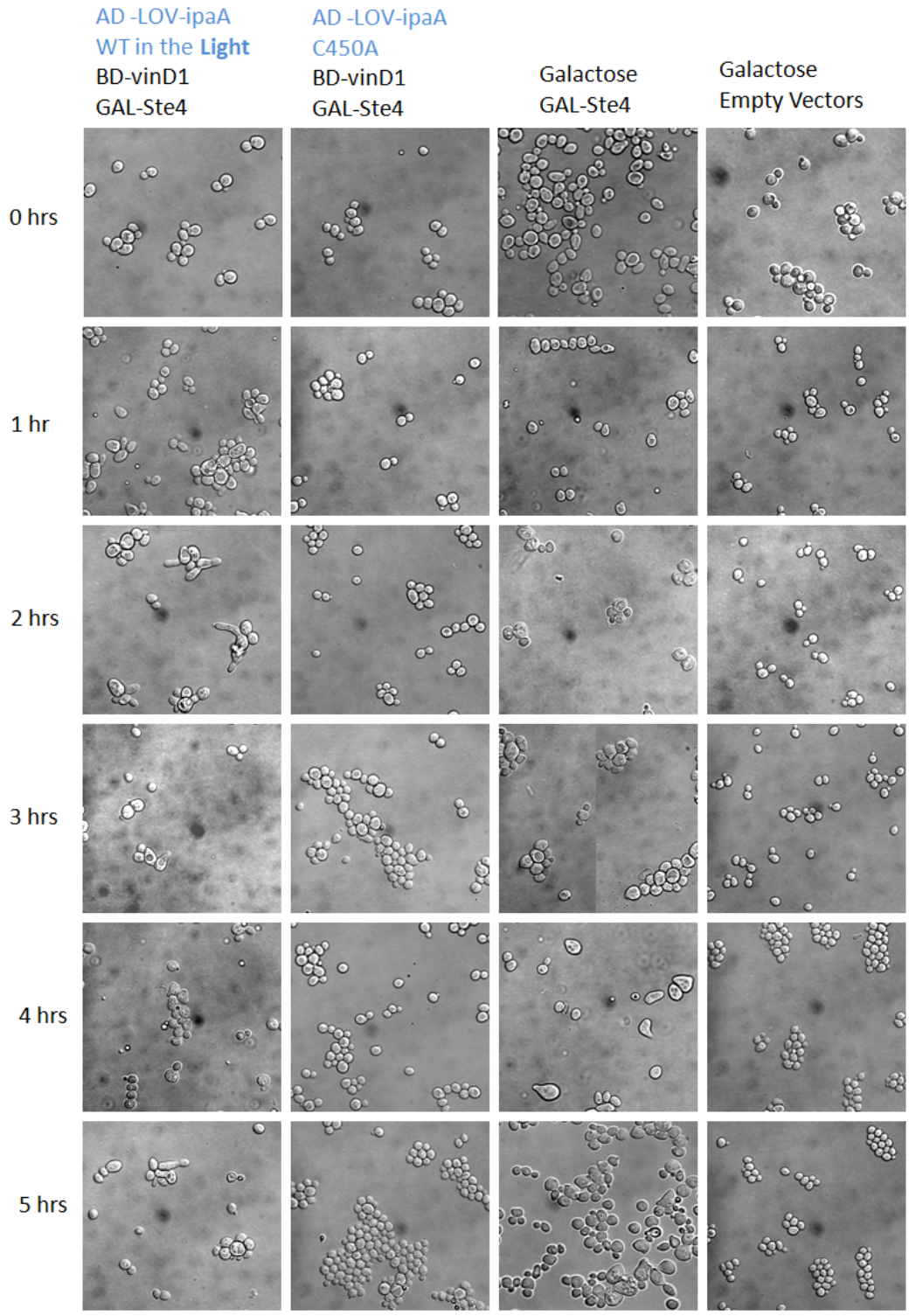

Figure 4.6: Blue light induces cell shmooing. Shmoo formation in *S. cerevisiae* cells transformed with GAL-Ste4, BD-vinD1, and AD-LOV-ipaA WT and induces through blue light was observed over the course of 5 hours. As a control, *S. cerevisiae* cells transformed with GAL-Ste4, BD-empty vector, and AD-empty vector were monitored for shmoo formation in tandem.

Figure 4.7: Blue light induces activation of the MAPK pathway. *S. cerevisiae* transformed with GAL-Ste4, BD-vinD1, and AD-LOV-ipaA WT were grown under dark (non-inducing) and blue light (inducing) conditions over the course of 120 min. Resulting activation of the downstream MAPK pathway is seen through the appearance of phospho-Fus3 and phospho-Kss1 MAP kinases. Untransformed *S. cerevisiae* strain YPH499 is used as a control.

can be monitored through the appearance of dually phosphorylated Fus3 protein as well as that of the phosphorylated, redundant Kss1 protein (28). We transformed cells with GAL-Ste4, BD-vinD1, and AD-LOV-ipaA WT, and grew transformed colonies to mid-log phase. Cultures were then exposed to blue light or dark conditions over the course of two hours. Cells were lysed and immunoblotted using a p44/42 antibody in order to probe for phosphorylated Fus3 and Kss1 proteins. The appearance of the phosphorylated proteins is evident only in the cultures exposed to light (Figure 4.7). Cultures only grown in the dark show no increase in levels of either protein over the course of an hour. A slight increase in phosphorylation is seen for samples in the dark after two hours, indicating a small amount of residual Ste4 expression in the dark.

4.4.4 Photoactivation of Gpa1 transcription

We tested the ability to photoactivate Gpa1 expression through the use of a halo assay. In the assay, *S. cerevisiae* cells transformed with the GAL1-Gpa1 gene are plated in a lawn of top agar on selective SD plates. Varying concentrations of α-factor are added as a single spot on the solidified top agar. This generates a gradient of pheromone radiating out from the spot, and induces growth arrest in cells sensitive to pheromone signaling (29; 30). Thus, a transformed strain's response to α-factor is observed as a function of the size of the halo

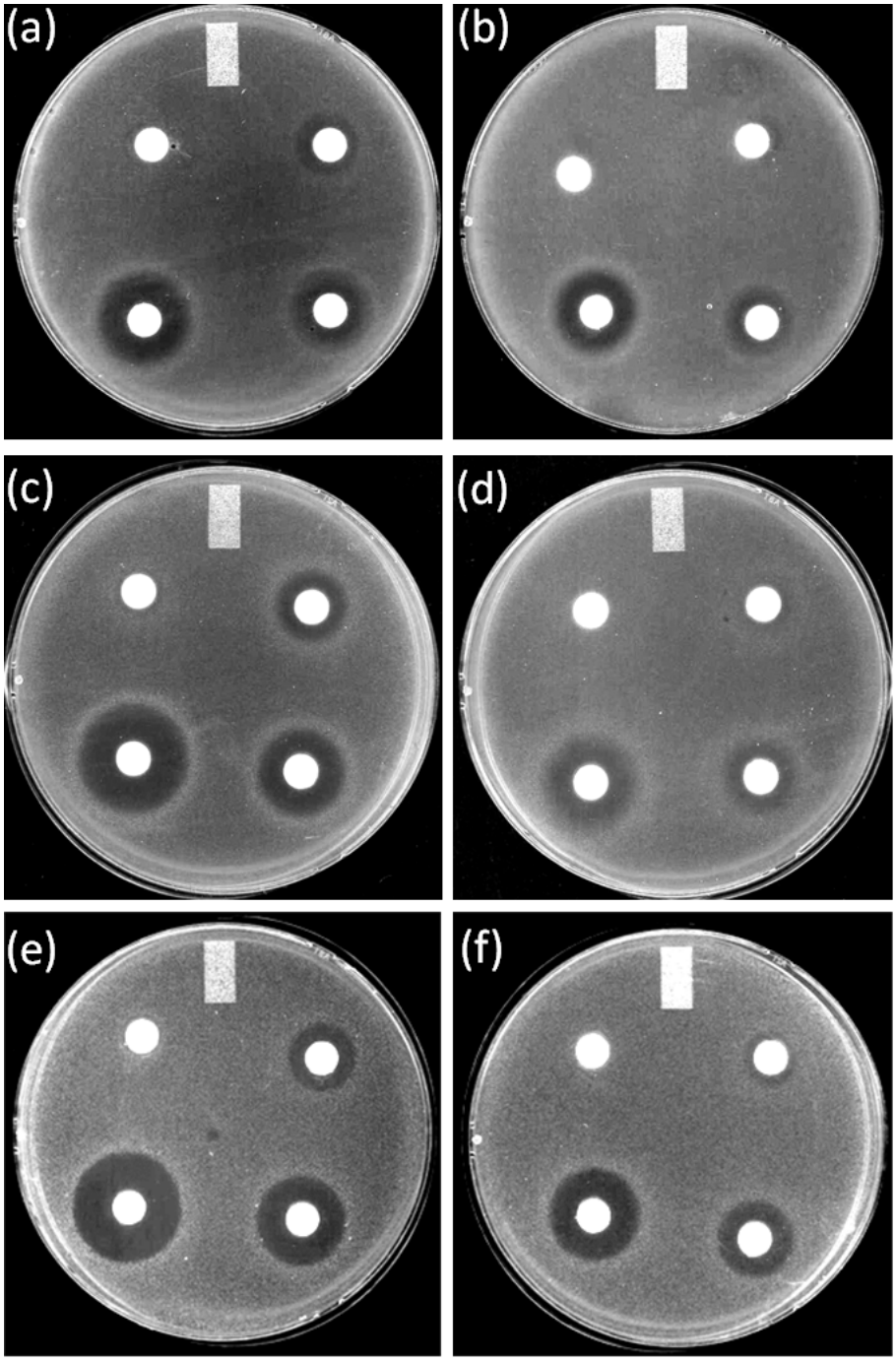

Figure 4.8: LOV-ipaA heterodimerization induces Gpa1 expression under blue light. Budding yeast transformed with GAL-Gpa1, BD-vinD1 and AD-LOV-ipaA WT were grown under (a) dark and (b) blue light conditions. Yeast transformed with GAL-Gpa1, BD-vinD1 and (c) AD-LOV-ipaA dark state, C450A mutation or (d) AD-LOV-ipaA lit state, I532E A536E mutation were grown. As a control, yeast transformed with BD-empty vector, AD-empty vector, and GAL-Gpa1 were grown under (e) glucose, non-inducing and (f) galactose, inducing conditions. Halo sizes in response to 1.5 μg, 4.5 μg, 15 μg, and 45 μg of α-factor (white pads, clockwise on each plate) are seen.

created by α-factor induced growth arrest. Overexpression of Gpa1 has been shown to dampen cells' sensitivity to α-factor.

In order to examine whether we could observe a phenotype in response to light-induced expression of Gpa1, we performed halo assays on cells transformed with GAL1-Gpa1, BD-vinD1 and AD-LOV-ipaA WT genes. These cells were replica plated and exposed to blue light (inducing) or dark (non-inducing) conditions over two days (Figure 4.8). Plates grown under blue light conditions showed less sensitivity to α-factor induced growth arrest. Halos on these plates were substantially smaller than those grown under dark conditions. As a control, cells expressing GAL1-Gpa1, BD-vinD1 and AD-LOV-ipaA C450A (dark state) or I532A A536E (lit state) genes were grown in dark conditions. In this case as well, cells expressing the AD-LOV-ipaA lit state gene were less sensitive than cells expressing the AD-LOV-ipaA dark state gene to pheromone induced growth arrest. This indicated that heterodimerization between AD-LOV-ipaA and BD-vinD1 rather than nonspecific light effects lead to insensitivity of cells to α-factor induced growth arrest.

A similar amount of insensitivity was observed in cells overexpressing Gpa1 through galactose induction. When cells expressing AD-empty vector, BD-empty vector and GAL1-Gpa1 were replica plated onto SD plates containing either galactose(inducing)or glucose (non-inducing) carbon sources, cells grown on galactose plates showed insensitivity to pheromone-induced growth arrest, but not those grown on glucose media.

Differences in pheromone-induced halo sizes were measured and averaged over three replicates. Cells grown on plates under inducing conditions required three times as much α factor to generate a halo equivalent in diameter to those cells grown on plates under non-inducing conditions (Table 4.2). Halo diameters were almost identical when cells were grown under blue light or under galactose induction Similarly, Halo diameters were almost identical, regardless of whether cells were grown under dark or under glucose induction. This indicates that we were able to demonstrate a clear phenotype of light-induced overexpression of Gpa1 in yeast cells.

AD-LOV-ipaA Inducing Condition	Dark State ——	Lit State ——	WT Dark	WT Blue Light	—— Glucose	—— Glalactose
α factor(μg)	Halo Diameter (cm)					
1.5	0.8	0.0	0.7	0.0	0.7	0.0
4.5	1.3	0.9	1.4	0.8	1.4	0.8
15	1.8	1.4	1.8	1.3	1.8	1.5
45	2.3	1.8	2.3	1.8	2.3	1.8

Table 4.2: Diameters of pheromone halos due to induced expression of Gpa1. Induction of Gpa1 overexpression by blue light or galactose was measured as a response to α factor concentration. Halo diameters versus α factor concentrations are given for yeast expressing GAL1-Gpa1 along with BD-vinD1 and AD-LOV-ipaA lit state, dark state, or WT grown under blue light (inducing) or dark (non-inducing) conditions. These can be compared to galactose induction of Gpa1.

4.5 Discussion

In this work, we sought to use LOV-ipaA binding to the vinculinD1 subdomain as a light-driven heterodimerization switch. We altered LOV-ipaA by introducing the L623A mutation that weakened its affinity to vinculinD1 by 500-fold. We introduced the mutated LOV-ipaA and vinD1 protein into a yeast-two hybrid system. LOV-ipaA was attached to the GAL4 activation domain, while the vinculinD1 subdomain was linked to the GAL4 binding domain. Light-induced heterodimerization of the two portions of GAL4 upon binding of LOV-ipaA to vinD1 induced expression of reporter genes LacZ, MEL1, HIS3 and ADE2. We applied the light-in inducible heterodimerization system to induce overexpression of Ste4 and Gpa1, two genes critical in the yeast pheromone response pathway.

Induction of Ste4 overexpression through blue light irradiation led to observance of two Ste4 phenotypes: growth arrest and shmoo formation. Both of these phenotypes were expressed weakly in blue light irradiated cells, when compared to cells induced by galactose. Biochemical data indicated strong activation of the MAPK pathway by blue light irradiation, however. This indicated strong overexpression of Ste4 over the course of two hours, but the activation may be too transient to show robust phenotypic activation over a longer course of time, which is required for growth arrest and shmoo formation. One other possibility for weak phenotype expriession might be heterogeneity of the transformed GAL-Ste4 cultures. In order to induce

overexpression with blue light in yeast cells, these cells must be transformed by three separate plasmids; these genes are not integrated into the yeast genome. Such a strategy might lead to over- or under-expression of one of the three components needed for a phenotypic response.

Gpa1 overexpression through blue light irradiation was more consistent. Gpa1 exxpressed the same phenotype, to the same extent, under blue light irradiation or under galactose induction. Experiments are still needed, however, to quantify the extent of Gpa1 overexpression upon irradiation with blue light, as compared to galactose induction.

We demonstrate that the LOV-ipaA photoswitch can be used as a tool for inducing gene expression using blue light. The pheromone mating response pathway can now be activated or inhibited by blue light, without the use of α-factor or other harsh or expensive chemical treatment of yeast cells. This technology can easily be adapted to induce expression of other critical yeast genes through light-induced heterodimerization, allowing for more studies into the workings of yeast genetics.

REFERENCES

1. Levskaya, A., Weiner, O., Lim, W., and Voigt, C. (2009) Spatiotemporal control of cell signalling using a light-switchable protein interaction. Nature **461**, 997–1001

2. Yazawa, M., Sadaghiani, A., Hsueh, B., and Dolmetsch, R. (2009) Induction of protein-protein interactions in live cells using light. Nature biotechnology **27**, 941–945

3. Wu, Y., Frey, D., Lungu, O., Jaehrig, A., Schlichting, I., Kuhlman, B., and Hahn, K. (2009) A genetically encoded photoactivatable rac controls the motility of living cells. Nature **461**, 104–108

4. Kennedy, M., Hughes, R., Peteya, L., Schwartz, J., Ehlers, M., and Tucker, C. (2010) Rapid blue-light-mediated induction of protein interactions in living cells. Nature Methods

5. Möglich, A. and Moffat, K. (2010) Engineered photoreceptors as novel optogenetic tools. Photochem. Photobiol. Sci.

6. Moglich, A., Yang, X., Ayers, R., and Moffat, K. (2010) Structure and function of plant photoreceptors. Annual Review of Plant Biology **61**, 21–47

7. Shimizu-Sato, S., Huq, E., Tepperman, J., and Quail, P. (2002) A light-switchable gene promoter system. Nature biotechnology **20**, 1041–1044

8. Leung, D., Otomo, C., Chory, J., and Rosen, M. (2008) Genetically encoded photoswitching of actin assembly through the Cdc42-WASP-Arp2/3 complex pathway. Proceedings of the National Academy of Sciences **105**, 12797

9. Crosson, S. and Moffat, K. (2001) Structure of a flavin-binding plant photoreceptor domain: insights into light-mediated signal transduction. Proceedings of the National Academy of Sciences **98**, 2995

10. Huala, E., Oeller, P., Liscum, E., Han, I., Larsen, E., and Briggs, W. (1997) Arabidopsis NPH1: a protein kinase with a putative redox-sensing domain. Science **278**, 2120

11. Swartz, T., Corchnoy, S., Christie, J., Lewis, J., Szundi, I., Briggs, W., and Bogomolni,

R. (2001) The photocycle of a flavin-binding domain of the blue light photoreceptor phototropin. Journal of Biological Chemistry **276**, 36493

12. Crosson, S. and Moffat, K. (2002) Photoexcited structure of a plant photoreceptor domain reveals a light-driven molecular switch. The Plant Cell Online **14**, 1067

13. Harper, S., Neil, L., and Gardner, K. (2003) Structural basis of a phototropin light switch. Science **301**, 1541

14. Halavaty, A. and Moffat, K. (2007) N-and C-terminal flanking regions modulate light-induced signal transduction in the LOV2 domain of the blue light sensor phototropin 1 from Avena sativa. Biochemistry **46**, 14001–14009

15. Harper, S., Neil, L., Day, I., Hore, P., and Gardner, K. (2004) Conformational changes in a photosensory LOV domain monitored by time-resolved NMR spectroscopy. Journal of the American Chemical Society **126**, 3390–3391

16. Swartz, T., Wenzel, P., Corchnoy, S., Briggs, W., and Bogomolni, R. (2002) Vibration spectroscopy reveals light-induced chromophore and protein structural changes in the lov2 domain of the plant blue-light receptor phototropin 1. Biochemistry **41**, 7183–7189

17. Zoltowski, B., Vaccaro, B., and Crane, B. (2009) Mechanism-based tuning of a LOV domain photoreceptor. Nature Chemical Biology **5**, 827–834

18. Cole, G., Stone, D., and Reed, S. (1990) Stoichiometry of g protein subunits affects the saccharomyces cerevisiae mating pheromone signal transduction pathway. Molecular and cellular biology **10**, 510

19. Nomoto, S., Nakayama, N., Arai, K., and Matsumoto, K. (1990) Regulation of the yeast pheromone response pathway by g protein subunits. The EMBO Journal **9**, 691

20. Whiteway, M., Hougan, L., and Thomas, D. (1990) Overexpression of the ste4 gene leads to mating response in haploid saccharomyces cerevisiae. Molecular and cellular biology **10**, 217

21. Gasch, A., Spellman, P., Kao, C., Carmel-Harel, O., Eisen, M., Storz, G., Botstein, D., and Brown, P. (2000) Genomic expression programs in the response of yeast cells to environmental changes. Molecular biology of the cell **11**, 4241

22. Klein, S., Reuveni, H., and Levitzki, A. (2000) Signal transduction by a nondissociable heterotrimeric yeast g protein. Proceedings of the National Academy of Sciences **97**, 3219

23. Bardwell, L. (2004) A walk-through of the yeast mating pheromone response pathway. Peptides **25**, 1465–1476

24. Cappell, S. and Dohlman, H. (2011) Selective regulation of map kinase signaling by an endomembrane phosphatidylinositol 4-kinase. Journal of Biological Chemistry **286**, 14852

25. Herskowitz, I. (1995) Map kinase pathways in yeast: for mating and more. Cell **80**, 187

26. Leberer, E., Thomas, D., and Whiteway, M. (1997) Pheromone signalling and polarized morphogenesis in yeast. Current Opinion in Genetics & Development **7**, 59–66

27. Dohlman, H. and Thorner, J. (2001) Regulation of g protein-initiated signal transduction in yeast: paradigms and principles. Annual review of biochemistry **70**, 703

28. Cappell, S., Baker, R., Skowyra, D., and Dohlman, H. (2010) Systematic analysis of essential genes reveals important regulators of g protein signaling. Molecular cell **38**, 746–757

29. Katada, T., Kusakabe, K., Oinuma, M., and Ui, M. (1987) A novel mechanism for the inhibition of adenylate cyclase via inhibitory gtp-binding proteins. calmodulin-dependent inhibition of the cyclase catalyst by the beta gamma-subunits of gtp-binding proteins. Journal of Biological Chemistry **262**, 11897

30. Reneke, J., Blumer, K., Courchesne, W., and Thorner, J. (1988) The carboxy-terminal segment of the yeast [alpha]-factor receptor is a regulatory domain. Cell **55**, 221–234

CHAPTER 5

CONCLUSION

5.1 PA-Rac and LOV-ipaA photoactivatable tools and applications

This thesis has described the development of two photoactivatable tools: PA-Rac and LOV-ipaA. However, only a small subsection of the the possible applications of each tool has been touched upon. The next few sections will cover current research in applying PA-Rac and LOV-ipaA to answer biological questions and understand signaling networks, as well as ways in which knowledge from the design of these photoswitches is aiding toward the goal of generalizable design of photoactivatable small GTPases and peptides.

5.2 Current uses of PA-Rac

PA-Rac has been used extensively to study the biology of Rac1 signaling and its effect on cell motility. These studies have been performed on the single cell level, as well as on the tissue and organismal level.

The first application of PA-Rac described was for single cells studies of motility (1). The effect of Rac1 activation on cell polarity was investigated. It was found that Rac1 induces cell polarity to induce protrusion locally, at the site of activation, while inducing retraction at the opposite side of the cell. It was found that myosin allows for this polarized cell movement to occur, while Rac1 activity through activation of PAK was the principle reason for overall protrusions in the cell. It was also seen that Rac1 activity in localized areas of the cell led to inhibition of RhoA activity in these places, possibly indicating RhoA is inhibited at cell

protrusions.

PA-Rac was used in zebrafish (2; 3) to study polarized cell migration. Activating Rac1 was found to direct polarized cell migration *in vivo*, in a *Danio rerio* embryo. Inhibiting the protein phosphoinositide 3-kinase (PI(3)K) while activating Rac1 allowed for membrane protrusion, but not polarized cell movement. This study has allowed scientists to understand how cell polarization occurs *in vivo*.

PA-Rac was also used to investigate the motility of a group of cells in the *Drosophila* ovary (4). These cells, called border cells, move about 175 μm in the egg chamber of a *D. melogaster* organism. Activation of Rac1 in one of the border cells proved sufficient to polarize and allow for cell motility in the entire group of border cells. This suggested that the cells jointly sense Rac1 activity level in order to induce polarized movement. The protein Jun N-terminal kinase was shown to be important for this intercellular communication, demonstrating yet another way in which PA-Rac was able to tease apart the mechanisms of cell signaling networks.

5.3 Future of PA-Rac: caging small GTPases

In section 2.4.3, the application of PA-Rac modeling to design PA-Cdc42 was described. Although the addition of Trp mutation on Cdc42 at its interface with the LOV2 domain led to caging of the small GTPase, the mutation also altered the effector binding region of Cdc42. This may alter the avidity of Cdc42 for its many effectors. Currently, efforts have been undertaken to identify other means to cage Cdc42 without disrupting its effector binding domain. One of the strategies being tested is the introduction of mutation sets G528A N538E and L514K L531E into the LOV2 domain, as described in section 3.4.3, to increase the dynamic range of LOV-ipaA. These same mutations are being applied to PA-Rac as well, in order to decrease its affinity of its effectors in the dark. The small GTPases RhoA and RhoG are being caged using the same strategy as that used to design PA-Rac. These efforts are ongoing and currently being tested.

5.4 Caging peptides using the LOV2 domain: lessons from LOV-ipaA

We are working on generalizing the caging of peptides through the use of the LOV2 domain. The challenge is altering the peptide and $J\alpha$ sequences so that they maintain peptide functionality but are compatible with the Jα helix (Figure 5.1). One face of the Jα helix is exposed to solvent while the other face forms hydrophobic interactions with a β-sheet in the LOV2 domain. Residues on the surface of the helix are expected to be tolerant to mutation, while the buried residues should be more conserved. Similarly, most peptides have sets of residues that are required for binding target proteins, while other positions can be varied. These observations indicate that it may be possible to identify more chimeric sequences for the Jα helix that maintain key interactions with the LOV2 domain but incorporate residues critical to peptide function.

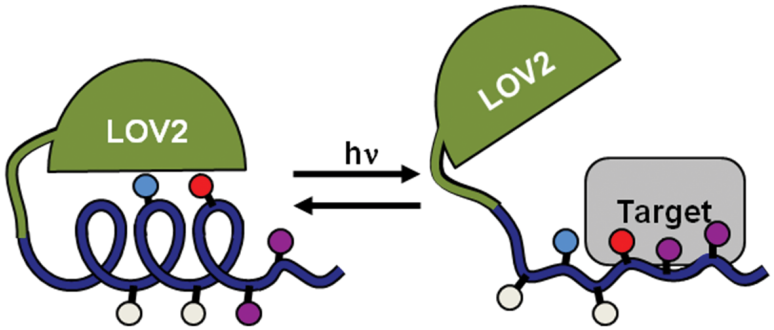

Figure 5.1: General design strategy for caging peptides using the LOV2 domain. Photoswitches are designed as sequence chimeras between the LOV2 Jα helix and the peptide to be caged. Residues that are important to LOV2-Jα interactions (cyan), important to peptide-target interaction (purple), important to both interactions (red), and residues that are important to neither interaction (white) are identified and mutated accordingly. Irradiation unfolds the Jα helix, and the peptide can bind its target.

We extended the design strategy used to cage ipaA in order to create a second photoswitchable peptide, LOV-SsrA. The SsrA peptide interacts with the protease delivery protein SspB from *E. coli* as a linear epitope using the seven residue sequence AANDENY (5). Caging of the SsrA peptide was considered an advancement of our peptide caging techniques, and a complimentary system to LOV-ipaA, for a variety of reasons. First, at functionally important residues both peptides align well with the Jα helix. Indeed, several alternative alignments were

identified for the SsrA peptide. Second, the peptides adopt alternative conformations when binding their targets, ipaA adopts a helix while SsrA binds in an extended conformation. By testing both peptides, we examine if our approach can be used to cage peptides regardless of the conformation they adopt when bound to their target protein. Third, the peptides have different intrinsic affinities for their target proteins. IpaA binds the D1 domain of vinculin very tightly, Kd less than 1 nM, while SrrA binds SspB with an affinity of about 30 nM. Fourth, for separate reasons they are well suited for controlling cell biology. The SsrA and SspB sequences are specific to bacteria, and therefore it is expected that they will not interact with other proteins and peptides in higher organisms. Fusing proteins of interest to a photoactivable SsrA and SspB should provide a general approach for light-induced heterodimerization, which can be used to localize proteins in the cell and activate cell-signaling pathways.

This approach may, in the future, be applied to a variety of peptides, since only a subset of residues on the Jα helix need to be conserved to maintain favorable interactions with LOV domain. Additionally, most protein-binding peptides contain residues that can be mutated without significantly weakening affinity for binding partners. In the case of LOV-ipaA and LOV-SsrA we also took advantage of the fact that not all of the peptide needs to be embedded in the Jα helix to create a steric block against effector binding. In this scenario, only a few residues from the N-terminal portion of the peptide need to be compatible with the folded Jα helix.

The switching power of the LOV-peptide switches can be manipulated by introducing mutations that stabilize the interaction between the Jα helix and the rest of the LOV domain, as well as by varying how deeply the caged peptide is embedded in the helix. Both the LOV-ipaA-vinculinD1 and the LOV-SsrAa-SspBb photoactivatable binding interactions can be harnessed as tools for photoactivatable heterodimerization. The LOV-ipaA- vinculin switch can be used in bacteria and in yeast cells, as these systems do not contain vinculin or vinculin binders that would affect the LOV-ipaA-vinculin interaction. The LOV-SsrA-SspB photoactivatable heterodimerization binders, on the other hand, should be useful in higher organisms such as mammalian cells. LOV-ipaA has a very slow off rate for vinculinD1, so it is better suited for long time-scale applications such as yeast mating. In contrast, LOV-SsrA binding to SspB is

rapidly reversible so can be used for more transient interactions, such as single cell motility experiments. In these ways, both LOV-ipaA and LOV-SsrA should be useful tools to spatially and temporally bring together proteins for activating signaling cascades.

5.5 Applications of the LOV-ipaA photoswitch

Apart from its use as a model system for caging peptides, LOV-ipaA is currently being researched for other applications. Since LOV-ipaA binds vinculin with high affinity in the lit state and weaker affinity in the dark state, it is being used to study vinculin-effector interactions. The photoswitch is added to mutated versions of full-length vinculin that alter its binding to polymerized actin and paxillin. LOV-ipaA acts as a regulatable activator of vinculin-actin and vinculin-paxillin interactions. This allows researchers to study the effects of full-length vinculin mutations on paxillin and actin binding when vinculin is in an on or off state.

Since the LOV-ipaA-vinculin binding interaction has been described so extensively, it is being used for screening of mutations in the LOV2 domain. The goal is to find mutations in the LOV2 domain of LOV-ipaA that favorably change its binding kinetics to vinculin. Mutations that maintain lit state binding affinity while decreasing the binding of the photoswitch to vinculin in the dark state are being particulary sought for.

LOV-ipaA was particularly successful at allowing for light induced heterodimerization in budding yeast. However, LOV-ipaA can only be used in orthogonal system such as yeast. The photoswitch cannot currently be used in mammalian cells a a light induced heterodimerization switch, as it would interact with endogenous vinculin in these cells. Efforts are being made to redesign both ipaA and the vinculinD1 subdomain at the ipaA interface. The end goal is to have an orthogonal interface, wherein redesigned LOV-ipaA only interacts with redesigned vindulinD1, rather than with endogenous vinculin, and redesigned vinculinD1 cannot interact with endogenous vinculin proteins such as talin and α-actinin.

5.6 A bright future for photoactivation

Photoactivation holds many future promises for the development of useful biological tools. This technology has already enabled us to study the underpinnings of signaling networks that lead to polarized cell motility, as well as to photoactivate yeast transcription at will. By generalizing the design of photoactivatable tools using the LOV2 domain, it will be possible to photoactivate many members of two classes of proteins; small GTPases and peptides. In the future, by combining the tools and systems in use today for genetically encoded photoactivation, we will be able to cage many more types of proteins using various different colors of light, even allowing for multiplexing of protein signaling in a cascade. One can envision a future in which any desired protein may be caged through genetically encoded means using a step-by-step protocol, and is uncaged using any one of a selectable number of wavelengths and colors of light. Such a future would lead to a dramatic advancement in our understanding of protein-protein signaling dynamics in a spatially and temporally precise manner. The future for photoactivation looks truly bright.

5.7 Appendix

5.7.1 Appendix A: Journal article adapted for Chapter 2

nature Vol 461|3 September 2009|doi:10.1038/nature08241

LETTERS

A genetically encoded photoactivatable Rac controls the motility of living cells

Yi I. Wu[1,3], Daniel Frey[4], Oana I. Lungu[1,2,3], Angelika Jaehrig[1,3], Ilme Schlichting[4], Brian Kuhlman[2,3] & Klaus M. Hahn[1,3]

The precise spatio-temporal dynamics of protein activity are often critical in determining cell behaviour, yet for most proteins they remain poorly understood; it remains difficult to manipulate protein activity at precise times and places within living cells. Protein activity has been controlled by light, through protein derivatization with photocleavable moieties[1] or using photoreactive small-molecule ligands[2]. However, this requires use of toxic ultraviolet wavelengths, activation is irreversible, and/or cell loading is accomplished via disruption of the cell membrane (for example, through microinjection). Here we have developed a new approach to produce genetically encoded photoactivatable derivatives of Rac1, a key GTPase regulating actin cytoskeletal dynamics in metazoan cells[3,4]. Rac1 mutants were fused to the photoreactive LOV (light oxygen voltage) domain from phototropin[5,6], sterically blocking Rac1 interactions until irradiation unwound a helix linking LOV to Rac1. Photoactivatable Rac1 (PA-Rac1) could be reversibly and repeatedly activated using 458- or 473-nm light to generate precisely localized cell protrusions and ruffling. Localized Rac activation or inactivation was sufficient to produce cell motility and control the direction of cell movement. Myosin was involved in Rac control of directionality but not in Rac-induced protrusion, whereas PAK was required for Rac-induced protrusion. PA-Rac1 was used to elucidate Rac regulation of RhoA in cell motility. Rac and Rho coordinate cytoskeletal behaviours with seconds and submicrometre precision[7,8]. Their mutual regulation remains controversial[9], with data indicating that Rac inhibits and/or activates Rho[10,11]. Rac was shown to inhibit RhoA in mouse embryonic fibroblasts, with inhibition modulated at protrusions and ruffles. A PA-Rac crystal structure and modelling revealed LOV–Rac interactions that will facilitate extension of this photoactivation approach to other proteins.

Recent NMR studies revealed the mechanism of a protein light switch in *Avena sativa* phototropin1 (refs 6, 12): a flavin-binding LOV2 domain interacts with a carboxy-terminal helical extension (Jα) in the dark. Photon absorption leads to formation of a covalent bond between Cys 450 and the flavin chromophore, causing conformational changes that result in dissociation and unwinding of the Jα helix. We fused the complete LOV2-Jα sequence (404–547) to the amino terminus of a constitutively active Rac1, anticipating that the LOV domain in its closed conformation would block the binding of effectors to Rac1, and that light-induced unwinding of the Jα helix would release steric inhibition, leading to Rac1 activation (Fig. 1a). Sampling of different junctional sequences in pull-down assays revealed that connecting Leu 546 of LOV2-Jα to Ile 4 of Rac1 led to substantial reduction in Rac1 binding to its effector PAK (Fig. 1b and Supplementary Fig. 1a). To ensure that the photoactivatable Rac1 would induce no dominant-negative effects and that its activity would not be subject to upstream regulation, mutations were introduced to abolish GTP hydrolysis and diminish interactions with nucleotide exchange factors, guanine nucleotide dissociation inhibitors (Q61L) and GTPase activating proteins (E91H and N92H) (Supplementary Fig. 2 and Supplementary text 'Characterization of Rac1 constructs'). This resulted in the photoactivatable analogue of Rac1 (PA-Rac1) used in the following studies. Pull-down assays showed that PA-Rac1 has greatly reduced affinity for its effector protein PAK in the dark, as does a PA-Rac1 construct containing a light-insensitive LOV2 mutation (C450A)[13]. Effector binding was restored in a PA-Rac1 construct containing a LOV2 mutant (I539E)[14] which mimics the unfolded 'lit state' (Fig. 1b and Supplementary Fig. 1b). Isothermal titration experiments indicated that the dark and lit state mutants of PA-Rac1 differed tenfold in effector binding (200 nM versus 2 μM) (Supplementary Fig. 3 and Supplementary Table 1), with lit state effector affinity similar to that of native Rac[15].

Activation of PA-Rac1 was examined in HeLa cells expressing a YFP fusion of PA-Rac1 to gauge expression level. The cells remained quiescent when illuminated with wavelengths longer than flavin absorbance (515, 568 or 633 nm, data not shown), but within seconds after switching to 458 nm, lamellipodial protrusions and membrane ruffles appeared around the cell edges (Fig. 1c and Supplementary Movie 1). To show that this effect was due to PA-Rac1, kymograms were used to quantify maximum protrusion length; irradiation of PA-Rac1 elicited protrusions that were four times as long as those seen in cells expressing either LOV domain alone or the light-insensitive PA-Rac1(C450A) mutant (Supplementary Fig. 4). An important advantage of PA-Rac1 is its ability to control precisely the subcellular location of Rac activation. We first examined this in mouse embryo fibroblasts (MEFs) stably expressing PA-Rac1, and cultured without serum to minimize cell activity before irradiation. Irradiation of 20-μm spots at the cell edge generated large protrusions clearly localized next to the point of irradiation (Fig. 1d and Supplementary Movie 2). Repeated irradiation led first to ruffles and then to protrusion. YFP–actin, YFP–PAK and YFP–Arp3 revealed actin polymerization at the edge of the Rac-induced protrusions with associated translocation of downstream effectors, and induction of localized PAK phosphorylation was shown by immunostaining (Supplementary Figs 5 and 6 and Supplementary Movies 3 and 4). Movement of a laser spot to different positions led to cessation of ruffling or protrusion at the initial irradiation position and new activities appearing where the laser spot was brought to rest (HeLa cells, Supplementary Movie 5), demonstrating reversible activation. In MEF cells, more prone to movement than HeLa cells, complex shape changes were produced by 'painting' the cell with the laser spot (Supplementary Movie 6). The area of protrusions in MEF cells was dependent on light dosage, indicating the valuable ability to control the level of Rac1 activation (Supplementary Fig. 7). PA-Rac1 diffusion was analysed using fluorescence recovery after photobleaching (FRAP) and using PA-Rac1 tagged with photoactivatable GFP[16] (Supplementary

[1]Department of Pharmacology, [2]Department of Biochemistry and Biophysics, and [3]Lineberger Comprehensive Cancer Center, University of North Carolina, Chapel Hill, North Carolina 27599, USA. [4]Department of Biomolecular Mechanisms, Max Planck Institute for Medical Research, Jahn-Strasse 29, 69120 Heidelberg, Germany.

Fig. 8 and Supplementary Movies 7 and 8), indicating that PA-Rac1 diffuses more slowly than cytosolic proteins, probably because it is membrane bound (10 µm spot, FRAP $D = 0.55\,\mu m^2\,s^{-1}$ or $t_{1/2} = 12.1$ s; PA-GFP $t_{1/2} = 14.6$ s). The half-life of dark recovery for PA-Rac1 was determined to be 43 s at room temperature. Simulation using this value indicated that, for two adjacent 10-µm spots, the unirradiated spot will achieve at most 7.5% the activation of the irradiated region (Supplementary Fig. 8c). Together these studies validate PA-Rac1 as a robust, genetically encoded and reversible caged protein effective in living cells.

We used PA-Rac1 to ask whether localized Rac activation is sufficient to specify cell polarity. In MEF cells, activating Rac1 at one spot near the cell edge not only generated protrusion locally, but also produced retraction on the opposite side of the cell (Fig. 2a and Supplementary Movie 9). To test whether this cross-cell coordination was due to a gradient of Rac1 activity, we fused the LOV domain to a dominant-negative mutant of Rac1 using the same linkage as in PA-Rac1. Irradiation of this PA-Rac1(T17N) led to nearby retraction rather than protrusion, and now generated protrusion in other areas of the cell (Fig. 2a and Supplementary Movies 10 and 11). The ability of Rac1 alone to control polarized movement was confirmed by repeated irradiation at the cell edge, which could be used to produce prolonged cell movement by generating consistent coordinated extension and retraction (MEF cells, Fig. 2b and Supplementary Movie 12; HEK293 cells, Supplementary Movie 13). In contrast to MEF and HEK293 cells, HeLa cells showed localized protrusion but could not be induced to retract or move simply by activating Rac (Supplementary Movie 3), indicating that Rac-induced motility is subject to modulation by other pathways.

PA-Rac1 enabled control of Rac1 activity without the prior cellular compensation seen with other techniques, that is, mutation or altered expression. Using this advantage, we examined the role of myosin, a key mediator of actin-based contractility, in Rac-induced motility. Global inhibition of myosin activity using the myosin ATPase inhibitor blebbistatin or the myosin light chain kinase inhibitor ML-7 strongly affected Rac's ability to specify the direction of cell movement, but minimally affected Rac-induced protrusion (Fig. 2c, d). Myosin may mediate Rac's control of directionality through induction of tail retraction[17], contraction of the cell cortex to direct protrusive force[18], or coupling of actin to adhesions differently at the front and rear[19]. In contrast, inhibition of PAK was found to strongly affect Rac-induced protrusion (Supplementary Fig. 9). Inhibition of the Rho-activated kinase ROCK using Y27632 suggested a role for ROCK in Rac-induced protrusion, but these results must be interpreted with caution owing to known off-target effects[20].

Where and how Rac regulates Rho *in vivo* remains largely unknown; this was examined by using PA-Rac1 together with a RhoA biosensor[8]. Localized activation of Rac1 led to immediate inhibition of RhoA, and this inhibition spread outwards from the irradiated spot (Fig. 3a and Supplementary Movie 14). This was not simply an artefact of biosensor photobleaching, as irradiating the photoinactive C450M mutant (Fig. 2c) of PA-Rac1 led to localized

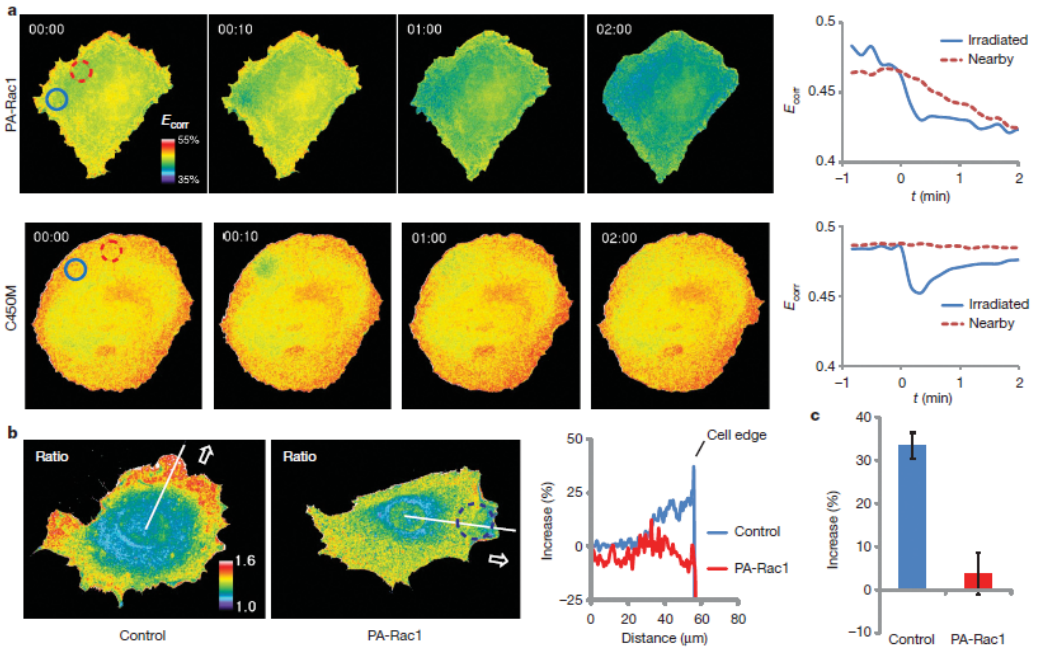

Figure 3 | Inhibition of RhoA by PA-Rac1. **a**, HeLa cells expressing RhoA biosensor and either PA-Rac1 or its C450M photoinactive mutant, illuminated in a 10-µm circle with a single pulse of 473-nm light. Changes in the FRET efficiency (E_{corr}) of the RhoA biosensor, indicative of RhoA activation, are shown in pseudocolour and as plots of average FRET efficiency within the irradiated circle (blue) and a nearby circle (red). In the PA-Rac1 cells, the irradiated spot showed bleaching of the biosensor followed by a relatively constant level of reduced RhoA activity. The nearby spot showed no bleaching, but a gradual decrease in RhoA activity reaching the low level achieved in the irradiated spot ($n = 3$ cells). In the control cells (C450M), the biosensor returned to near initial activation readouts after bleaching, and no change was seen in the nearby spot ($n = 3$ cells). Time shown is in minutes and seconds. **b**, RhoA activation in constitutive pseudopods[8,21] versus pseudopods induced by PA-Rac1 (473 nm, 20-µm circle shown, Supplementary Movie 15). **c**, The bar graph shows the per cent increase in biosensor FRET/CFP ratio in the region 1 µm from the cell edge versus the mean of the flat region at the left of the line scan. Means ± 95% confidence intervals, 18 lines from 6 cells per bar.

Fig. 8 and Supplementary Movies 7 and 8), indicating that PA-Rac1 diffuses more slowly than cytosolic proteins, probably because it is membrane bound (10 µm spot, FRAP $D = 0.55\,\mu m^2 s^{-1}$ or $t_{1/2} = 12.1$ s; PA-GFP $t_{1/2} = 14.6$ s). The half-life of dark recovery for PA-Rac1 was determined to be 43 s at room temperature. Simulation using this value indicated that, for two adjacent 10-µm spots, the unirradiated spot will achieve at most 7.5% the activation of the irradiated region (Supplementary Fig. 8c). Together these studies validate PA-Rac1 as a robust, genetically encoded and reversible caged protein effective in living cells.

We used PA-Rac1 to ask whether localized Rac activation is sufficient to specify cell polarity. In MEF cells, activating Rac1 at one spot near the cell edge not only generated protrusion locally, but also produced retraction on the opposite side of the cell (Fig. 2a and Supplementary Movie 9). To test whether this cross-cell coordination was due to a gradient of Rac1 activity, we fused the LOV domain to a dominant-negative mutant of Rac1 using the same linkage as in PA-Rac1. Irradiation of this PA-Rac1(T17N) led to nearby retraction rather than protrusion, and now generated protrusion in other areas of the cell (Fig. 2a and Supplementary Movies 10 and 11). The ability of Rac1 alone to control polarized movement was confirmed by repeated irradiation at the cell edge, which could be used to produce prolonged cell movement by generating consistent coordinated extension and retraction (MEF cells, Fig. 2b and Supplementary Movie 12; HEK293 cells, Supplementary Movie 13). In contrast to MEF and HEK293 cells, HeLa cells showed localized protrusion but could not be induced to retract or move simply by activating Rac (Supplementary Movie 3), indicating that Rac-induced motility is subject to modulation by other pathways.

PA-Rac1 enabled control of Rac1 activity without the prior cellular compensation seen with other techniques, that is, mutation or altered expression. Using this advantage, we examined the role of myosin, a key mediator of actin-based contractility, in Rac-induced motility. Global inhibition of myosin activity using the myosin ATPase inhibitor blebbistatin or the myosin light chain kinase inhibitor ML-7 strongly affected Rac's ability to specify the direction of cell movement, but minimally affected Rac-induced protrusion (Fig. 2c, d). Myosin may mediate Rac's control of directionality through induction of tail retraction[17], contraction of the cell cortex to direct protrusive force[18], or coupling of actin to adhesions differently at the front and rear[19]. In contrast, inhibition of PAK was found to strongly affect Rac-induced protrusion (Supplementary Fig. 9). Inhibition of the Rho-activated kinase ROCK using Y27632 suggested a role for ROCK in Rac-induced protrusion, but these results must be interpreted with caution owing to known off-target effects[20].

Where and how Rac regulates Rho *in vivo* remains largely unknown; this was examined by using PA-Rac1 together with a RhoA biosensor[8]. Localized activation of Rac1 led to immediate inhibition of RhoA, and this inhibition spread outwards from the irradiated spot (Fig. 3a and Supplementary Movie 14). This was not simply an artefact of biosensor photobleaching, as irradiating the photoinactive C450M mutant (Fig. 2c) of PA-Rac1 led to localized

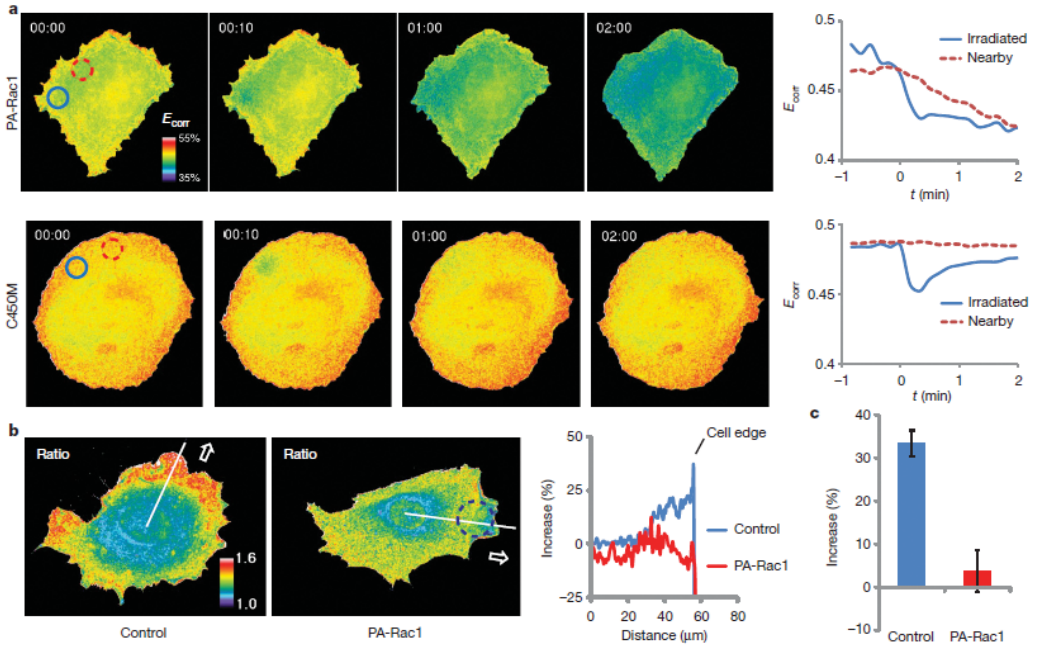

Figure 3 | Inhibition of RhoA by PA-Rac1. **a**, HeLa cells expressing RhoA biosensor and either PA-Rac1 or its C450M photoinactive mutant, illuminated in a 10-µm circle with a single pulse of 473-nm light. Changes in the FRET efficiency (E_{corr}) of the RhoA biosensor, indicative of RhoA activation, are shown in pseudocolour and as plots of average FRET efficiency within the irradiated circle (blue) and a nearby circle (red). In the PA-Rac1 cells, the irradiated spot showed bleaching of the biosensor followed by a relatively constant level of reduced RhoA activity. The nearby spot showed no bleaching, but a gradual decrease in RhoA activity reaching the low level achieved in the irradiated spot ($n = 3$ cells). In the control cells (C450M), the biosensor returned to near initial activation readouts after bleaching, and no change was seen in the nearby spot ($n = 3$ cells). Time shown is in minutes and seconds. **b**, RhoA activation in constitutive pseudopods[8,21] versus pseudopods induced by PA-Rac1 (473 nm, 20-µm circle shown, Supplementary Movie 15). **c**, The bar graph shows the per cent increase in biosensor FRET/CFP ratio in the region 1 µm from the cell edge versus the mean of the flat region at the left of the line scan. Means ± 95% confidence intervals, 18 lines from 6 cells per bar.

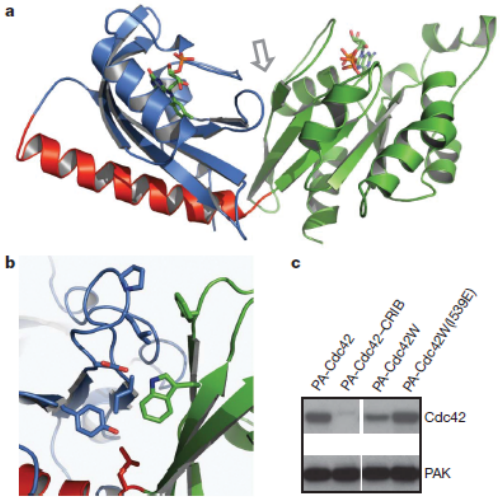

Figure 4 | Crystallization and structural modelling of PA-Rac1. a, Dark state crystal structure of PA-Rac1. Blue, LOV domain; red, Jα helix; green, Rac1. **b**, Interacting residues at the LOV–Rac interface (arrow in panel **a**), including Trp 56. **c**, Mutating Cdc42 to include the Trp involved in stabilizing the LOV2–Rac1 interaction substantially improved LOV inhibition of Cdc42. Lane 1, PA-Cdc42; linking LOV to Cdc42 using the same truncations that produced good inhibition for Rac does not inhibit Cdc42–PAK binding. Lane 2, PA-Cdc42–CRIB; covalently linking the CRIB domain of PAK to PA-Cdc42 blocks PAK binding. Lane 3, PA-Cdc42(F56W) (PA-Cdc42W); introduction of the tryptophan substantially improves LOV inhibition of Cdc42 binding to PAK. Lane 4, lit state mutant of PA-Cdc42(F56W) (PA-Cdc42W(I539E), showing that Cdc42 inhibition is sensitive to the lit/dark state of the LOV domain. Supplementary Movie 16 and Supplementary Fig. 14 demonstrate the ability of PA-Cdc42(F56W) to produce filopodia and protrusions in living cells.

biosensor photobleaching and recovery, but no prolonged local inhibition or wave of inhibition (Fig. 3a). There were marked differences between constitutive MEF protrusions and protrusions induced by pulsed PA-Rac1 irradiation. In contrast to constitutive protrusions, RhoA activity was greatly reduced in protrusions induced by PA-Rac (Fig. 3b). Inhibition of RhoA seems to be compartmentalized or controlled kinetically when Rac is activated in the context of normal motility, as both active Rac and active Rho are seen at the leading edge[7,8,21]. PA-Rac activation led to large ruffles moving from the site of irradiation rearwards towards the nucleus (Supplementary Movie 15), suggesting that Rac regulates rearwards membrane flow. In control experiments, irradiation of cells expressing the photoinactive C450M mutant did not produce polarized ruffling or show reduced RhoA activity (data not shown).

To understand the structural basis of the PA-Rac1 switch for future application to other proteins, we performed Rosetta structure prediction simulations[22] on several LOV2–Rac1 constructs, and determined high-resolution crystal structures of photoactive and inactive PA-Rac1 in the dark state. The crystal structures confirmed that the LOV domain occludes effector binding in the dark state (Fig. 4a and Supplementary Table 2). LOV-Jα adopted a closed conformation that superimposes with the recently published structure of isolated LOV-Jα (ref. 23). In the conformational ensemble predicted by simulations of the dark state, the effector binding site of Rac was sterically blocked by the LOV domain in a majority of the low-energy models (Supplementary Tables 3–5 and Supplementary Figs 10–13). Consistent with pull-down assays (Fig. 1b and Supplementary Fig. 1a), adding or removing even one residue from the connection between LOV and Rac resulted in conformational ensembles with exposed effector binding sites. In the dark state, Rac was seen to form an extensive interface with the LOV domain (Fig. 4b), occluding Rac binding interactions. Given the substantial structural similarity between Rac1 and Cdc42, we hypothesized that the LOV domain could also be used to cage Cdc42. However, the linkage used for PA-Rac1 failed to reduce Cdc42 binding to PAK (Fig. 4c and Supplementary Fig. 1d). Using the PA-Rac1 crystal structure as a template, a model was built of the Cdc42–LOV dark state. At the interface between Rac and LOV a hydrophobic cluster is formed between residues Phe 37 and Trp 56 from Rac and Leu 422, Pro 423, Ile 428, Tyr 508 and Leu 546 from LOV. Consistent with this being a weak, non-evolved interaction, most of the hydrogen-bonding potential at the Rac–LOV interface is satisfied by buried and partially buried water molecules instead of inter-domain hydrogen bonds (Fig. 4b). This interface model was used to identify a mutation to Cdc42, F56W, at the Rac–LOV interface, that was predicted to stabilize the dark state. Pull-down assays showed that this mutation substantially improves dark-state inhibition of PAK binding, and produces differential affinity for Cdc42 effector in the dark versus the lit state (Fig. 4d). In living cells, irradiation of the mutated PA-Cdc42 led to production of filopodia and in some cases protrusions and/or ruffles, consistent with Cdc42 induction of filopodia and activation of Rac[24] (Supplementary Fig. 14 and Supplementary Movie 16). These results argue that PA-Rac1 can serve as a blueprint for engineering other caged GTPases.

We have engineered genetically encoded photoactivatable Rac1 analogues that enable precise spatial and temporal control of Rac activity in live cells, with reversible activation at 458 or 473 nm. Localized Rac activation or deactivation was sufficient to generate polarized cell movement. Rac could be activated without cellular compensation, enabling us to probe the role of myosin and PAK in Rac-mediated motility. Spatially regulated Rac inhibition of Rho was demonstrated in living cells. Structural studies indicate that a non-evolved interaction at the Rac–LOV interface can be engineered to cage other GTPases. This study and other recent work[25–28] show that coupling genetically encoded light-modulated domains to other proteins provides a versatile new route to control protein activities in living cells.

METHODS SUMMARY

Imaging experiments were conducted on an Olympus FluoView 1000 laser scanning confocal microscope and an Olympus IX81-ZDC inverted microscope. Biosensor imaging was performed as previously described[8,29]. Simultaneous biosensor imaging and activation of PA-Rac was achieved using a MAG Biosystems FRAP-3D add-on (Photometrics) for galvanometer control of laser position.

Full Methods and any associated references are available in the online version of the paper at www.nature.com/nature.

Received 21 March; accepted 30 June 2009.
Published online 19 August 2009.

1. Goeldner, M. & Givens, R. *Dynamic Studies in Biology: Phototriggers, Photoswitches and Caged Biomolecules* (Wiley-VCH, 2005).
2. Fortin, D. L. *et al.* Photochemical control of endogenous ion channels and cellular excitability. *Nature Methods* **5**, 331–338 (2008).
3. Raftopoulou, M. & Hall, A. Cell migration: Rho GTPases lead the way. *Dev. Biol.* **265**, 23–32 (2004).
4. Ridley, A. J. *et al.* Cell migration: integrating signals from front to back. *Science* **302**, 1704–1709 (2003).
5. Christie, J. M., Salomon, M., Nozue, K., Wada, M. & Briggs, W. R. LOV (light, oxygen, or voltage) domains of the blue-light photoreceptor phototropin (nph1): binding sites for the chromophore flavin mononucleotide. *Proc. Natl Acad. Sci. USA* **96**, 8779–8783 (1999).
6. Harper, S. M., Neil, L. C. & Gardner, K. H. Structural basis of a phototropin light switch. *Science* **301**, 1541–1544 (2003).
7. Kraynov, V. S. *et al.* Localized Rac activation dynamics visualized in living cells. *Science* **290**, 333–337 (2000).
8. Pertz, O., Hodgson, L., Klemke, R. L. & Hahn, K. M. Spatiotemporal dynamics of RhoA activity in migrating cells. *Nature* **440**, 1069–1072 (2006).
9. Burridge, K. & Wennerberg, K. Rho and Rac take center stage. *Cell* **116**, 167–179 (2004).

10. Ridley, A. J., Paterson, H. F., Johnston, C. L., Diekmann, D. & Hall, A. The small GTP-binding protein rac regulates growth factor-induced membrane ruffling. *Cell* **70**, 401–410 (1992).
11. Sander, E. E., ten Klooster, J. P., van Delft, S., van der Kammen, R. A. & Collard, J. G. Rac downregulates Rho activity: reciprocal balance between both GTPases determines cellular morphology and migratory behavior. *J. Cell Biol.* **147**, 1009–1022 (1999).
12. Yao, X., Rosen, M. K. & Gardner, K. H. Estimation of the available free energy in a LOV2-Jα photoswitch. *Nature Chem. Biol.* **4**, 491–497 (2008).
13. Salomon, M., Christie, J. M., Knieb, E., Lempert, U. & Briggs, W. R. Photochemical and mutational analysis of the FMN-binding domains of the plant blue light receptor, phototropin. *Biochemistry* **39**, 9401–9410 (2000).
14. Harper, S. M., Christie, J. M. & Gardner, K. H. Disruption of the LOV-Jα helix interaction activates phototropin kinase activity. *Biochemistry* **43**, 16184–16192 (2004).
15. Thompson, G., Owen, D., Chalk, P. A. & Lowe, P. N. Delineation of the Cdc42/Rac-binding domain of p21-activated kinase. *Biochemistry* **37**, 7885–7891 (1998).
16. Patterson, G. H. & Lippincott-Schwartz, J. A photoactivatable GFP for selective photolabeling of proteins and cells. *Science* **297**, 1873–1877 (2002).
17. Vicente-Manzanares, M., Zareno, J., Whitmore, L., Choi, C. K. & Horwitz, A. F. Regulation of protrusion, adhesion dynamics, and polarity by myosins IIA and IIB in migrating cells. *J. Cell Biol.* **176**, 573 (2007).
18. Burridge, K. & Chrzanowska-Wodnicka, M. Focal adhesions, contractility, and signaling. *Annu. Rev. Cell Dev. Biol.* **12**, 463–518 (1996).
19. Giannone, G. *et al.* Lamellipodial actin mechanically links myosin activity with adhesion-site formation. *Cell* **128**, 561–575 (2007).
20. Davies, S. P., Reddy, H., Caivano, M. & Cohen, P. Specificity and mechanism of action of some commonly used protein kinase inhibitors. *Biochem. J.* **351**, 95–105 (2000).
21. Kurokawa, K. & Matsuda, M. Localized RhoA activation as a requirement for the induction of membrane ruffling. *Mol. Biol. Cell* **16**, 4294–4303 (2005).
22. Rohl, C. A., Strauss, C. E., Misura, K. M. & Baker, D. Protein structure prediction using Rosetta. *Methods Enzymol.* **383**, 66–93 (2004).
23. Halavaty, A. S. & Moffat, K. N- and C-terminal flanking regions modulate light-induced signal transduction in the LOV2 domain of the blue light sensor phototropin 1 from *Avena sativa*. *Biochemistry* **46**, 14001–14009 (2007).
24. Nobes, C. D. & Hall, A. Rho, rac, and cdc42 GTPases regulate the assembly of multimolecular focal complexes associated with actin stress fibers, lamellipodia, and filopodia. *Cell* **81**, 53–62 (1995).
25. Lee, J. *et al.* Surface sites for engineering allosteric control in proteins. *Science* **322**, 438–442 (2008).
26. Moglich, A., Ayers, R. A. & Moffat, K. Design and Signaling Mechanism of Light-Regulated Histidine Kinases. *J. Mol. Biol.* **385**, 1433–1444 (2008).
27. Strickland, D., Moffat, K. & Sosnick, T. R. Light-activated DNA binding in a designed allosteric protein. *Proc. Natl Acad. Sci. USA* **105**, 10709–10714 (2008).
28. Leung, D. W., Otomo, C., Chory, J. & Rosen, M. K. Genetically encoded photoswitching of actin assembly through the Cdc42-WASP-Arp2/3 complex pathway. *Proc. Natl Acad. Sci. USA* **105**, 12797–12802 (2008).
29. Hodgson, L., Shen, F. & Hahn, K. M. Biosensors for characterizing the dynamics of Rho family GTPases in living cells. *Curr. Protoc. Cell Biol.* (in the press).

Supplementary Information is linked to the online version of the paper at www.nature.com/nature.

Acknowledgements We are grateful for help and constructs from W. Briggs, K. Moffat, A. Tripathy, G. Bokoch and K. Jacobson. Diffraction data were collected at the Swiss Light Source, beamline X10SA, Paul Scherrer Institute, Villigen, Switzerland. We thank the Dortmund-Heidelberg team for data collection, and A. Pauluhn and M. Fuchs for their support in setting up the beamline. This research was supported by the American Heart Association (Y.I.W.) and the National Institutes of Health (K.M.H. grants GM057464 and GM64346).

Author Contributions Y.I.W. initiated the project, demonstrated the validity of caging Rac with LOV, and performed the studies of Rac biological function. He was assisted by A.J. in cloning and protein expression. D.F. and I.S. determined and analysed the crystal structures. O.I.L. performed molecular modelling and isothermal calorimetry studies under the direction of B.K. K.M.H. coordinated the study and wrote the final version of the manuscript, based on contributions from all authors.

Author Information The structural coordinates of PA-Rac1 and its mutants have been submitted to the Protein Data Bank under accessions 2wkp (wild type), 2wkq (C450A) and 2wkr (C450M). Reprints and permissions information is available at www.nature.com/reprints. Correspondence and requests for materials should be addressed to K.M.H. (khahn@med.unc.edu) or Y.I.W. (yiwu@med.unc.edu).

METHODS

DNA cloning. The cDNA encoding the LOV2 domain of *Avena sativa* (oat) Phototropin1 (404–546), including the C-terminal helical extension (Jα), was a gift from K. Moffat. Chimaeric fusion constructs consisting of LOV2-Jα fused to Rac1 or Cdc42 were generated using an overlapping PCR approach so that precise junctional sequences could be engineered without being limited by restriction sites. These included truncations/extensions of the LOV2-Jα C terminus (539–547), the N terminus (2–4) of the GTPases, or insertions of designed Schellman caps (KEAGADQI and KELKEAGADQI)[1]. The QuickChange (Stratagene) protocol was used to introduce additional point mutations, including C450A or C450M, and I539E to mimic the dark and lit state of the LOV domain, respectively. PA-Rac1 was constructed as follows: LOV2-Jα(404–546)–Rac1(4–192)/Q61L/E91H/N92H. These constructs were inserted into a pTriEx (Novagen) vector for transient expression in mammalian cells as well as in bacteria. For crystallization, C-terminally truncated PA-Rac1 (Δ181–192) was subcloned into the pQE-30 vector (Qiagen). Fluorescent proteins mVenus[2], mCherry[3] and mPA-GFP[4] were inserted at the N terminus of the LOV domain with a short GSGS linker to monitor expression and subcellular localization. After initial characterization, PA-Rac1 with different fluorescent protein tags was subcloned into pBabe-TetCMV vector for retroviral production and establishment of stable MEF Tet-Off cell lines. High-fidelity Pfu Turbo DNA polymerase (Stratagene) was used in PCR reactions and all plasmids were verified by DNA sequencing.

Pull-down assay of effector binding. mVenus-tagged LOV2-Jα and Rac1 fusion constructs were coexpressed with Flag-tagged PAK1 in HEK293 (LinXE) cells by transient transfection using Fugene 6 (Roche). The cells were lysed in 50 mM Tris pH 7.5, 150 mM NaCl and 1% Triton X-100 (lysis buffer) with addition of EDTA-free protease inhibitor cocktail (Roche). After brief centrifugation, the supernatants were incubated with Flag/M2-agarose (Sigma) followed by washes with lysis buffer, and elution with lysis buffer containing 200 μg ml^{-1} 3×Flag peptide (Sigma). All procedures were done at 4 °C under red light, facilitated using Handee spin columns (Pierce). The purified protein complexes as well as cell lysates were fractionated on 4–12% NuPAGE gels (Invitrogen) followed by western blot analysis using antibodies against fluorescent protein (JL-8, Clontech) and PAK (N-20, Santa Cruz). Myc pull-down experiments were performed similarly using anti-Myc agarose and Myc peptide (Sigma) to investigate the interaction of PA–Rac constructs with p50RhoGAP.

Expression, purification and characterization of proteins used for crystallization. C-terminal truncated PA-Rac1 (Δ181–192) was expressed in *Escherichia coli* strain XL-10 Gold (Stratagene) at 30 °C overnight. All purification steps were done under yellow light at 4 °C. Cells were lysed in 20 mM Tris pH 8.5, 50 mM NaCl, 5 mM $MgCl_2$ and 2 mM 2-mercaptoethanol. Protein was purified with a Ni-NTA-FastFlow column (Qiagen) exploiting the N-terminal 6×His tag. The elution was dialysed against 10 mM Tris pH 8.5, 20 mM NaCl, 5 mM $MgCl_2$ and 2 mM 2-mercaptoethanol. The protein was bound to a MonoQ column (GE Healthcare) and eluted with a linear gradient (0–250 mM NaCl in 50 CV). Fractions containing the protein were concentrated (30 kDa cutoff, Millipore) and further purified by Superose 6 gel filtration chromatography (GE Healthcare, 10 mM Tris pH 8.5, 20 mM NaCl, 5 mM $MgCl_2$ and 2 mM DTE). Before crystallization the protein was concentrated to 10 mg ml^{-1} (30 kDa cutoff, Millipore). All proteins were characterized spectroscopically. PA-Rac1 showed reversible light/dark conversion. The dark recovery rate of PA-Rac1 was measured as described previously[5]. The inactive C450A mutation showed no effect on light illumination whereas truncated C450M (Δ181–192) was prone to aggregation on light illumination and, therefore, no data for light/dark conversion could be measured.

Crystallization. Crystallization was carried out under dimmed red light at 20 °C. PA-Rac1 and its C450A and C450M mutants were crystallized using the vapour diffusion method by mixing equal volumes of protein (10 mg ml^{-1}) and precipitant solution (100 mM calcium acetate/100 mM sodium cacodylate/12% (w/v) PEG 8000 or 4% (w/v) PEG 4000/100 mM potassium chloride). Yellow pencil-shaped crystals appeared overnight and grew to a final size of 50 × 50 × 1,000 μm^3 in a week. To avoid photoactivation, crystal handling was done by shielding the microscope light bulb with a 2-mm-thick RG630 filter (ITOS). Before cooling the crystals in liquid nitrogen they were transferred stepwise to precipitant solution supplemented with 20% (v/v) ethylene glycol for cryoprotection.

Data collection and structure determination. Diffraction data were collected at the X10SA beamline (Swiss Light Source) under standard cryogenic settings. Data were reduced using the XDS suite[6] (Supplementary Table 2) and the structure was solved by molecular replacement[7] using subsequentially 2V0U[8] and 1MH1[9] as the initial models. During several rounds of refinement with PHENIX[10] and manual model building in COOT[11], FMN, GTP, Mg^{2+}, Ca^{2+} and solvent molecules were included in the model. Structures were validated using MOLPROBITY[12] and PROCHECK[13] (see Supplementary Table 2 for final statistics).

Structural modelling for linker optimization. The Rosetta program[14,15] was used to predict the dark state structure of LOV2–Rac1 based on the solved crystal structures of dark state LOV2[8] (Protein Data Bank (PDB) code 2V0U) and Rac1[9] (PDB code 1MH1). Structure prediction simulations were performed on LOV2–Rac1 545-4, 546-4 and 547-4 constructs. In these simulations, the torsion angles of the residues connecting the two proteins were optimized with Monte Carlo sampling. Using the Rosetta domain assembly protocol[16], we first applied 1,000 Φ and Ψ backbone torsion angle movements of up to 180° each to three residues connecting LOV2 to Rac1 in a low-resolution representation. Small backbone torsion angle moves of up to 4° were then performed on a high-resolution representation of LOV2–Rac1, followed by a global repacking of all side-chain rotamers. After every 15 cycles of small moves and repacking, further repacking was restricted to the rotamers at the interface and next to the LOV2–Rac1 linkers. This sequence of refinement was repeated for a total of 150 cycles. Next, we adopted a series of small moves, global rotamer repacking, as well as backbone minimization within 5 residues of the LOV2–Rac1 linker for high-resolution optimization cycles. After every ten cycles, only rotamers at the interface and next to the LOV2–Rac1 linkers were repacked. A total of 100 such high resolution optimizations were used to generate models, which were further scored using Rosetta's energy function. One-thousand models, each representing a different folding trajectory, were generated per construct from simulations using the domain assembly protocol.

The complex structure of Rac3 and the CRIB domain of PAK4 (PDB code 2OV2) was used to model the interaction of CRIB-containing effectors with LOV2–Rac1 constructs. The crystal structure of Rac1[9] (PDB 1MH1) was superimposed onto the complex structure by mapping the Cα atoms of Rac1 onto those of Rac3. This derived complex structure was then superimposed onto the LOV2–Rac1 models to create model–CRIB complexes. Side-chain rotamers at the interface of each complex were optimized using rotamer repacking[17]. These complexes were scored using the Rosetta energy function. A low-scoring model–CRIB complex indicated the model could bind CRIB, whereas a high-scoring model–CRIB complex indicated clashes between atoms of the model and the CRIB domain, resulting in reduced binding.

Models generated in a simulation were grouped into clusters according to their pairwise root mean square deviation (r.m.s.d.). The r.m.s.d. (in Å) of the Cα atom positions of each model from all other models in the simulation was calculated. Those models falling within a radius of 3 Å r.m.s.d. from each other were grouped into a cluster. A cluster member representing the centre of each cluster was chosen.

Isothermal titration calorimetry. Dark and lit state mimetics of PA-Rac1, C450A and I539E were cloned into a pTriEx vector with an N-terminal six histidine tag. Residues 65–150 of PAK1, comprising the extended CRIB domain, were cloned into a pET23 vector, with a C-terminal 6xhistidine tag. All proteins were expressed in *E. coli* strain BL21(DE3) cells (Stratagene) at 16 °C overnight in the dark. Cells were lysed in 50 mM sodium phosphate pH 7.0, 300 mM NaCl and 5 mM $MgCl_2$. Proteins were purified under yellow light using TALON Metal Affinity Resin (Clontech) and eluted with 150 mM imidazole at pH 7.0. The proteins were dialysed against 50 mM sodium phosphate, 150 mM NaCl, 7.15 mM 2-mercaptoethanol, 5 mM $MgCl_2$ and 1% glycerol. Protein concentrations were quantified based on the estimated molar extinction coefficients (280 nm) of the corresponding polypeptides or the reported molar extinction coefficient (447 nm) of LOV2-FMN, and were confirmed with SDS–PAGE followed by Coomassie staining.

ITC experiments were performed by injecting the dark state mutant C450A of PA-Rac1 (0.14 mM) or the lit state mutant I539E (0.13 mM) into the CRIB domain of PAK1 (10 μM) using a Microcal VP-ITC calorimeter at 25 °C. Each titration consisted of 29 injections of 10 μl of mutants of PA-Rac1. The baseline of each titration was determined and subtracted from all of the data points. Titration data for the heat change per injection were fitted to a one-site binding model using Origin software (OriginLab).

Cell culture. HeLa, HEK293 (ATCC) and parental MEF/3T3 Tet-Off cells (Clontech) were maintained in DMEM containing 10% FBS following the supplier's culturing instructions. Stable MEF lines were passaged with addition of 1 ng ml^{-1} doxycycline, sufficient to suppress protein expression under the Tet-CMV promoter. Doxycycline was removed 24 h before live cell imaging. It was important to control expression level because small amounts of Rac activity from PA-Rac were apparently present before irradiation, as evidenced by increased ruffling at high expression levels. This was probably due to the equilibrium amount of active Rac present in the dark state. For constructs tagged with fluorescent proteins, expression level could be roughly approximated as proportional to brightness/unit area, enabling use of cells with similar expression.

Live cell microscopy. Cells for live cell imaging were seeded on coverslips coated with 5 μg ml^{-1} fibronectin in Ham's F-12K medium free of Phenol red and containing 2% fetal bovine serum (FBS). Coverslips were mounted in an Attofluor live cell chamber (Invitrogen) placed in a microscope stage with a heated stage adaptor (Warner). Initial characterization and photoactivation of PA-Rac1, diffusion studies by FRAP and PA-GFP, and protrusion/retraction analyses were carried out using an Olympus FluoView 1000 confocal scanning microscope system equipped with a ×60 1.42 NA oil objective and lasers at 405, 458, 488, 515, 568 and 633 nm. Fluorescence images were acquired using 0.1% power from a 30 mW multi-line Ar ion laser (Olympus, minimum power possible without introducing a neutral density filter) and scanned at 2 μs per pixel. The illumination used for photoactivation of PA-Rac1 was between 0.1% power for 10 μs and 1% power for 1 ms in a 10-μm spot, at 458 nm. A more precise measure of the light dose used for activation was obtained by measuring the power after the objective using a power meter (Thorlabs), as described in Supplementary Fig. 7.

Biosensor images were acquired using an Olympus IX81-ZDC microscope equipped with a CoolSNAP HQ2 14-bit camera (Photometrics) and ET-CFP/YFP filters (Chroma) as described previously[18,19]. Band-pass and neutral density filters were switched using motorized filter wheels under computer control (Ludl). CFP, FRET and YFP images were acquired using a 100 W Hg arc lamp with a 3% ND filter for 500, 250 and 250 ms, respectively. FRET/CFP ratio images were calculated after shading correction, background subtraction, binary masking and image registration using MetaMorph and MatLab software as described previously[18–20].

Our imaging conditions, exposure times and filters resulted in a donor (ECFP) bleed-through factor (into the FRET channel) of 0.25 and an acceptor (Citrine) bleed-through factor of 0.07, using the previously described approach[18–20]. The E-FRET calculation was used as a measure of apparent FRET efficiency of the RhoA biosensor, producing a G factor of 1.57. Photobleaching-corrected FRET efficiency (E_{corr}) images were processed based on acceptor photobleaching as previously described[21]. Imaging YFP acceptor fluorescence of the RhoA biosensor was carried out using band-pass filters 500/20 (excitation) and 545/30 (emission).

Simultaneous photoactivation and biosensor imaging was achieved using the FRAP-3D instrument (MAG Biosystems), an illumination system with galvanometer-driven laser positioning. A laser source at 473 nm was incorporated into the illumination pathway using beam-combining mirrors (Chroma, or a 94%/6% Magic Mirror from Olympus).

Immunocytochemistry. MEF cells expressing mVenus-PA-Rac were plated onto coverslips with etched grids (Bellco) that were coated with fibronectin as described above. The cells were locally irradiated at 473 nm through a ×20 phase-contrast objective. Immediately after protrusions were induced, the cells were fixed in 3.7% formalin (Sigma), permeabilized in 0.2% Triton X-100, incubated with anti-phospho-PAK antibody (Cell Signaling), and finally incubated with Alexa Fluor 594-conjugated secondary antibody (Molecular Probes). The numbers on the etched-grid coverslips were used to locate the immunostained cells that had been previously irradiated.

Measurement of protrusion length. Protrusions were analysed by drawing up to 8 lines per cell, perpendicular to the cell border and at least 45 degree apart (a few lines were dropped because of cell junctions). More than 14 cells were analysed for each construct. The line scans were analysed as kymographs, oriented as shown in Supplementary Fig. 4. The protrusion length was defined as the maximal distance of the membrane from the left hand border of the kymograph after irradiation minus the average distance of the cell border from the left hand edge of the kymograph before irradiation.

Fluorescence recovery after photobleaching (FRAP). MEF cells expressing mVenus-tagged PA-Rac1 were irradiated (515 nm, 10% power for 100 μs) at a 10-μm spot using the Olympus FluoView1000 confocal scanning microscope and laser detailed above. The intensity of mVenus fluorescence was monitored (515 nm, 0.1% power for 2 μs) before and after photobleaching at 2-s intervals. The intensity of fluorescence within the bleached spot was normalized against the integrated intensity of the entire cell. The data were plotted and fitted to a single-exponential decay to obtain $t1/2$ (τ_D). A $t1/2$ of 12.1 s and Fi (immobile fraction) of 18.6 ± 0.6% were obtained ($n = 26$). The diffusion coefficient ($D = 0.55\ \mu m^2 s^{-1}$) was estimated using $D = \omega^2/4\tau_D$ (where ω is the radius of the circular bleached spot), assuming exclusively free lateral diffusion[22,23].

PA-GFP tracking. MEF cells expressing mPA-GFP-tagged PA-Rac1 were irradiated (405 nm, 6 mW diode laser, 10% power for 10 μs) in a 10-μm spot to switch on PA-GFP. The fluorescence of PA-GFP was monitored using a 488-nm laser, acquiring an image every 2 s. The intensities of fluorescence within the irradiated spot and an adjacent spot of the same size were quantified and normalized against the entire cell. The decay of activated PA-GFP fluorescence was fitted to a single exponential decay, yielding a $t1/2$ of 14.6 s.

Inhibitor studies. MEF cells expressing mVenus-tagged PA-Rac1 were incubated with 1 μM myosin II inhibitor blebbistatin, 1 μM MLCK inhibitor ML-7, or 10 μM ROCK inhibitor Y-27632 (Calbiochem). Cells underwent the cell shape changes previously described[24] and then reached a stable state within 30 min. After this cells were irradiated with the 458-nm laser at a 10-μm spot to induce PA-Rac activation.

Protrusion/retraction analysis. Fluorescence images of MEF cells expressing mVenus-tagged PA-Rac1 and its mutants were masked based on intensity thresholding to produce binary images. Regions of protrusion were isolated by subtracting the binary image at a given time point from that at time 0. Conversely the binary images of retraction were obtained. Areas not part of protrusions or retractions, those that overlapped the time 0 image, were obtained by subtracting the above two images from that at time 0. Each binary image was assigned a different colour: red, protrusion; blue, retraction; green, area overlapping with time 0; and white, background. These operations were carried out using MetaMorph software.

Polarity index calculation. To obtain the polarity index ($\cos\theta$) of the migrating MEF cells, x and y coordinates were obtained for the centroid before movement (x_0,y_0), the centroid after movement (x_1,y_1), and for the centre of the irradiation spot (x_2,y_2), using MetaMorph software. The cos and sin values of the angles were obtained using simple triangle calculations. First two angles were defined using an arbitrarily selected horizontal line θ_1 = angle between the arbitrary line and the line from (x_0,y_0) to (x_1,y_1), and θ_2 = angle between the arbitrary line and the line between (x_0,y_0) and (x_2,y_2). The cos used to characterize polarity (see main text and Fig. 2d) was obtained using the following formula: $\cos\theta = \cos(\theta_1 - \theta_2) = \cos\theta_1\cos\theta_2 + \sin\theta_1\sin\theta_2$.

5.7.2 Appendix B: Matlab code used to analyze fluorescence polarization assays in Chapter 3

```
clear all

%  ------------------------------------------
% starting protein concentrations (M)

ipa_tot = 43e-9;
vin_tot = 47e-9;
lov_vin_start = 0.0;
nlov = 6;
lov_array = [80e-9 150e-9 300e-9 1000e-9 3000e-9 5000e-9 ];
% experimental results (t= seconds)
tout_exp = dlmread('time.csv');
ntout_exp = 38;
ipa_vin_exp(:,1) = dlmread('D80nm.csv');
ipa_vin_exp(:,2) = dlmread('D150nm.csv');
ipa_vin_exp(:,3) = dlmread('D300nm.csv');
ipa_vin_exp(:,4) = dlmread('D1um.csv');
ipa_vin_exp(:,5) = dlmread('D3um.csv');
ipa_vin_exp(:,6) = dlmread('D5um.csv');


% time steps (seconds)
dt = 1e-2;    % time step
nits = 12e5;    % number of time steps
nout = 1200;
dt_out = (nits/nout)*dt;
tout = [0:dt_out:nout*dt_out];   % time points for collecting data

nk1r = 1;    % dissociation of ipa_vin
k1r_array = [.0024];
kd_ipa_vin = [ 2e-9 ];  % kd of ipa_vin

nk2f = 1;     %  association of lov_vin
k2f_array = [1e3];%
nkd = 1;
kd_array = [73e-9];  % equilibrium dissociation constant for lov binding to
vin

for i_k1r = 1:nk1r
    for i_k2f = 1:nk2f
        for i_kd = 1:nkd

 % initialize kinetic parameters
        k1r = k1r_array(i_k1r);         % Rate constant for ipa_vin breakup
        k1f = k1r/kd_ipa_vin;          % Rate constant for ipa_vin association
        kd  = kd_array(i_kd);           % equilibrium dissociation constant
for Lov / vin binding
        k2f = k2f_array(i_k2f);         % rate constant for
        k2r = k2f * kd;                 % rate constant for Lov dissociating
from vin

        % loop over various Lov_tot concentrations
        sum_sqr_deviation_pol = 0;
```

```
for l = 1:nlov

    %ipa_tot = ipa_tot_start;
    %vin_tot = vin_tot_start;
    lov_tot = lov_array(l);
    lov = lov_tot;

    % calculating ipa_vin
    a = 1;
    b = -(ipa_tot + vin_tot + kd_ipa_vin);
    c = vin_tot * ipa_tot;
    ipa_vin = (-b - (b*b - 4*a*c)^0.5)/2;
    ipa_vin_start = ipa_vin;

    lov_vin = lov_vin_start;
    vin = vin_tot - ipa_vin - lov_vin;
    ipa = ipa_tot - ipa_vin;

    % output vectors
    ipa_vin_out(:,l) = zeros(1,nout+1);
    pol_out(:,l) = zeros(1,nout+1);

    % fill output variable for time = 0
    n = 1;
    ipa_vin_out(n,l) = ipa_vin;
    fraction_bound = ipa_vin/ipa_tot;
    %dpol = pol_min - pol_max;
    pol_out(n,l) = fraction_bound;

    % numerical integration of kinetic reaction
    for i = 1:nits
        delta_k1f = dt*k1f*ipa*vin;
        delta_k1r = dt*k1r*ipa_vin;
        delta_k2f = dt*k2f*lov*vin;
        delta_k2r = dt*k2r*lov_vin;
        lov_vin = lov_vin + delta_k2f - delta_k2r;
        ipa_vin = ipa_vin + delta_k1f - delta_k1r;
        vin = vin + delta_k1r + delta_k2r - delta_k1f - delta_k2f;
        ipa = ipa + delta_k1r - delta_k1f;
        lov = lov + delta_k2r - delta_k2f;

        % collect data for making plots
        if mod (i,floor(nits/nout)) == 0
            n = n+1;
            %lov_vin_out(n,l) = lov_vin;
            ipa_vin_out(n,l) = ipa_vin;
            fraction_bound = ipa_vin/ipa_tot;
            %dpol = pol_min - pol_max;
            pol_out(n,l) = fraction_bound;
        end
    end

    % compare rmsd of experiment to simulated curves
```

```
                ntp = floor(time_point/dt_out)+1;  % how to find time_point
in _out arrays
                fraction_bound = ipa_vin_out(ntp,1)/ipa_tot;
                pol = fraction_bound;
                square_deviation_pol = ((pol) - ipa_vin_exp(nt,1))^2;
                sum_sqr_deviation_pol = sum_sqr_deviation_pol +
square_deviation_pol;
            end
        end
        rmsd = (sum_sqr_deviation_pol/(nlov*ntout_exp))^0.5;

        end % i_kd
    end  % i_k2f
end  % i_k1r

plot(tout, pol_out(:,1),'b', tout_exp, ipa_vin_exp(:,1),'ob');
hold on
plot(tout, pol_out(:,2),'r', tout_exp, ipa_vin_exp(:,2),'or');
plot(tout, pol_out(:,3),'g', tout_exp, ipa_vin_exp(:,3),'og');
plot(tout, pol_out(:,4),'c', tout_exp, ipa_vin_exp(:,4),'oc');
plot(tout, pol_out(:,5),'m', tout_exp, ipa_vin_exp(:,5),'om');
plot(tout, pol_out(:,6),'k', tout_exp, ipa_vin_exp(:,6),'ok');
hold off
xlabel('time (seconds)');
ylabel('fraction bound');
```

5.7.3 Appendix C: Yeast two-hybrid experiments with controls

LOV-ipaA L623A Lit state and dark state mimetic yeast two-hybrid assay and controls. SD media conditions are indicated. *S cerevisiae* strain Y2Hgold containing the Gal4 activation domain (AD) linked to the construct indicated was mated with strain Y187 containing the Gal4 binding domain (BD) linked to the construct indicated. Mated colonies were serially diluted (1:5), replica plated, and grown for 3 days at 30 °C

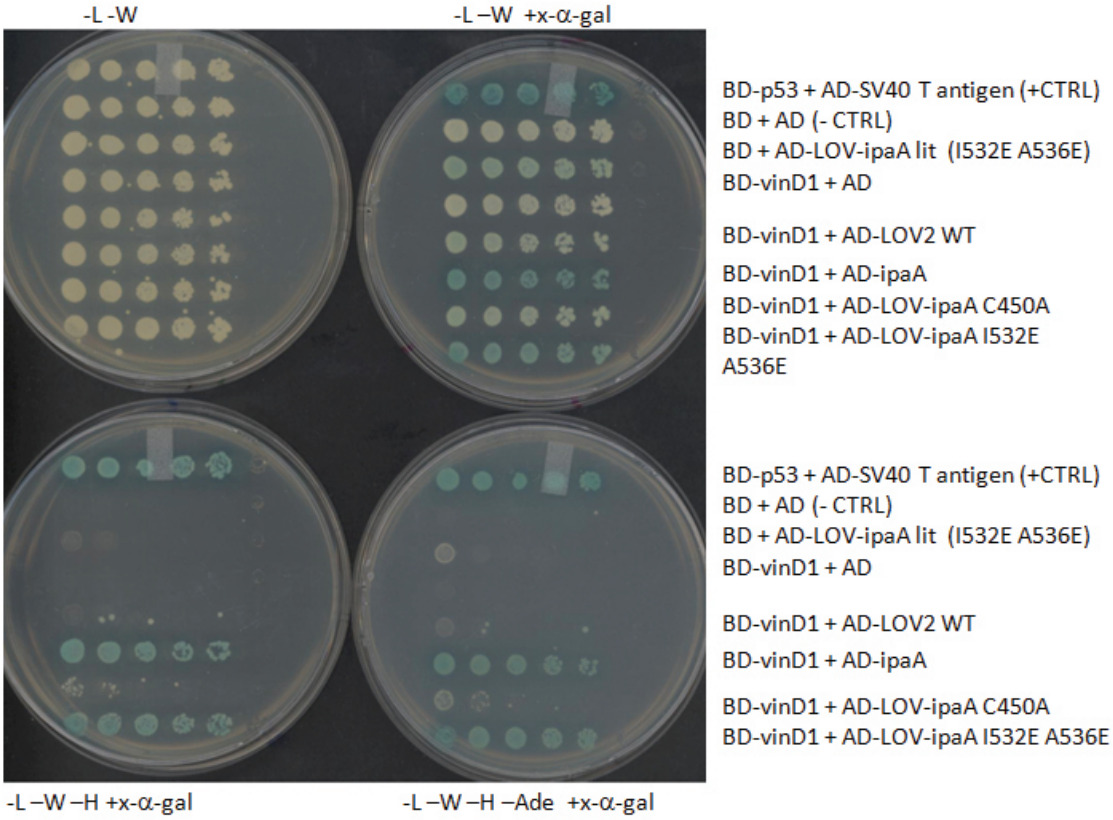

LOV-ipaA L623A WT yeast two-hybrid assay and controls. SD media conditions are indicated. *S cerevisiae* strain Y2Hgold containing the Gal4 activation domain (AD) linked to the construct indicated was mated with strain Y187 containing the Gal4 binding domain (BD) linked to the construct indicated. Mated colonies were serially diluted (1:5), replica plated, and grown for 3 days at 30 °C in either blue light or in the dark, as indicated.

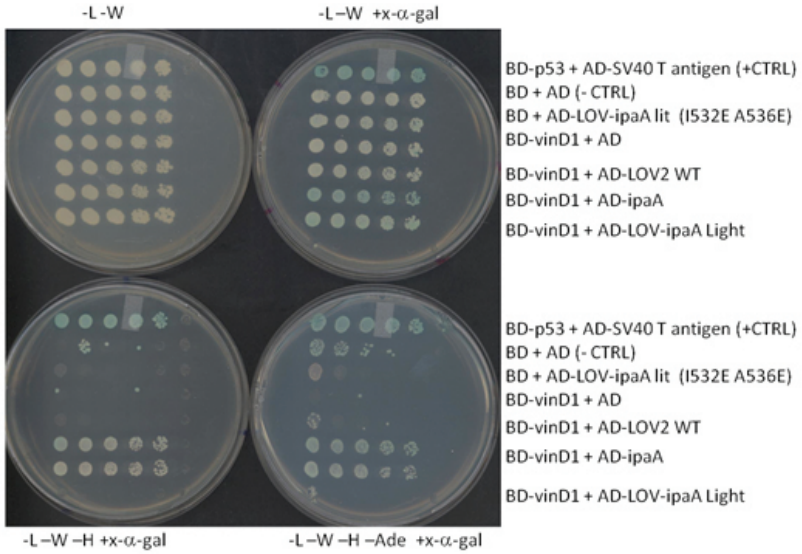

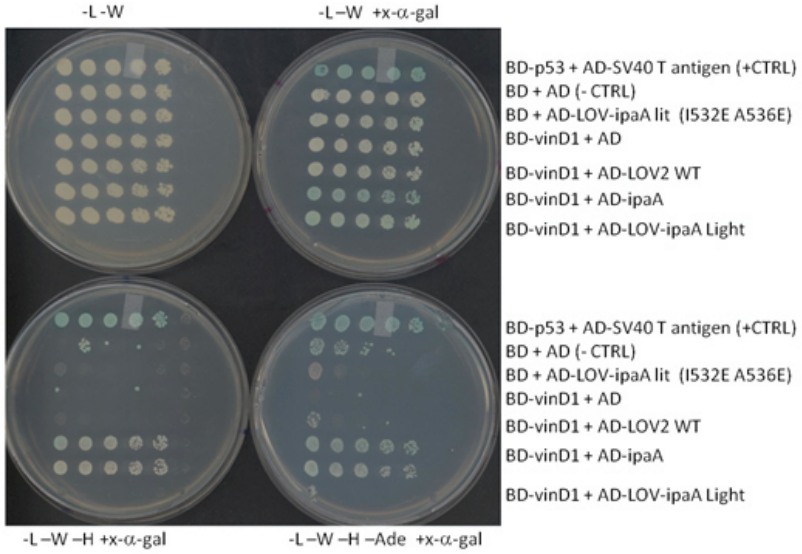

LOV-ipaA WT lit state and dark state mimetic yeast two-hybrid assay and controls. SD media conditions are indicated. *S cerevisiae* strain Y2Hgold containing the Gal4 activation domain (AD) linked to the construct indicated was mated with strain Y187 containing the Gal4 binding domain (BD) linked to the construct indicated. Mated colonies were serially diluted (1:5), replica plated, and grown for 3 days at 30 °C

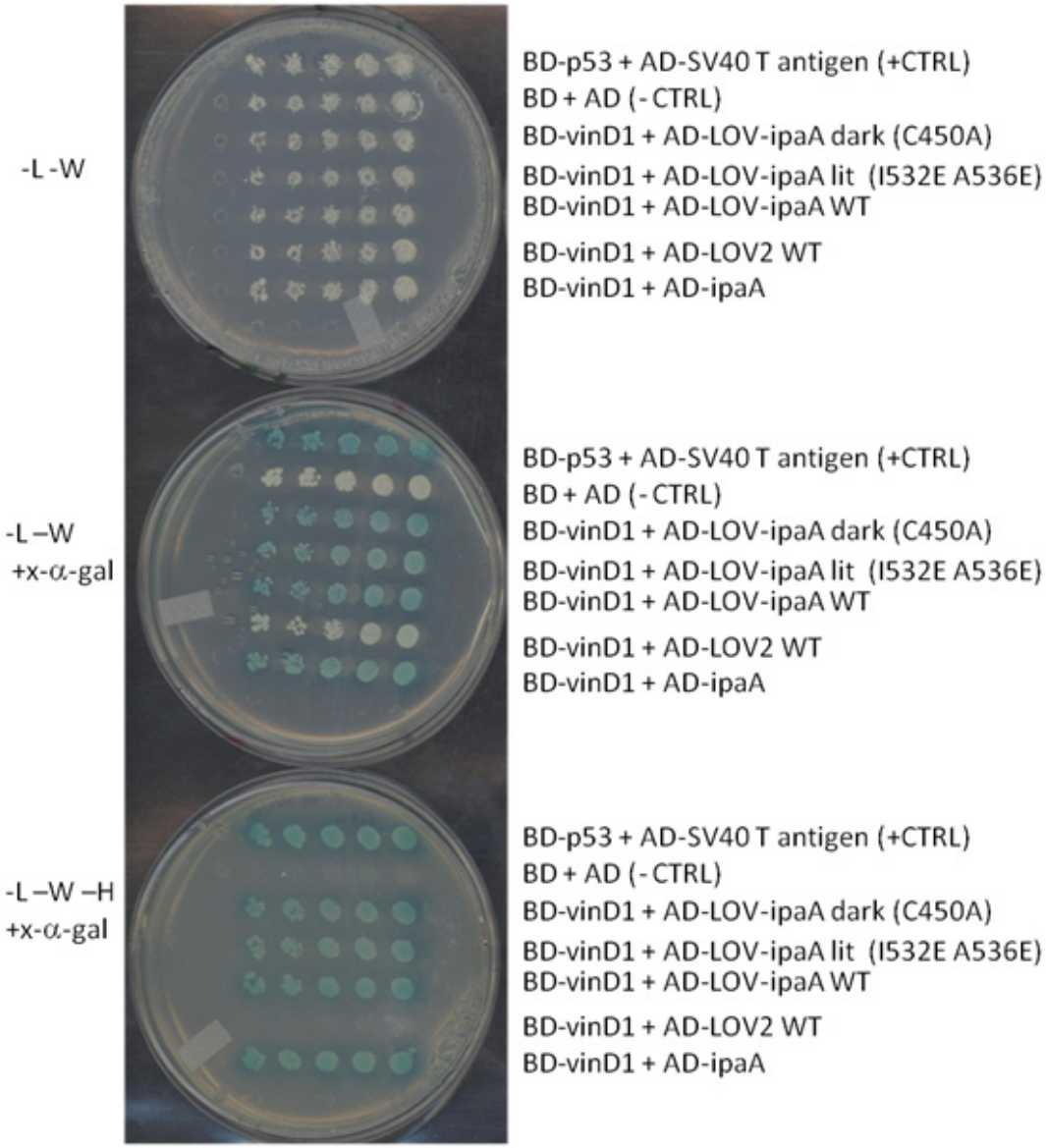

5.7.4 Appendix D: Photoactivation of Ste4 expression plates

Budding yeast transformed with GAL-Ste4, BD-vinD1, and AD-LOV-ipaA WT or empty pRS316 vector were grown under dark (non-inducing) and blue light (inducing) conditions. Resulting growth arrest is seen on serially diluted colonies.

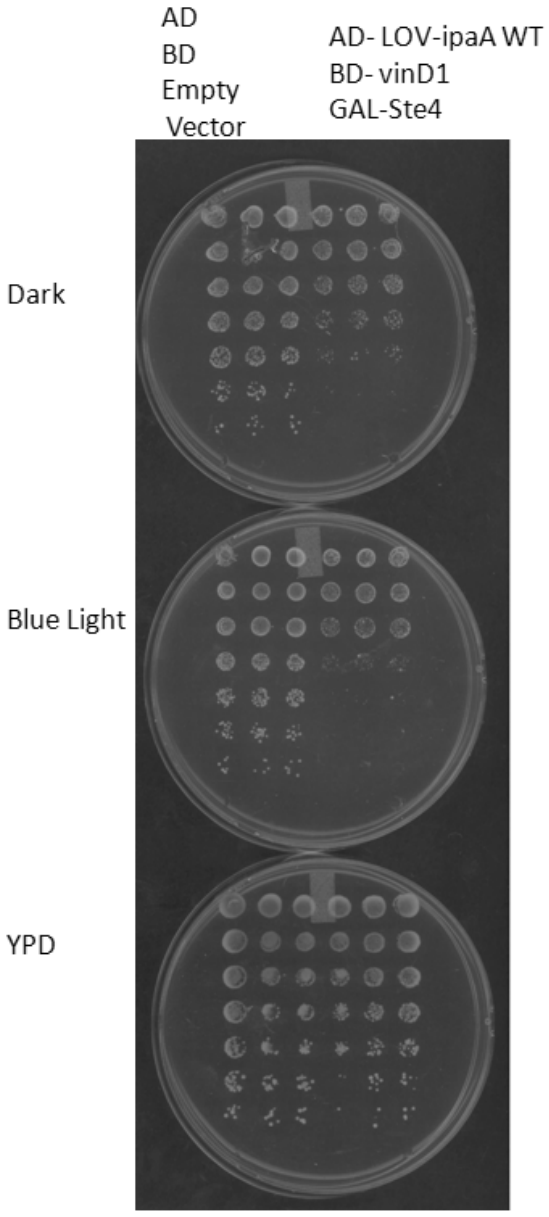

Budding yeast transformed with GAL-Ste4, BD-vinD1, and AD-LOV-ipaA C450A or empty pRS316 vector were grown under dark (non-inducing) and blue light (inducing) conditions. Resulting growth arrest is seen on serially diluted colonies.

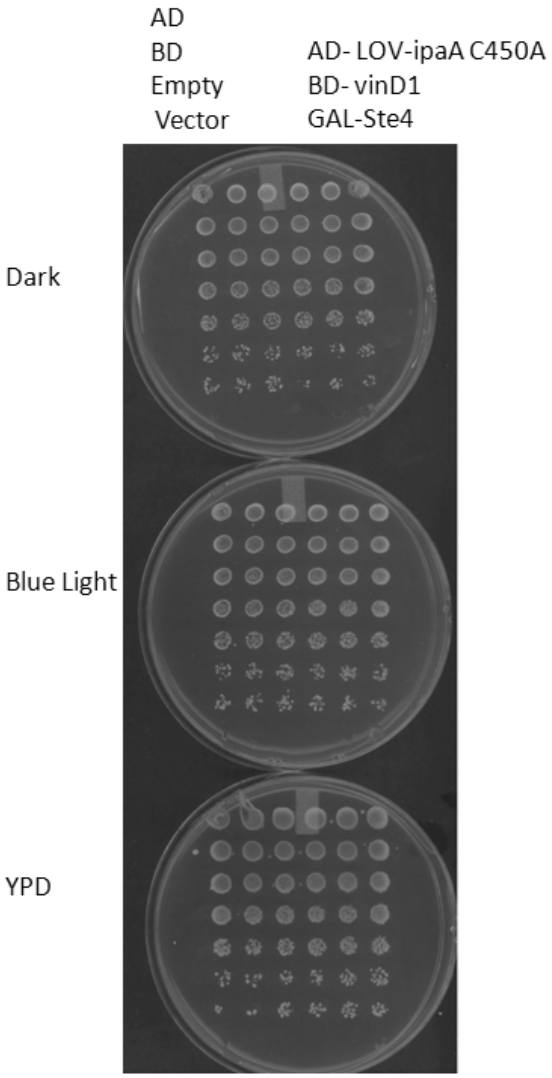

Budding yeast transformed with GAL-Ste4 or empty pRS316 vector were grown under glucose (non-inducing) and galactose (inducing) conditions. Resulting growth arrest is seen on serially diluted colonies.

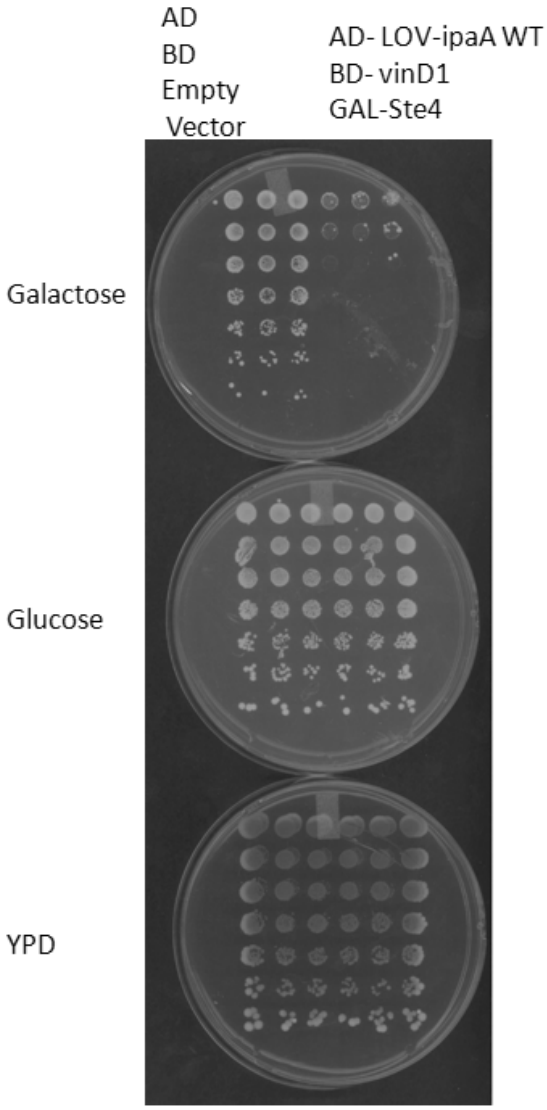

REFERENCES

1. Wu, Y., Frey, D., Lungu, O., Jaehrig, A., Schlichting, I., Kuhlman, B., and Hahn, K. (2009) A genetically encoded photoactivatable Rac controls the motility of living cells. Nature **461**, 104–108

2. Yoo, S., Deng, Q., Cavnar, P., Wu, Y., Hahn, K., and Huttenlocher, A. (2010) Differential regulation of protrusion and polarity by PI (3) K during neutrophil motility in live zebrafish. Developmental cell **18**, 226–236

3. Walters, K., Green, J., Surfus, J., Yoo, S., and Huttenlocher, A. (2010) Live imaging of neutrophil motility in a zebrafish model of whim syndrome. Blood **116**, 2803

4. Wang, X., He, L., Wu, Y., Hahn, K., and Montell, D. (2010) Light-mediated activation reveals a key role for Rac in collective guidance of cell movement in vivo. Nature cell biology **12**, 591

5. Levchenko, I., Grant, R., Wah, D., Sauer, R., and Baker, T. (2003) Structure of a delivery protein for an AAA+ protease in complex with a peptide degradation tag. Molecular cell **12**, 365–372